NPS - 59SL72081A

NAVAL POSTGRADUATE SCHOOL

Monterey, California

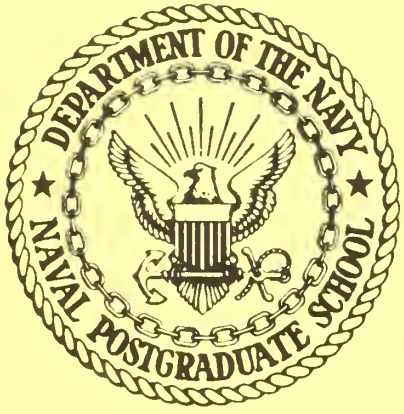

INTERACTION OF SEMI-CONFINED TURBULENT JETS

FINAL REPORT

BY

TURGUT SARPKAYA

8 AUGUST 1972

NAVAL POSTGRADUATE SCHOOL

Monterey, California

Rear Admiral Mason B. Freeman, USN
Superintendent

M. U. Clauser
Provost

ABSTRACT

The present investigation is concerned with the theoretical and experimental study of the interaction of semi-confined, subsonic, turbulent jets, the application of the results to fluidics being one of the primary objectives in mind. The theoretical results obtained both through the use of the free-streamline theory and a new momentum analysis for both the single and symmetric control-jet configurations are presented in the first part of the report. The second part covers the detailed experimental investigations of the jet deflection and the velocity-and turbulence-profile measurements obtained with a hot-wire anemometer for both the single-control-jet and symmetric beam-deflection type amplifiers. Finally, the results of the two parts of the study are compared and the advantages and shortcomings of the various analyses are presented.

NPS - 59SL72081A

8 August 1972

FOREWORD

The work described in this report was sponsored by the U. S. Army Research Office - Durham. The generous support of the sponsor is gratefully acknowledged.

The author expresses his special appreciation to a group of Naval Officers: LT N. Gungor, LT S. B. Weeks, LCDR E. Turken, and LT G. L. Hiriart who through their maturity, dedication, invaluable assistance, and untiring work proved themselves to be the most outstanding students on earth.

TABLE OF CONTENTS

I. INTRODUCTION

There are so many instances in nature and in engineering when the problem of free or semi-confined, two-dimensional or axisymmetric, jet-jet and jet-wall impingement is of great importance that the task of preparing a complete list of examples together with suitable comments is of itself a major undertaking. Such a broad survey will not be undertaken here for the present study was primarily motivated by a desire to understand the phenomenon of jet impingement or interaction in fluidic elements in general and in beam-deflection amplifiers in particular and by an attempt to provide a rational approach to imparting and processing information as well as transmitting power with fluids in fluidic control systems.

An essential prerequisite to a rational approach to the information and power transmission through a fluid medium is that the interaction of some type of flow, containing the major portion of power, with one or more secondary flows, essentially intermittent in nature, be achieved with as little energy loss as possible and that the exact mode of interaction as well as the characteristics (e.g. velocity, pressure and noise distributions as functions of space, time, and the specified amplifier geometry, etc.) of the resulting flow be understood and analytically predicted.

A dozen of years, since the invention of fluidics, and hundreds of papers which resulted in a descriptive set of rules-of-thumb rather than in a prescriptive set of design criteria have taught us that the mastery of the simultaneous use of both the brains and brawns of a fluid medium, i.e., imparting and processing information as well as transmitting power with fluids, is at best an exceedingly complex proposition and that the source of major difficulty lay not so much in the control theory but rather

in the prediction of the behavior of the motion of the working fluid. The understanding of the jet impingement even in its simplest forms, leaving aside the complex boundaries, had to be acquired as part of the development of this new technology for it did not exist in the annals of fluid dynamics. The acquisition of this vital information began, as it then appeared logical on the basis of past experience, with the study of relatively idealized situations, e. g. taking one fixed operational condition at a time. At first it appeared that considerable progress was being made and that the theoretical and experimental findings so arrived at will somehow be unified and everything will fall in its proper place in a cross-flow puzzle. The intensive research by many investigators in the past decade has yielded many results and numerous pieces of understanding of the idealized operational conditions but these black dots and black boxes of information did not integrate, with the exception of a few cases, into a meaningful and quantitative picture. The reasons for this dissappointingly small progress were numerous:

I. 1: Lack of understanding of the physics of turbulence;

I. 2: Lack of measurements and/or analysis of the characteristics of confined two-dimensional laminar and turbulent jets;

I. 3: Lack of understanding of the characteristics of the entrainment interface, dependence of entrainment on the configuration of the adjacent jets and boundaries;

I. 4: Lack of understanding of the entire impingement process; and in general,

I. 5: The lack of isolation and identification of the nature and location of the important noise sources.

We will now briefly comment on each of these factors which significantly limit the rationalization of the design of most of the fluid amplifiers.

I. 1. The shortcomings of simple relations, like eddy viscosity formula

and the mixing length, are well-known. Satisfactory relations have been obtained with them only for relatively simple flow situations. The decisive disadvantage of these relations is that their application to a particular flow problem requires ad hoc assumptions with regard to the magnitude and distribution of eddy viscosity or mixing length. This is even more so for an amplifier in which the flow is considerably more complex, and a turbulent shear assumption uniformly applicable to the flow field in the amplifier is not likely to exist.

I. 2. Many fluidic devices operate in the turbulent flow regime for a variety of practical and hydrodynamic reasons. This then leads to the consideration of a pseudo two-dimensional turbulent jet. One then obtains a velocity distribution equation, the form and the complexity of which depend primarily on the assumptions made regarding the Reynolds stresses. Available theories consider the turbulence structure to be two-dimensional, i. e., $w' = 0$, like the jet itself and ignore (out of necessity) the effect of the boundary layers on the confining walls (top and bottom cover plates of the amplifier). One such profile is that obtained by Görtler as

$$u = \frac{\sqrt{3}}{2}\sqrt{\frac{J\sigma}{\rho x}}\,(1 - \tanh^2\eta)\,, \quad v = \frac{\sqrt{3}}{4}\sqrt{\frac{J}{\rho\sigma x}}\,[2\eta(1 - \tanh^2\eta) - \tanh\eta] \tag{1}$$

$$\eta = \sigma y/x \quad , \quad Q = \sqrt{3Jx/\rho\sigma} \quad , \quad m = \sqrt{3J\rho x/\sigma}$$

where u and v are the velocity components, J the momentum of the jet per unit length, m the total mass flux, and σ an empirical constant which may vary anywhere from 7. 7 to 15 depending on the circumstances. Obviously, alternative expressions may be obtained by adopting different hypotheses for the turbulent shear stresses. These do not, however, affect the main conclusions we arrive at here regarding their applicability to the analysis of jet impingement in fluidic elements. Firstly, it is

clear that the theoretical analyses consider a jet which has at the origin ($x = 0$), no net flux of mass but only a momentum flux J. Thus the expression given above for the volume flow rate Q is not due to the source generating the jet but rather due to the fluid entrained by the jet which has a momentum flux of J. This then leads to the considerations concerning the true origin of a jet which has a momentum flux of J with a finite flow rate Uw at the nozzle exit. It is easy to show that the jet could have entrained a flow of Uw in a distance of approximately $x_o = \sigma w/3$ which is also the distance to the nearly true origin of the jet from the nozzle exit. This is nearly so because at $x = x_o$, i.e. at the nozzle, the jet attained the same mass and momentum flux but not the same energy and the similar velocity profile predicted by the analysis. Clearly, the origin of the jet depends on σ and, in other words, on what happens to the jet further downstream, such as jet curvature etc. It is further clear that the theoretical solutions provide better approximation to the flow produced by the slit as U increases or equivalently the nozzle area decreases. However, the problems with such analyses begin after the jet leaves the nozzle. There is always a region near the origin where the equations are not valid and the jet undergoes a transition in a distance of approximately 3 to 8 nozzle widths. As will be noted later, the length of the transition region strongly depends on the availability of the entrainable flow or in other words on the distance between the two cover plates (aspect ratio); the configuration of the boundaries on the two sides of the jet; the direction, energy, and the momentum of the impinging jets; Reynolds number, etc. The variation in turbulence structure in and outside the potential core, the three-dimensional structure of flow and turbulence, the variable and boundary-dependent entrainment conditions, the rolling up of intense shear layers at the entrainment interface, and above all the finiteness of the nozzle introduce such complexities into the analysis that there is at present no solution of the complete equations of motion even for a steady two-dimensional confined jet discharging

from an orifice in the form of a finite slit. Suffice it to say that the region of interest is exactly the region where the existing analyses or approximations are not applicable. The far field or the fully developed region of the jet is not a good region in which to try to further the understanding of either the resultant jet or of the noise generation by turbulence. In other words, a vast amount of detail about the velocity and pressure distributions, about the individual sources of noise, and intermixing among the power and control jets and their interacting with the local entrainment and turbulence would be lost by this fully-developed behavior of the jet in the far field. The understanding of the near field or the developing region offers a better opportunity for the prediction of the behavior of the amplifiers and of the different sources existing in the nozzle and the strong shear region. But no detailed velocity and pressure measurements are available to shed any light on this inner field, not mentioning the complications due to turbulence and doubly-connected vortex sheets. Besides the complete absence of pressure measurements, the measurements of the statistical properties of the flow within the potential region are very crude and scarce. For this lack of data, the usual, but not necessarily valid, assumption of potential flow inside the jet has to be blamed.

Several attempts have been made to develop empirical velocity-distribution relationships for the purpose of predicting the behavior of fluid amplifiers. Among these notable is the one proposed by Simson (1), which describes the power jet over both the transition and the fully established zone, involves a reasonable turbulent shear stress, renders the slope of the velocity profile zero as the ratio of the local velocity to the center-line velocity approaches unity, and which maintains a constant jet momentum. Simson proposed that (see Fig. 1)

$$u/u_c = \left[1 - (y_e/kx)^{7/4}\right]^2 \quad \text{with} \quad y_e = y - w/2 \tag{2}$$

where $k = 1.378\ w/x_o$ for $x_o = 5w$. In the transition zone $u = u_c$ and in the fully established region

$$u_c/U = \sqrt{x_o/x} \tag{3}$$

As previously noted, the length of the transition zone depends on the aspect ratio, Reynolds number, availability of the entrainable flow, etc., and may vary from 3w to 7w. Furthermore, both the transition and the fully established region significantly change their characteristics when the power jet is acted upon and deflected by one or more control jets placed at some angle of inclination to the power jet. In passing, it suffices to note that the analysis of the two-dimensional laminar jet is equally complex because of the laminar boundary layers developing along the top and bottom plates of the amplifier. The instability of laminar jets, particularly to small swirl, render them practically unuseable in fluidic elements in spite of the appetizing features of laminar jets such as lower noise, lower power consumption, and significantly higher energy, relative to a turbulent jet, at a given section downstream.

Obviously, attention has been directed here to turbulent jets issuing from several slits into a two-dimensional confined space. There is, to be sure, an extensive literature on the structure of turbulent free jets (see e.g. Schlichting (2), Krzywoblocki (3), Gurevich (4), Davis (5), and their references) the bulk of which deals with the decay of subsonic jets issuing from round nozzles into a quiescent medium. Analytical and semi-empirical methods for determining jet characteristics likewise have been largely restricted to subsonic and properly expanded supersonic jets. In the special approach of the present study, however, it is of interest to determine not only the local details of the flow within the core of both the single and impinging two-dimensional jets, but also the effects of interaction on the decay and spreading rates downstream.

Knowledge of these effects should enable one to consider the problem of confined-jet impingement in terms of downstream boundaries such as load ports and in terms of various recovery factors such as pressure, momentum, and energy recovery.

I. 3. Fluid jets, confined-two-dimensional or axisymmetric, have the characteristics of entraining, i. e. drawing in the surrounding fluid so that the mass flow rate of the jet increases with axial distance from the jet origin. Metaphorically speaking, the auditory nerves, stimulated by the noise of the jet, can almost filter out the words "let me entrain you."

The property under consideration here is the mass flow rate in the jet, m, and in particular the rate of change of mass flow rate dm/dx, which is equal to the local entrainment rate dm_e/dx. For a two dimensional jet between the boundaries $\pm h/2$ (with the aspect ratio of h/w)

$$m(x) = \int_{-\infty}^{\infty} \int_{-h/2}^{h/2} u(x, y, z)\, dz\, dy \qquad (4)$$

where ρ is the fluid density, u is the fluid velocity in the axial direction, and x, y, and z are the coordinate axes in the direction of flow, in the plane of the jet parallel to the cover plates, and normal to the x-y plane, respectively.

In fully developed axisymmetric free jets, the mass flow rate of the jet is observed to increase linearly with axial distance according to the relation (Ricou & Spalding (6)),

$$dm/dx = \sqrt{J\rho}\ C_1 \qquad (5)$$

where J is the momentum flux of the jet, ρ is the density of the surrounding fluid and C_1 is a constant ($C_1 \cong 0.28$).

Measurements of velocity profiles and the calculation therefrom of the jet mass flow rate in the region immediately downstream of a round nozzle, i.e., in the region over which the velocity profile changes from that of the entering jet to that of fully developed flow, were made by Voorheis & Howe (7), Albertson et al. (8), Grimmett (9), Polomik (10), Ricou (11), Donald & Singer (12), and Hill (13). In spite of the quantitative differences between the results of various measurements, it appears that the jet mass flow rate increases nonlinearly in the initial region, the entrainment rate being lower than in the fully developed jet. Be that as it may, these measurements are made with axisymmetric jets and the results may not be used in the prediction of the entrainment characteristics of confined turbulent jets for the entrainment rate and/or the entrainment interface are reduced and the doubly-connected vortex sheets are bounded and influenced by the top and bottom boundary layers. Furthermore, and perhaps obviously, the results of the available analytical solutions for two-dimensional, fully-developed, turbulent jets cannot be expected to predict the entrainment rate in the flow development region. For example, the mass flow rate calculated by Görtler as $m = \sqrt{3J\rho x/\sigma}$ would, if it were applicable to the initial flow region, yield

$$dm/dx = 0.5\sqrt{3J\rho/\sigma x} \qquad (6)$$

according to which the maximum entrainment should occur in the flow-development region, a fact contrary to the experimental measurements, at least for those made for axisymmetric jets where entrainment appears to vary according $dm/dx = C_1\sqrt{J\rho x}$ for $x/w \lesssim 15$. The reason for this is rather obvious since Görtler's analysis is applicable only to the fully-developed region of a two-dimensional flow where the similarity of the jet profiles holds true. There are, however, more fundamental and practical reasons which have precluded the use of the results obtained from the analysis of confined, two-dimensional, turbulent jets in the prediction of the entrainment in the flow development region. We will

now touch upon these reasons briefly.

It is a well-known fact that differential entrainment causes differential pressure, i. e., jets bow to entrainment deprivation. This is called the Coanda effect. A jet will continue to deflect under the influence of time-and position-dependent differential entrainment (the deflection and the kinematics of the entrainment interface depending heavily on the local surface curvature) until a stable state of equilibrium is reached. One such state may be the attachment of the jet to a wall of sufficient length or the attachment of the wall to the jet (as in the case of a shower curtain attaching to the jet rather than to the edges of the tub). This process is of primary importance in the operation of wall attachment devices. In other words, the real amplifier geometry, comprized of additional elements such as control-jet walls, nozzles, or obstructions, dramatically alter the flow entrainment in the flow-development region. Many variations of the proportional amplifiers have been proposed and/or patented by controlling the entrainment deprivation, to varying degrees, in the vicinity of impingement of two or more jets. In passing it should be noted that the use of two or more axisymmetric jets is not practicable since experiments have shown that the weaker of the two jets interacts with and passes around the other if the latter were an elastic cylinder (bending of the jet, vortex shedding, etc.). On the other hand, the confinement of the jets between two parallel plates brings in additional pressure and entrainment problems which prohibit the analysis of the resulting flow without resorting to the use of a fair number of simplifying assumptions and empirical coefficients. In fact, a close look at the interaction region shows that it is not possible to establish via analytical methods how the flow and pressure fields in a proportional or beam-deflection amplifier vary with geometry. Furthermore, it appears, on the basis of the past experience, that a geometry and flow combination which is relatively more amenable to some form of analytical study is not necessarily the most satisfactory combination from a

flow and/or pressure recovery stand point. In fact, it has been possible, as noted above, to shape the geometry of the interaction region (additional vents, curved control-port walls, etc.) so as to make use of the interplay between the enhanced or decreased entrainment and the jet, at the expense of rendering the resulting flow relatively less amenable to analysis.

I. 4. We will now briefly describe the characteristic features of the impingement process. Numerous experiments with air and water of the impingement of confined two-dimensional jets have shown that the power as well as the control jets retain to a large measure (with some contraction to be discussed later) their identity during interaction, the main jet acting simply as a brick wall or deflector. The four shear layers (two at outsides of the control jets, i.e., between the ambient flow and the control jets, and two between the control jets and the power jet) rapidly develop (with increasing entrainment) and the profile of the combined jet acquires a Gaussian form in about 3 to 6 nozzle widths. Two relatively strong control jets ($Q_c/Q_p > 0.3$) often pinch the main jet and give rise to a jet contraction and central-line acceleration. The two control jets also undergo some contraction and acceleration depending on the set-back and the width of the control nozzles, aspect ratio, Reynolds number, jet deflection, etc. These effects do in turn alter the velocity and pressure distributions, the entrainment characteristics, and the subsequent development of the composite jet. It is further expected that the level and distribution of noise, generated in the shear layers, will also be affected by this pinching or contraction process. Fortunately enough, however, control flow rates in excess of 0.25 to 0.30 of the supply flow are not of practical importance in either the wall-attachment or beam-deflection amplifiers since such relatively large control flows may lead to control jet velocities or pressures considerably larger than that of the power jet (for the sizes of set-backs currently used for many

other reasons) and negate the very purpose of pressure, momentum, and energy amplification through the use of fluidic elements even though this would tend to minimize the intensity of the noise generated in the inner shear layers. The relationship between these practical reasons and the analytical necessity, at least in inviscid flows, of preventing the velocity and pressure discontinuities within the flow field will be discussed later. It suffices to state that the concept of fluid amplification through jet interaction is incompatible with the prevention of velocity discontinuity and the shear-layer generated noise. In other words, noise must be an element to content with and to be alleviated after the fact if the idea of fluid amplification is to be employed within a range of acceptable signal-to-noise ratios.

It is apparent from the foregoing description of the impingement process that the jets behave as inviscid jets shortly after leaving their respective nozzles and remain nearly so only within a short distance of the interaction region (approx: one nozzle width). Thereafter, the shear layers tend to alleviate the intensity of the reasons leading to their existence and eventually yield a velocity profile which is free from the two internal shear layers and a resultant jet which behaves as a fully-developed, gradually expending, turbulent jet. Thus, there is not a unique mode of interaction which would assist in the formulation of a mathematical model uniformly applicable everywhere from the nozzle to the fully-developed flow region. Furthermore, there are many possible geometric and kinematic variables for the interaction process and it is not economically feasable to experimentally investigate the characteristics of the mode of operation of each and every possible combination.

The realization of the many limitations of the understanding of the characteristics of impinging, seemingly two-dimensional, semi-confined

turbulent jets led, in the first decade of fluidics, to the evolution of several flow models with varying degrees of approximations and complexities. There are, to be sure, essential differences, as well as similarities, among these models, and all must be carefully assessed before a design choice is made.

It has been customary to study the behavior of such interactions for analytical expediency, and at times with some realism, by regarding the deflection of the jet either as a consequence of pressure differentials alone or as a result of the balance of momenta of the jets involved. It now appears that the pressure in the interaction region is rarely ambient everywhere and consequently the deflection of a two-dimensional jet by a laterally impinging jet is determined not only by the momenta of the interacting jet system but also by the pressure forces resulting from the fluid reacting with the nearby solid walls. Although the deflection of the power jet due to the momenta of the interacting jets may be calculated to some degree of accuracy (e.g., assuming a simple inviscid jet model, by assuming a submerged-jet model and using experimentally obtained velocity profiles, etc.), the prediction of the influence of curtailed or enhanced entrainment and of the non-uniform pressure field on the jet deflection and for that matter on all other static and dynamic gain characteristics of the amplifier is nearly an impossible task. Thus, however convenient and familiar these ideas may be, it is important to recognize that they may not be correct for every geometry and flow combination. One can either alleviate the problem by properly venting the amplifier and placing the control-jet boundaries sufficiently far from the power jet, thus approximating a momentum-controlled operation, or as a last resort, by carrying out a series of experiments by carefully varying the geometry in the neighborhood of a given design so as to develop suitable sensitivity functions and/or gain prediction functions. Such experiments may also be used to develop proper autocorrelation functions

between various important variables to describe the nonlinear interactions between various parameters of the flow and geometry as proposed by Watton (14). Such a procedure would, however, avoid the real fluid dynamical problems of fluidics for the sake of practical expediency.

Dexter (15) employed the "submerged jet" model assuming that viscous mixing with the surrounding fluid has reached the stage where the velocity profile of the deflected jet is of Gaussian form. Moynihan & Reilly (16) employed the "self-preservation" model in which each jet is assumed to have retained its identity during interaction and is not subjected to any viscous effects as it proceeds downstream. According to this model, the jet-deflection angle is given by

$$\tan \beta = \frac{w_c \left[(1 + C_{c1}^2) P_{c1} - (1 + C_{c2}^2) P_{c2} \right] + \Sigma F_{wy}}{w_p \left[(1 + C_p^2) P_p \right] + \Sigma F_{wx}} \qquad (7)$$

which reduces to the experimental determination of the contraction coefficients of the power and control jets (C_p, C_{c1}, C_{c2}) and of the static pressure forces F_{wx} and F_{wy}. The analytical determination of these parameters does not, at least at present, appear to be possible. Douglas & Neve (17) extended the works in the references just cited by applying the two models to the appropriate regions of the resultant jet and modifying their results with a suitable "Coanda coefficient." Needless to point out, such a coefficent is strongly dependent on the particular amplifier geometry used and on the flow conditions.

Zalmanzon et al. (18) presented the results of an inviscid-flow analysis for the single-control-jet type beam-deflection amplifier, such as an 'AND' gate, and claimed good correlation between the theoretical results and a few experimental data points. Their analysis which

precluded the cases of velocity discontinuity between the two jets, was limited to the prediction of only one deflection angle or flow ratio for a given geometry. Obviously, the deflection angle can be calculated as a continuous function of the ratio of flows in the supply and control jets only if a velocity or pressure discontinuity is permitted at the interface of the jets as in real jet interactions. Sarpkaya et al. (19) presented a theoretical analysis, through the use of the free-streamline theory, for both the single and symmetric control-jet configurations and a series of experimental results obtained with a hot-wire anemometer for both the single-control-jet and symmetric beam-deflection amplifiers. Even though such an analysis is capable, as will be seen later, of accounting for the relative positions of the power and control streams and even though the predictions appear to agree with relatively idealized experimental observations, there are several drawbacks of the free-streamline analysis which limit its direct application to the prediction of the characteristics of the commonly used beam-deflection amplifiers of relatively complex geometry. The major drawback stems from the fact that the mathematics of the analysis becomes, as will be noted later, exceedingly complex for the type of the geometries encountered in practice. In spite of this and other shortcomings, however, the free-streamline theory indicates with precision the geometry of the relatively simple and noise-free amplifiers and a correspondance between the results of the theory and of experiments which is usually close and sometimes astonishingly so.

The foregoing being the state of the fluid dynamics of impingement and of the prediction of deflection of jets, it is easy to realize that the dynamic characteristics of the jet-deflection devices would be even more complex to predict with any degree of confidence. In general, they depend on the entire state of the amplifier such as the input, output and venting impedances, the size of the amplifier, and the Reynolds number.

I. 5. The noise in beam-deflection devices, which may generally be defined as any unwanted signal in the system not necessarily introduced through the controls of the first stage, remains as one of the most troublesome problems of the analog devices. Evidently, the noise is amplified, as if it were a signal, during staging and the operation of the system is thus confined to relatively low levels of amplification. As previously noted, its prevention (within the inner shear layers) requires comparable magnitude of power and control jet velocities, a proposition which is in glaring contrast to the concept of fluid amplification.

The noise in jet-deflection devices has been studied by a number of investigators (20, 21). In general, it is noted that it is advantageous to match the resonant frequencies of the edge-tone and the cavities; the major source of noise is the shear layers between the power and control jets and between the control jets and the entraining flow, as previously noted; the noise tends to increase monotonically with aspect ratio (for aspect ratios less than approximately two, the potential core region or the noise-free region of the jet increases thereby increasing the signal-to-noise ratio, but this improvement is at the expense of gain); decreasing the size of the amplifier decreases the relative noise; signal-to-noise ratio increases with the supply pressure; and that providing many parallel paths with a common output connection decreases the noise amplitude (since, as just noted, the length of the relatively noise-free potential core rapidly increases with decreasing aspect ratios). Evidently, the noise is an inevitable consequence of the very method of pressure and/or flow amplification through the interaction of two or more jets of different velocities. The interaction or the so-called mixing region is a region of strong velocity discontinuities and free-shear layers where vortex sheets with an array of double-branched vortex cores initially inhibit the uniform dissipation of energy. The energy concentration and velocity jumps

decrease as the cores stretch and grow until one arrives at a random turbulent flow where all three components of velocity fluctuations are important. Thus, ideally speaking, the noise could be considerably reduced if the velocity distribution of the power jet could be so structured that it would, at its edges, have velocities comparable in magnitude to those of the control jets. This would tend to minimize the formation or the intensity of the free-shear layers.

It appears, on the basis of the foregoing brief review of the current state of the art of the jet-interaction devices, that the unsolved and perhaps unsolvable problems of the basic beam-deflection amplifiers (e.g., increasing the pressure gain, overcoming the difficulties of interconnection, reducing the sensitivity to control levels, increasing the signal-to-noise ratio, and, most importantly, analytically predicting the static and dynamic characteristics of the amplifier) are indeed vast in extent and that the most fruitful avenues of investigation into the partial understanding of its characteristics would be a series of investigations ranging from purely analytical studies (e.g. the assumption of an inviscid fluid and the application of the free-streamline theory) to relatively more empirical studies such as the development of sound control volumes through the measurement and proper interpretation of the velocity and pressure distributions along the chosen boundaries. These together would enable one to use the momentum-balance technique with greater degree of confidence in predicting the behavior of flow in elements whose geometries are within the neighborhood of those experimentally studied. Finally, a purely empirical method would be the development of prediction equations for both the static and dynamic behaviors of the amplifier in a manner similar to that proposed by Watton (14) where a series of specially designed experiments are sequentially carried out on a variable geometry amplifier and then the coefficients of the design matrix are determined via the application of a regression technique. The ultimate

criterion for such a semi-analytical work is not how well the predicted details of the flow may exhibit irregularities that are most probably caused either by the imperfections in the amplifier and the experimental apparatus or by the errors in the coefficients of the prediction matrix, but rather and more appropriately, how well the characteristic features of the experimental data are reproduced. The emerging fact is that one can arrive at a viable technology only by properly blending certain amount of analysis, certain amount of experimentation, and a fair amount of empiricism. The fact that one deliberates about the accomplishments of the past and the shortcomings of the existing analyses and the adoption of hybrid methods is in itself an indication of the arrival of a period of consolidation and retrospect in fluidics.

I. 6. The specific aims of the present investigation:

The present investigation is concerned with the theoretical and experimental study of the interaction of semi-confined, subsonic, turbulent jets, the application of the results to fluidics being one of the primary objectives in mind. The theoretical results obtained both through the use of the free-streamline theory and the momentum analysis for both the single and symmmetric control-jet configurations are presented in the first part of the study. The second part covers the experimental results (detailed velocity and turbulence-structure measurements, jet deflection, etc.) obtained with a hot-wire anemometer for both the single-control-jet and symmetric beam-deflection type amplifiers. Finally, the results of the two parts of the study are compared and the advantages and shortcomings of the various analyses are presented.

2. ANALYSIS

2.1 General Remarks

The shortcomings of the various versions of the previous analyses, based mostly on momentum considerations, and the rapidly varying characteristics of the impinging jets of unequal velocities in the interaction region have already been described in detail together with the major underlying reasons. The evolution of the jets from an initially nearly inviscid-like behavior to a thoroughly mixed, gradually expanding, turbulent, single-jet like behavior under the action of viscous shear and pressure forces will never permit the use of a single analytical method uniformly applicable to all regions. The best that one can hope for is to develop two or more methods of solution, each applicable to a different region, and then combine them, primarily through the use of experimentally observed facts. In the following, we will first present the application of the free-streamline theory to several basic jet-interaction patterns and then consider a relatively more approximate but practically more convenient momentum analysis.

2.2 Free-Streamline Analysis

As in all applications of the free-streamline theory, the pressure and magnitude of velocity along the free-streamlines are assumed constant. It is further assumed that both the pressure and velocity are continuous along the separation lines between the power jet and the control jets.

Experiments show that each control jet retains a large measure of its integrity, and the power and control jets undergo an acceleration or

a "vena-contracta" effect during the initial phase of the interaction particularly for relatively strong control jets. The combined jet attains a Gaussian profile only after a distance of $x = Ka$ from the pivoting point where K is a coefficient which ranges from 2 to 6 depending on the flow ratio and the geometry of the system and "a" is the width of the power nozzle. The effective pivot point of the deflected, combined jet is, for all intents and purposes, at the intersection of the axes of power and control nozzles.

It is apparent from the foregoing that the flow in the region in which the momentum exchange and the turbulent mixing take place does not, strictly speaking, follow the assumptions made in the free-streamline theory. Nevertheless, at this stage of time in fluidics where there are no better analyses, it seems wisest simply to parametrize the phenomenon with such a fairly classical analysis and then explore its consequences before adding additional complexities. Subsequently, the results of the analysis may be properly modified with the additional insight gained through their comparison with the experiments. With this understanding, the analysis of the various types of pertinent jet interactions follow.

2.21 Analysis of the Contraction of an Undeflected Power Jet Under the Influence of Two Equal Control Jets.

A schematic drawing of the flow configuration, together with the resultant jet, is shown in Fig. 2a. The flow in the physical plane may be transformed to an Ω-plane through the use of the Planck's transformation with the usual assumptions of the free-streamline theory. Thus writing,

$$\Omega = - \operatorname{Ln} q/V_j + i\theta \tag{8}$$

and carrying out the necessary manipulations, one obtains Fig. 2b.

It is a well-known fact that any polygon, such as the one shown in Fig. 2b, may be transformed to the upper or the lower half of a real plane through the use of the Schwartz-Christoffel transformation given by

$$\Omega = M \int \prod_{k=1}^{n} (t - t_k)^{-\alpha_k/\pi} dt + N \tag{9}$$

where M and N are constants to be determined and t_k and α_k are given by

$$t_1 = -1 \ , \ \alpha_1 = \pi/2 \ ; \quad t_2 = +1 \ , \ \alpha_2 = \pi/2 \ ; \quad t_3 = \infty \ , \ \alpha_3 = \pi$$

Then one has

$$\Omega = M \int \frac{dt}{\sqrt{t^2 - 1}} + N \tag{10}$$

The evaluation of this integral and the use of the t_k values assigned to the points A and C in the t-plane yield

$$\Omega = \tfrac{1}{2} c h^{-1} t \qquad a = \tfrac{1}{2}\left[\left(\frac{V_j}{V_A}\right)^2 + \left(\frac{V_A}{V_j}\right)^2\right] \tag{11}$$

$$c = \tfrac{1}{2}\left[\left(\frac{V_j}{V_c}\right)^2 + \left(\frac{V_c}{V_j}\right)^2\right]$$

or

$$\left(\frac{V_j}{V_c}\right)^2 = c + \sqrt{c^2 - 1} \qquad \text{and} \qquad \left(\frac{V_j}{V_A}\right)^2 = a + \sqrt{a^2 - 1} \tag{12}$$

The velocity potential in the t-plane is given by

$$W(t) = 1/\pi \{V_j n \operatorname{Ln}(t+1) - V_A m \operatorname{Ln}(t+a) - V_c b \operatorname{Ln}(t-c)\} = \Phi + i\Psi \tag{13}$$

and the parameters θ and t along the free-streamline DE are related by

$$t = \cos 2\theta \quad \text{or} \quad \cos\theta = \sqrt{(1+t)/2} \tag{14}$$

The appropriate distances in the physical plane (Fig. 2a) and the contraction coefficient may be evaluated by noting that

$$n + \int_{1}^{-1} dx = m + s \tag{15}$$

where the integral in Eq. (15) may be written, through the use of Eqs. (13) and (14), as

$$\int_{+1}^{-1} dx = -\frac{1}{\pi V_j} \int_{1}^{-1} \sqrt{\frac{1+t}{2}} \left[\frac{V_j \cdot n}{t+1} - \frac{m V_A}{t+a} - \frac{b V_c}{t-c} \right] dt \tag{16}$$

Evaluating the integrals appearing in Eq. (16), combining with Eq. (15), and rearranging, one finally has

$$\frac{1}{C_c} = \frac{m+s}{n} = \frac{\pi+2}{\pi} - \frac{\frac{V_c}{V_j}\frac{b}{n}}{\pi\sqrt{2}} F \tag{17}$$

where C_c is defined by

$$C_c = n/(m+s) \tag{18}$$

and the function F is given by

$$F = \frac{1+c}{a-1}\left(2\sqrt{2} - 2\sqrt{a-1}\,\tan^{-1}\sqrt{\frac{2}{a-1}}\right) + \left(2\sqrt{2} - \sqrt{1+c}\,\ln\frac{\sqrt{1+c}+\sqrt{2}}{\sqrt{1+c}-\sqrt{2}}\right) \tag{19}$$

To complete the solution of the problem, one needs two more relationships: the equation of the conservation of mass and the condition of velocity and pressure continuity along the contact streamline between the control and power jets. The first relationship is given by

$$V_A m + V_C b = V_j n \tag{20}$$

and the second relationship simply reduces to

$$V_C b/V_A m = Q_C/Q_A = Q_r = (a - 1)/(c + 1) \tag{21}$$

Equations (17) through (21) uniquely establish the relationships between the power and control jet velocities, geometry of the physical plane, and the contraction coefficient. It should be noted in passing that for a given geometry (b/m and s/m), there is only one velocity ratio (V_C/V_A) which satisfies the aforementioned conditions.

The results, obtained through the use of a computer, are presented in graphical form in Figs. 3 through 5. Figure 3 shows the variation of b/m with s/m for constant values of Q_r (mass-flux ratio of the control and power jets). The asymptotic values of b/m, obtained from Eqs. (11), (12), and (21), are given by

$$\left(\frac{b}{m}\right)_{min} = \frac{Q_r}{\sqrt{(2Q_r+1)+\sqrt{(2Q_r+1)^2-1}}} \tag{22}$$

and are shown in Fig. 3 for the corresponding values of Q_r.

Figure 4 shows the variation of b/m with s/m for constant values of

the velocity ratio V_C/V_A and Fig. 5 shows the variation of the contraction coefficient C_c with b/m for constant values of Q_r.

A careful examination of Figs. 3, 4, and 5 point out several facts of major importance to fluidics:

(1) The achievement of a smooth impingement with no discontinuity in velocity across the streamline common to the power and control jets, where the relative flow rate is reasonably small to yield an acceptable flow amplification, requires the use of very small control-nozzle widths (i.e. very small b/m values), (see Fig. 3), and hence fairly large velocity ratios (see Fig. 4). In other words, the velocity and the supply pressure of the control jets must be of the same order of magnitude as those of the power jet if no mixing or shear-layer generated noise is desired. Evidently, therefore, noise in jet deflection amplifiers cannot be avoided if a reasonable pressure or energy recovery is to be achieved.

(2) There is only one particular velocity or flow ratio for a given set of specific values of the amplifier geometry. Any variation in input-flow ratio from that predicted on the basis of no velocity discontinuity will result in the development of free-shear layers (in real fluids) of varying intensity and in unwanted noise in the amplifier output.

(3) Finally, it is apparent from Fig. 5 that the contraction coefficient C_c decreases, i.e. the acceleration of the combined jet increases, as b/m and/or Q_r increases. This finding is in conformity with the experimental observations, as previously noted.

2.22 Analysis of the Deflection of Power Jet under the Influence of a Single Control Jet.

Figure 6 shows the jet interaction under consideration together with the corresponding successive transformation planes pertinent to the solution. The application of the free streamline theory and the evaluation of the resulting integrals yield

$$\Omega = -\operatorname{Ln}\frac{q}{V_j} + i\theta = \operatorname{Ln}\frac{\sqrt{t+1}+\sqrt{t-h}}{\sqrt{h+1}} \quad , \quad \beta = \tan^{-1}\sqrt{h} \quad , \quad \frac{d'}{a} = \alpha + \eta\frac{b}{a} \tag{23}$$

$$\frac{t}{a} = \frac{1}{\pi\sqrt{h+1}}\left[\frac{d'}{a}\operatorname{Ln}\frac{\sqrt{h+1}+1}{\sqrt{h+1}-1} - \frac{b}{a}\eta\pi\sqrt{f-1} + 2\frac{b}{a}\eta\sqrt{f-1}\tan^{-1}\sqrt{\frac{f-1}{h+1}}\right. \tag{24}$$

$$\left. - \alpha\sqrt{k+1}\operatorname{Ln}\frac{\sqrt{h+1}+\sqrt{k+1}}{\sqrt{k+1}-\sqrt{h+1}}\right] + \frac{b}{a} - \frac{d'}{a}\sqrt{\frac{h}{h+1}}$$

$$\frac{s}{a} = \frac{1}{\pi\sqrt{h+1}}\left[\frac{d'}{a}\sqrt{h}\operatorname{Ln}\frac{\sqrt{h+1}+\sqrt{h}}{\sqrt{h+1}-\sqrt{h}} + 2\alpha\sqrt{k-h}\tan^{-1}\sqrt{\frac{k-h}{h+1}} - \pi\alpha\sqrt{k-h}\right. \tag{25}$$

$$\left. - \frac{b}{a}\eta\sqrt{f+h}\operatorname{Ln}\frac{\sqrt{h+1}+\sqrt{f+h}}{\sqrt{f+h}-\sqrt{h+1}}\right] - \frac{d'}{a}\frac{1}{\sqrt{h+1}} + 1$$

$$\alpha = \frac{V_A}{V_j} = \frac{\sqrt{h+1}}{\sqrt{k+1}+\sqrt{k-h}} \quad , \quad \eta = \frac{V_E}{V_j} = \frac{\sqrt{h+1}}{\sqrt{f-1}+\sqrt{f+h}} \quad , \quad \frac{\eta}{\alpha} = \frac{V_E}{V_A} \tag{26}$$

As in the previous analysis, one needs two more relationships to complete the solution of the problem: (1) the equation of the conservation of mass and (2) the condition of velocity and pressure continuity along the contact streamline between the control and power jet. The first condition

is given by

$$a.V_A + b.V_E = d'.V_j \qquad (27)$$

and the second condition reduces to

$$a.V_A/b.V_E = f/k \qquad (28)$$

As before, the analysis shows that there is only one particular velocity or flow ratio for a given set of specific values of the amplifier geometry, (see Fig. 7). Any variation in input-flow ratio from that predicted on the basis of no velocity discontinuity will result in the development of free-shear layers (in real fluids) of varying degrees of intensity and in unwanted noise signal in the amplifier output.

2.23 Analysis of the Deflection of Power Jet under the Influence of Two Unequal Control Jets in a Symmetric Beam-Deflection Amplifier.

A similar but relatively more complex analysis was carried out for the symmetrical beam-deflection amplifier shown in Fig. 8. The transformation planes (also depicted in Fig. 8) yield

$$\Omega = \mathrm{Ln}\,\frac{\sqrt{1-k^2}+\sqrt{1-t^2}}{\mp\sqrt{t^2-k^2}}, \quad (+) \text{ for } t \leqslant -k \text{ and } t \geqslant 1, \quad (-) \text{ for } -k \leqslant t \leqslant 1 \qquad (29)$$

$$\eta = \frac{V_A}{V_J} = \frac{k}{1+\sqrt{1-k^2}} \qquad \alpha = \frac{V_C}{V_J} = \frac{\sqrt{c^2-k^2}}{\sqrt{1-k^2}+\sqrt{1-c^2}} \qquad \gamma = \frac{V_G}{V_J} = \frac{\sqrt{g^2-k^2}}{\sqrt{1-k^2}+\sqrt{1-g^2}} \qquad (30)$$

$$\sin\beta = \sqrt{\frac{f^2-1}{f^2-k^2}} \qquad (31)$$

The complex function for the flow in the t-plane is given by

$$w(t) = 1/\pi \{V_j d' \mathrm{Ln}(t+f) - V_A a \mathrm{Ln} t - V_C b \mathrm{Ln}(t+c) - V_G b \mathrm{Ln}(t-g) \qquad (32)$$

Then the various distances in the physical plane may be evaluated through the use of the following expressions:

$$z = \int \left(-\frac{1}{V_j}\frac{dw}{dt}\right) e^{\Omega}\, dt \quad \text{and} \quad e^{\Omega} = \pm\sqrt{\frac{t^2-k^2}{t^2-k^2}} + i\sqrt{\frac{t^2-1}{t^2-k^2}} \qquad (33)$$

The integration and separation of the real part of z yield

$$a + 2s = 2\frac{\sqrt{1-k^2}}{\pi}\left[\pi\frac{a}{k}\sin^{-1}k - \frac{\alpha b}{\sqrt{c^2-k^2}}\mathrm{Ln}\frac{\sqrt{1-c^2}}{\sqrt{1-k^2}+\sqrt{c^2-k^2}}\right.$$

(33)

$$\left. - \frac{\gamma b}{\sqrt{g^2-k^2}}\mathrm{Ln}\frac{\sqrt{1-g^2}}{\sqrt{1-k^2}+\sqrt{g^2-k^2}} - \frac{d}{\sqrt{f^2-k^2}}\mathrm{Ln}\frac{\sqrt{f^2-1}}{\sqrt{1-k^2}+\sqrt{f^2-k^2}}\right]$$

The integration of the imaginary part of z yields,

$$\frac{2b}{\pi(1+k)}\left\{\left[\left(\frac{1+ck}{k+c}\right)\alpha + \left(\frac{1-gk}{k-g}\right)\gamma - \left(\frac{1+fk}{k+f}\right)\frac{d'}{b}\right]K + \frac{\alpha(1-k)(c-1)}{k+c}\Pi_c\left(\frac{2(k+c)}{(k+1)(c+1)}\right)\right.$$

(34)

$$\left. \pm\frac{\gamma(1-k)(1+g)}{g-k}\Pi_c\left(\frac{2(k-g)}{(k+1)(1-g)}\right) - \frac{d'}{b}\frac{(1-k)(f-1)}{k+f}\Pi_c\left(\frac{2(k+f)}{(k+1)(f+1)}\right)\right\} = 0$$

in which Π_c is the third kind incomplete elliptic integral. It is evaluated through the use of Jacobian Zeta function and Heuman's Lambda function.

The two additional relationships needed to uniquely define the solution are given by

$$d' = (\alpha+\gamma)b + \eta . a \quad \text{(conservation of mass)} \tag{35}$$

and

$$V_A.a.f + V_C.b.(f - c) + V_G.b.(f + g) = 0 \quad \text{(condition of no velocity discontinuity)} \tag{36}$$

As before, the analysis shows that there is only one particular velocity combination and one jet deflection for a given set of the specific values of the amplifier geometry. Any variation in control-jet and power jet velocities from that predicted on the basis of no-velocity-discontinuity results in the development of free-shear layers together with their well-known consequences. The analysis also shows that the achievement of a smooth impingement and jet deflection with no discontinuity in velocity across the streamlines common to the power and control jets requires the use of very small control-nozzle widths (see Fig. 9) and hence fairly large velocity ratios. In other words, the velocity and the supply pressure of the control jets must be of the same order of magnitude as those of the power jet if shear-layer generated noise is to be avoided. Evidently, therefore, either the resultant pressure recoveries must be kept very low or the noise must be separately reckoned with.

It is apparent from the foregoing three analyses that (1) the free streamline theory is capable of predicting the relative positions of the power and control streams (unlike the momentum equation without the pressure terms); (2) the achievement of a relatively high flow and/or pressure recovery is in conflict with the achievement of a high signal-to-noise ratio; and that (3) the flows (combining or dividing) in which there is a velocity or pressure discontinuity cannot be analyzed by means of free-streamline theory. Since the primary purpose of fluidics has been and will continue to be the realization of high flow-and pressure recoveries, the fluidic elements currently in use employ relatively small differential control flows and pressures. The consequences of these practical considerations are rather obvious and have already been elucidated in section-I. Suffice it to state that each control jet retains a large measure of its integrity during interaction, the power jet acts simply as a flexible wall, and the combined jet attains a Gaussian profile 3 or 4 nozzle widths downstream of the pivoting point. Thus the flow in a high-flow or pressure recovery proportional amplifier particularly in the region in which the momentum-exchange and the turbulent mixing take place does not follow the assumptions made in the free-streamline theory. It is, therefore, necessary, to develop additional methods of analysis (however approximate) to deal with the relatively more complex problems of confined-jet interaction encountered in practice.

2.3 Momentum Analysis

The deflection of the combined jet is determined by the geometry of the system and the momenta of the power and control jets. It is, therefore, of special interest to derive an expression, however approximate, which will predict the deflection of the combined jet for a given amplifier geometry and control-and power-jet supply pressures.

The present analysis significantly differs from those previously made (15, 16, and 17) in two important aspects: (1) two control volumes are used, one along the boundaries where the velocity and pressure distributions across the jets are uniform and one along the exit boundaries of the control and power-nozzles where the velocity and pressure are non-uniform; and (2) the respective stagnation pressures at the exits of the corresponding nozzles are assumed to be uniform, i.e. no energy loss due to viscous-shear dissipation. Additional and rather usual assumptions are that (1) the entrainment on both sides of the combined jet are equal but opposite in direction, i.e. there is no momentum contribution by the entrained flow; and that (2) the flow is two dimensional, i.e. the aspect ratio of the amplifier does not affect the analysis. The foregoing is the minimum number of assumptions that could be made to arrive at the desired results without introducing approximate velocity or pressure-distribution functions through the use of experimentally obtained data.

The equations of momentum along the x-and y-directions may be written with reference to Fig. 10 (presented here for convenience and also included

among the figures compiled at the end of this report) as follows,

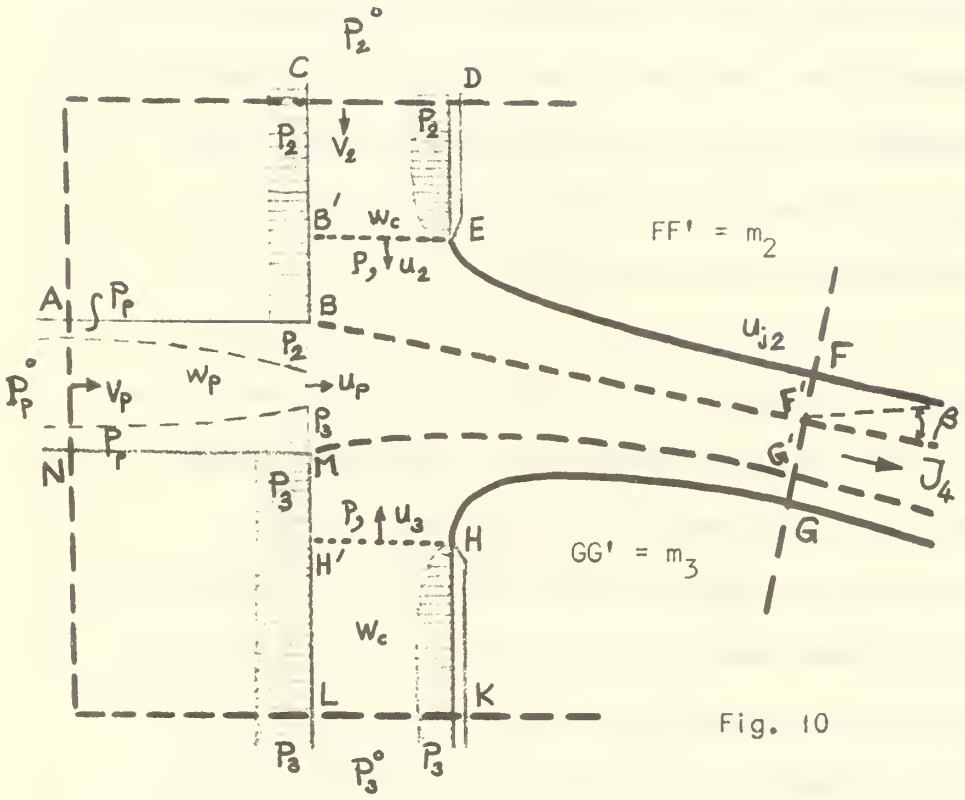

Fig. 10

$$J_P + P_P w_P + P_2 \overline{BC} + P_3 \overline{ML} - \int_D^E p\,dy - \int_K^H p\,dy = J_4 \cos\beta \tag{37}$$

$$J_2 - J_3 + P_2 w_c - P_3 w_c + \int_A^B p\,dx - \int_N^M p\,dx = J_4 \sin\beta \tag{38}$$

from which one has

$$\tan\beta = \frac{J_2 - J_3 + (P_2 - P_3) w_c + \int_A^B p\,dx - \int_N^M p\,dx}{J_P + P_P w_P + P_2 \overline{BC} + P_3 \overline{ML} - \int_D^E p\,dy - \int_K^H p\,dy} \tag{39}$$

It is apparent from the foregoing equations that the first control volume designated by ABCDEFGHKLMN has been used and the contribution of the wall pressures has been taken into consideration.

The relationship between the supply pressures and the velocity and static pressures along the lines AN, CD, and HH' are given by

$$P_2^\circ = P_2 + \frac{\rho V_2^2}{2}, \quad P_3^\circ = P_3 + \frac{\rho V_3^2}{2}, \text{ and } \quad P_p^\circ = P_p + \frac{\rho V_p^2}{2} \tag{40}$$

Now, let us consider the section HH' and assume that the stagnation pressure across HH' remains constant, i.e. no energy loss. Then one has

$$P + \frac{\rho}{2} u_3^2 = P_3^\circ \tag{41}$$

Obviously, similar expressions may be written for B'E and BM also. It should be noted that whereas V_3, p_3; V_2, p_2; and V_p and p_p are uniform across KL, CD, and AN, u_2, u_3, and u_p are functions of distance along HH', EB', and BM.

The velocity distribution along the curved jet issuing, say from HH' may be written as

$$u\,(r_3 + x) = C_3 \tag{42}$$

where r_3 is the radius of curvature of the streamlines and may be determined as follows. Writing,

$$u_3 = \frac{C_3}{x + r_3} \quad \text{and} \quad p + \frac{\rho}{2} \frac{C_3^2}{(x + r_3)^2} = P_3^\circ \tag{43}$$

and using the boundary condition that

$$\begin{aligned} x &= 0 \quad u = u_{3j} = \sqrt{2P_3^\circ/\rho} \text{ and} \\ x &= w_c \quad p = p_3 = p_3^\circ - \rho V_3^2/2 \quad (P = P_3,\ u_3 = V_3 \text{ at } H') \end{aligned} \tag{44}$$

one has

$$r_3 = \frac{\sqrt{\frac{\rho}{2P_3^\circ}}\, V_3 w_c}{1 - \sqrt{\frac{\rho}{2P_3^\circ}}\, V_3}, \qquad C_3 = r_3 \sqrt{\frac{2P_3^\circ}{\rho}} \tag{45}$$

and

$$u_3 = \frac{\dfrac{V_3 w_c}{1 - \sqrt{\frac{\rho}{2P_3^\circ}}\, V_3}}{x + \dfrac{\sqrt{\frac{\rho}{2P_3^\circ}}\, V_3}{1 - \sqrt{\frac{\rho}{2P_3^\circ}}\, V_3}} \tag{46}$$

It is important to note that the pressure distribution along the boundaries ML and BC are assumed to be uniform and equal to p_3 and p_2 respectively, in accordance with the experimental observations (16). This assumption is quite sound and does not introduce any appreciable error in the analysis, as will be seen later in connection with the discussion of the pressure distributions obtained in the present study.

Combining Eqs. (43) and (46), one obtains the pressure distribution along the line HH' as

$$p = p_3^0 - \frac{\rho}{2} \left\{ \frac{\dfrac{V_3 w_c}{1 - \sqrt{\frac{\rho}{2P_3^\circ}}\, V_3}}{x + \dfrac{\sqrt{\rho/2P_3^\circ}\, V_3 w_c}{1 - \sqrt{\rho/2P_3^\circ}\, V_3}} \right\}^2 \tag{47}$$

The momentum flux J_3 across HH' is given by

$$J_3 = \int_0^{w_c} \rho u_3^2 \, dx \tag{48}$$

which reduces to

$$J_3 = 2 P_3^\circ r_3^2 \left[\frac{1}{r_3} - \frac{1}{w_c + r_3} \right] \tag{49}$$

The pressure-integrated force across HH' is given by

$$\int_H^{H'} p \, dx = \int_H^{H'} \left[P_3^\circ - \frac{\rho V_3^2}{2} \right] dx = P_3^\circ w_c - \frac{1}{2} J_3 \tag{50}$$

Thus the total momentum-flux through HH' is given by

$$\vec{M}_3 = P_3^\circ w_c + \frac{1}{2} J_3$$

Likewise, one can write for the total momentum-flux through EB' as

$$\vec{M}_2 = P_2^\circ w_c + \frac{1}{2} J_2$$

where J_2 is given by

$$J_2 = 2 P_2^\circ r_2^2 \left[\frac{1}{r_2} - \frac{1}{w_c + r_2} \right] \tag{51}$$

with

$$r_2 = \frac{V_2 w_c \sqrt{\frac{\rho}{2 P_2^\circ}}}{1 - \sqrt{\rho / 2 P_2^\circ} \; V_2} \tag{52}$$

The momentum flux through BM may be evaluated as follows. Writing,

$$u\,(r_p + y) = C_p \qquad \text{and} \qquad p + \rho \frac{u_p^2}{2} = p_p^\circ \tag{53}$$

and using the boundary conditions that

$$p = p_2 \text{ at } y = w_p/2 \qquad \text{and} \qquad p = p_3 \text{ at } y = -w_p/2$$

and simplifying, one finally has

$$C_p = \frac{w_p}{1-K}\sqrt{\frac{2}{\rho}(p_p^\circ - p_2)} = \frac{K w_p}{1-K}\sqrt{\frac{2}{\rho}(p_p^\circ - p_3)} \tag{54}$$

$$r_p = \frac{w_p}{2}\frac{1+K}{1-K}, \qquad v_p = \frac{1}{1-K}\sqrt{\frac{2}{\rho}(p_p^\circ - p_2)}\,\operatorname{Ln}\sqrt{\frac{p_p^\circ - p_3}{p_p^\circ - p_2}} \tag{55}$$

where

$$K = \sqrt{\frac{p_p^\circ - p_2}{p_p^\circ - p_3}} \tag{56}$$

Then the momentum flux across MB is given by

$$\vec{M}_p = \rho \int_{-w_p/2}^{w_p/2} u^2\,dy + \int_{-w_p/2}^{w_p/2} p\,dy \qquad \text{with} \quad p = p_p^\circ - \rho\frac{u^2}{2} \tag{57}$$

Carrying out the indicated integrations and simplifying, one finally has

$$\vec{M}_p = p_p^\circ w_p + \sqrt{(p_p^\circ - p_3)(p_p^\circ - p_2)}\; w_p \tag{58}$$

The equations of momentum given by Eqs. (37) and (38) can then be recast through the use of the second control volume designated by HH'MBB'EH to yield

$$\vec{M}_p + (P_2 + P_3)\, s = J_4 \cos\beta \tag{59}$$

and

$$\vec{M}_2 - \vec{M}_3 = J_4 \sin\beta \tag{60}$$

Equation (39) then reduces to

$$\tan\beta = \frac{\vec{M}_2 - \vec{M}_3}{\vec{M}_p + s(P_2 + P_3)} \tag{61}$$

or

$$\tan\beta = \frac{(P_2^* - P_3^*) + V_2\sqrt{sP_2^*/2} - V_3\sqrt{sP_3^*/2}}{P_p^* + \sqrt{(P_p^* - P_3)(P_p^* - P_2)} + \frac{s}{W_p}(P_2 + P_3)} \tag{62}$$

Now to complete the analysis and to render β a function of the supply pressures alone, we must establish the necessary relationships between V_2 and p_2^0, and V_3 and p_3^0. For this purpose, consider the flow within the boundary designated by DEFF'BCD or by LMG'GHKL. For all intents and purposes, the flow within these boundaries may be regarded as a consequence of the sudden deflection of a jet issuing from a nozzle with a setback s (s = BB'= MH') by a plane wall BF' or MG'. Such a flow may easily be analyzed by means of free-streamline theory to predict FF' or GG' as a function of B'E, BB', and the angle of deflection of the rigid wall BF' or MG'. The results of such an exact analysis are presented in

Fig. 11. It is immediately apparent that FF'/B'E, (FF' = m_2 , B'E = w_c) varies almost linearly with BB'/B'E, (BB' = s and B'E = w_c), and that the contraction coefficient of the jet designated by m_2/w_c or by m_3/w_c increases with increasing angles of deflection (positive values of β) and vice-versa. The results of this analysis enable us to determine V_2 in terms of p_2^0 and V_3 in terms of p_3^0 as follows. Writing,

$$\frac{\rho}{2} U_{2j}^2 = P_2 + \frac{\rho}{2} V_2^2 = P_2^\circ \tag{63}$$

and from the mass-flux considerations

$$V_2 \cdot w_c = u_{2j} \cdot m_2 \tag{64}$$

Combining Eqs. (63) and (64) and simplifying, one finally has

$$P_2 = P_2^\circ \left(1 - \frac{m_2^2}{w_c^2}\right), \quad P_3 = P_3^\circ \left(1 - \frac{m_3^2}{w_c^2}\right), \quad V_2 = \sqrt{\frac{2 P_2^\circ}{\rho}} \frac{m_2}{w_c} \tag{65}$$

It is apparent from the foregoing analysis that Eqs. (62), and (65) yield the deflection angle as a function of the geometry of the amplifier and the total-control and supply pressures. The deflection angles calculated from the equations cited are presented in the section dealing with the discussion of the results. Suffice it to say that, in spite of the simplifications introduced into the analysis, the agreement between the results obtained experimentally and those predicted theoretically is astonishingly good. Better agreement may be achieved by taking into consideration the energy loss due to shear and the boundary-layer effects within the nozzles. Such an improvement has not been attempted here for it would have introduced additional unknown parameters into the analysis and thereby obscure the fundamental features of the method presented.

3. EXPERIMENTAL EQUIPMENT AND PROCEDURE

The experimental apparatus consisted of a series of jet assemblies, hot-wire anemometer system, a velocity calibrator, and a pressure transducer system.

3.1 Jet Assembly

The jet assembly consisted of a power jet and either one or two control jets depending on the particular type of amplifier studied. Two power-nozzle widths (1/8 in. and 1/4 in), two control-jet widths (1/4 in. and 5/8 in.), three aspect ratios (2, 4, and 8), and various set-backs were used. A typical amplifier geometry together with the concave-convex type convergent nozzles is shown in Fig. 12. A one inch long honey-comb section was used at the uncontracted part of each nozzle for the purpose of straightening the flow. The air supply system consisted of a micro-filter (to remove oil and dust), primary and secondary pressure regulators, and various precision-calibrated flow meters.

The pressure taps were placed at the contracted section of each nozzle. The distances between taps were kept constant at 1/4 in. A special type of arrangement was made to connect each tap into the pressure transducer while the others were kept closed. The holes for these taps were placed at the centerline of the top and bottom plexiglass plates.

The jet deflection angle was determined through the use of several different procedures. The first three consisted of the use of lamp-black and oil mixtures, the use of powdered, colored, paint in the power and

control lines, and the use of a thin string glued to the common corner of the intersecting jets. All of these methods yielded the deflection angle to an accuracy of ±2 degrees. The powdered, colored paint (a different color for each jet) provided on a large piece of freshly painted (white oil paint) paper, glued on the inner face of one of the plexiglass side walls, an excellent definition of the evolution of the mixing region by forming regions of primary and complementary colors. The fourth method which yielded the deflection angle to a finer degree of accuracy was, of course, the use of the measured velocity profiles.

3.2 Hot-Wire Anemometer System

A model 1050, constant temperature hot-wire anemometer system, manufactured by the Thermo-Systems Inc., was used to measure the mean velocity and turbulence intensities. A double-cross wire with an angle of 45 degrees between the wires was used. The readings were taken by means of D-C voltmeters and RMS voltmeters which were accurate to 0.001 volts.

A specially designed probe holder which was fitted into the slots in the jet assembly, enabled the probe to move along the lines parallel to the power-nozzle axis in any plane. Two different type of micrometer mechanisms on the holder provided transverse and vertical movements of the hot-wire across the jet with an accuracy of 0.001 inch. The calibration curves were obtained by use of Thermo-Systems Calibrator, Model-1125. The stagnation pressures in the calibration process were measured with an inclined liquid manometer.

4. PRESENTATION AND DISCUSSION OF RESULTS

4.1 Two Normally Impinging Plane Turbulent Jets

4.11 Deflection Angles

The measured jet deflection angles for two perpendicularly impinging plane turbulent jets are shown in Fig. 13 for a representative amplifier geometry together with those obtained from the free-streamline theory and a simple momentum equation (pressures assumed to be uniform throughout the interaction region). Firstly, it is apparent that the single point predicted by the free-streamline theory agrees with that obtained experimentally. Secondly, the deflection angles based on the simple momentum equation (often used in the literature) do not agree well at all. This is to be expected since the equation ignores the non-uniform pressure distribution and does not take into account the control-channel setback. Additional data are presented in theses by Gungor (22) and Weeks (23). Suffice it to say that the deflection angle is uniquely determined by the geometry of the system and the ratio of the two velocities.

4.12 Velocity and Turbulence-Intensity Distributions

The evolution of the velocity distribution in the mixing region is shown in Figs. 14 through 19. It is apparent from these figures that, close to the channel exit, the two velocity maximums are far apart with a large velocity minimum or "trough" between them. This preservation, for a short distance, of the identity of the main and control jets has been attributed by Douglas and Neeve(17) to a "brick-wall effect".

Further down the jet axis, the peaks move closer together as the momentum transfer across the turbulent-shear layer decreases. At present, there does not seem to be any means to theoretically predict the evolution of the velocity distribution. A similarity variable of limited generality may be devised along the lines suggested by Pai(24).

Representative turbulence-intensity profiles are shown in Figs. 20 through 22. In the mixing region, the turbulence intensities are higher on the control-jet side than on the main-jet side. This is caused by the relatively low local mean velocities. The intensity of the shear-layer generated turbulence decreases with increasing distance from the channels, as would be expected. Additional data presented in References (22, 23, and 25) have also shown that the length of the mixing region increases with increasing control flow; a maximum mixing length of 6w occurs for equal control and power jet velocities; and that the jets maintain their identity almost near to the end of the mixing region. Then, and almost suddenly, the two velocity peaks reduce to a single and symmetric peak. Thus the transformation of two jets impinging with widely different velocities, into a single jet is more of a sudden rather than gradual process. For jets of nearly identical velocities, however, this transformation appears to be gradually completed within a distance of 4w to 6w.

Experiments have also shown that (22, 23, 25) the normalized maximum velocity in the jet increases at first, indicating a vena-contracta effect and convective acceleration, and then gradually, and almost linearly, decreases with distance along the jet. It is interesting to note that

the maximum velocity in the combined jet remains considerably higher than that of the power nozzle in a region approximately twice the length of the mixing region. The vena-contracta takes place at about $x = 2.5w$ and the maximum velocity there reaches a value as much as 25% higher than that of the power jet. It is, thus, apparent that while the location of the vena-contracta is nearly independent of the velocity ratio, the mixing of the two streams on impact is governed by the ratio of the control and power-jet velocities.

4.2 Dual Control-Jet Beam-Deflection Amplifier

4.21 Deflection Angles

The measured jet-deflection angles are shown in Figs. 23 through 28 in terms of the average and differential control-port velocities normalized with respect to the power-jet velocity for three different Reynolds numbers. Needless to state, these two parameters cannot account for the supply pressures in the control and power nozzles but they do account for the corresponding supply flows. In order to account for both the supply pressure and flows in a proportional amplifier, one has to consider an approximate momentum analysis along the lines previously described.

It is apparent from Figs. 23-28 that the deflection angle is, in general, a linear function of the normalized differential control-jet velocities. This linearity is distorted at very small and large values of the normalized differential velocity. The non-linearity at small jet-deflection angles increases with increasing normalized average control-port velocity. At larger angles of deflection, it increases with

decreasing average control-port velocity. For all the Reynolds numbers considered, a proportional amplifier becomes less sensitive to the normalized differential-velocity signals (i.e. smaller increase in the deflection angle with a higher change in the differential velocity) for the higher values of the normalized average control-port velocity.

Figures 29 through 31 show the deflection angles plotted for three different Reynolds numbers in terms of the parameters cited above. It is apparent that the effect of the Reynolds number on the deflection angle is almost negligible when normalized average control-port velocity is kept constant.

4.22 Velocity, noise, and turbulence-intensity distributions

These parameters were measured both at the mid-plane of the amplifier and in the planes 1/16 inch away from the top and bottom cover plates. Since the results have shown (Ref. 26) that there is very little or no difference between the two sets of measurements, only the representative data obtained at the mid-plane for Re = 31550 and the deflection angle δ (measured from the undeflected position of the jet) are presented herein.

Figures 32 through 38 show the evolution of the velocity profile and the noise distribution at various sections along the jet. As previously noted, in connection with the impingement of two jets, initially both the control and power jets maintain their identity and only at a distance of approximately 4w to 6w merge into a Gaussian profile. The noise, defined as

$$\frac{\sqrt{P_t'^2}}{\rho U_{max}^2/2} = \frac{(\bar{P}_t - P_s - \rho\bar{U}^2/2)}{\rho U_{max}^2/2} = \frac{\{\overline{u'^2} + \overline{v'^2} + \overline{w'^2}\}}{U_{max}^2}$$

remains fairly constant in the jet-establishment region (at distances less than 4w), increases almost linearly with distance in the fully-developed region, and reaches a value of approximately 5% at a distance of 8w. Similar results have been obtained for different angles of deflection, Reynolds numbers, and distances from the side walls. A comparison of the noise levels in the deflected jet with those found in the undeflected jet has shown that they are, with minor differences, quite comparable and that once the deflected jet is fully established, its noise level cannot be significantly altered by varying some of the upstream parameters, while maintaining the deflection angle constant.

Figures 39 through 45 show the turbulence intensities (normalized with respect to the local mean velocity) at the mid-plane at various distances from the pivot point for a Reynolds number of 31550 (based on throat width and mean throat-velocity of the power jet) and for a jet deflection angle of 6 degrees to the right of the power nozzle, (V_p = 242 ft/sec, V_L = 26.8 ft/sec, and V_R = 13.4 ft/sec.).

It is immediately apparent that all three components of turbulence are of the same order of magnitude and all must be taken into consideration in the calculation of noise. Secondly, the use of a single component of turbulence may appreciably underestimate the noise level captured by the receivers. Thirdly, the turbulence level at sections near the pivoting point are higher at the side of the control port with lower velocity. This, obviously, is due to the presence of relatively stronger

shear layers between the high-velocity power jet and the very low velocity control jet at the right side of the nozzle, i.e., due to larger velocity discontinuity between the two jets. At sections away from the pivoting point, the combined jet acquires a Gaussian distribution, the jets lose their identity, and the turbulence intensities on both sides of the jet become nearly identical. Finally, it is apparent that there is, in each profile, a relatively quiet region near the axis of the jet as one would normally expect. On both sides of this region, turbulence intensities rapidly increase. The significance of this observation lies in the fact that the use of a center dump and two adjacent load ports generally amount to dumping the noise-free region of the jet and capturing the parts which contain the largest noise.

Measurements of turbulence intensities at lower and higher Reynolds numbers and near the top and bottom plates have yielded essentially the same type and order of magnitude turbulence intensities and will not be discussed further.

4.23 Static Pressure Distributions

The static wall pressures for three representative Reynolds numbers are shown in Figs. 46 through 48. The general characteristics of these figures are such that (1) the pressures are higher at higher flow rates; (2) for lower Reynolds numbers, the pressures at the lower control-flow side become less than the ambient pressure; and that (3) the pressure on the innner wall of each control port remain fairly uniform. This latter experimental fact has been successfully used in the application of the momentum method to the prediction of the deflection angles.

4.24 Deflection Angles in Terms of the Control-and Power-Jet Supply Pressures and Their Comparison with Those Obtained via the Momentum Method.

The measured as well as analytically predicted (via the Eqs. 62 and 65 and Fig. 11) deflection angles are shown in Fig. 49 in terms of the parameters $\tan \gamma$. $p_p^0 / \Delta p_c^0$ and $(p_{LC}^0 + p_{RC}^0)/p_p^0$ for the amplifier shown in the insert of Fig. 23, ($w_c/w_p = 2.5$ and $s/w_c = 0.40$). Three facts are immediately apparent: (1) the tangent of the deflection angle normalized with $\Delta p_c^0/p_p^0$ varies only slightly with the normalized, average, total control-port pressure, the slight decrease in $\tan \gamma$ being due to the previously discussed pinching of the power jet with increasing control-port pressures; (2) Tan γ varies almost linearly with $\Delta p_c^0/p_p^0$ for a given amplifier geometry; and that (3) the momentum analysis presented in this report is capable of accurately predicting the deflection angles in terms of the geometry of the amplifier and the total pressures of the control and power jets. This latter conclusion has been further substantiated by applying the analysis to an amplifier with $s/w_c = 1$ and $w_c/w_p = 1$, and comparing the results with those obtained experimentally. Nevertheless, it suffices to note that it is not yet possible, if it is at all possible, to analytically optimize the characteristics of a proportional amplifier for the calculation of the deflection angle via Eqs. (62) and (65) involves a successive iteration in calculating the appropriate contraction coefficients for the control jets through the use of the free-streamline theory (Fig. 11). The analysis is, however, capable of predicting, to a first order of approximation, the deflection

angles of a proportional amplifier of given geometry and thereby allowing the designer to make the necessary changes at the design stage. The degree of the complexity of the general problem, known to all fluidicists, is a sufficient measure of the degree of usefulness of the method developed.

5. CONCLUSIONS

The extensive theoretical and experimental study of the deflection angles; turbulence, noise, and pressure distributions in the interaction and flow development region of two and three interacting jets of unequal velocities have shown that:

(1) Amplifier geometries which will yield very little noise for a unique combination of jet velocities also yield very small flow and/or pressure recoveries;

(2) The free-streamline theory is capable of predicting the geometrical characteristics of relatively noise-free jet interactions;

(3) There is, at present, no way of purely-analytically predicting the performance characteristics of an amplifier in which there are strong shear layers between the two adjacent jets;

(4) A momentum analysis based on a properly selected control volume together with a theoretical analysis of the contraction of the control jets, as presented herein, is capable of predicting, to a first order of approximation, the deflection angle in terms of the geometry of the amplifier and the supply pressures of the control-and power jets.

(5) The increase of the strengths of control jets (higher, normalized

average, control flow) results in the pinching of the power jet, in non-linearity of the jet deflection, and in lower noise and sensitivity;

(6) The velocity profile may be assumed to have reached a Gaussian profile at a distance of 6 nozzle widths from the pivoting point. This information, based on experimental measurements, together with a knowledge of the deflection angles, based on theoretical considerations, enables one to predict, to a first order of approximation, the transfer characteristics of a given proportional amplifier in terms of the size and location of the receiver ports;

(7) All components of turbulence are of the same order of magnitude and must be taken into consideration in the determination of the noise level;

(8) The noise level remains relatively low and constant in the jet-establishment region and increases almost linearly in the fully-developed region;

(9) The minimum noise level is in the order of 5% due to the contributions of the jet interaction and flow entrainment and could be considerably higher at normal operating conditions due to the several other factors such as the aspect ratio, receiver shape, cavity oscillations, etc.;

(10) The deflection of the jet does not materially affect the noise level at a given axial distance larger than 4 nozzle widths;

(11) In the design and operation of a proportional amplifier, one must avoid the use of a center dump, must capture the noise-free region of the combined jet, place the receivers as close as possible to the pivoting point without rendering the amplifier unstable, and use as low

control flows as practically possible to achieve a given jet deflection.

(12) It appears, on the basis of the extensive theoretical and experimental work reported herein, that the unresolved and perhaps unresovable problems of the basic beam deflection amplifier are indeed vast in extent and that the most fruitful avenues of additional research into the understanding of its characteristics may be (a) the further development of the control volumes devised herein through additional measurements of the velocity and pressure distributions along the chosen boundaries, and (b) the development of prediction equations for both the static and dynamic behaviors of the amplifier in a manner similar to that proposed by Watton(14) where a series of specially designed experiments are sequentially carried out on a variable geometry amplifier and then the coefficients of the design matrix are determined via the application of a regression technique. The ultimate criterion for such a semi-analytical work is not how well the experimental data are reproduced, for the observed as well as the predicted details of the flow may exhibit irregularities that are perhaps caused either by the imperfections in the amplifier and the experimental apparatus or by the errors in the coefficients of the prediction matrix, but rather and more appropriately how well the characteristic features of the experimental data are reproduced. Clearly, the analyses presented in this report are sufficient to design a proportional amplifier to a first order of approximation to which the regression analysis may be applied to predict the additional static and dynamic characteristics of elements whose geometries are within the neighborhood of the original design. For a more comprehensive discussion of the experimental, analytical, and phenomenological problems of proportional as well as wall-attachment amplifiers, the reader is referred to Ref. 27.

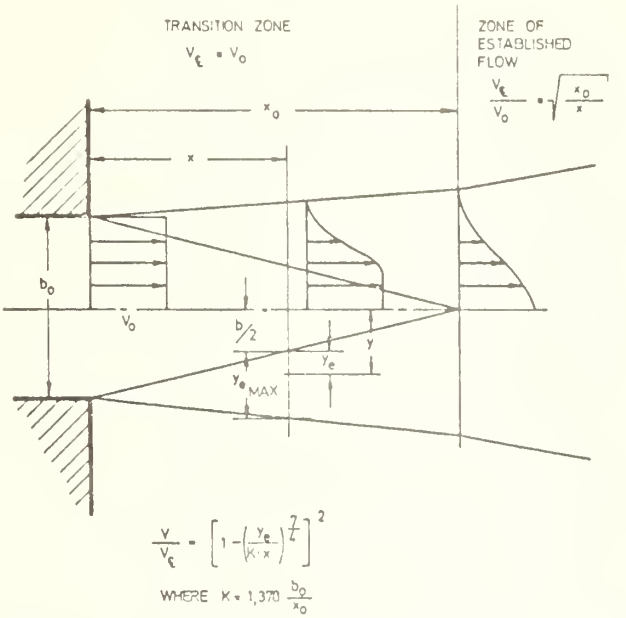

Fig. 1 The power jet velocity profile by A.K. Simson (ref 1).

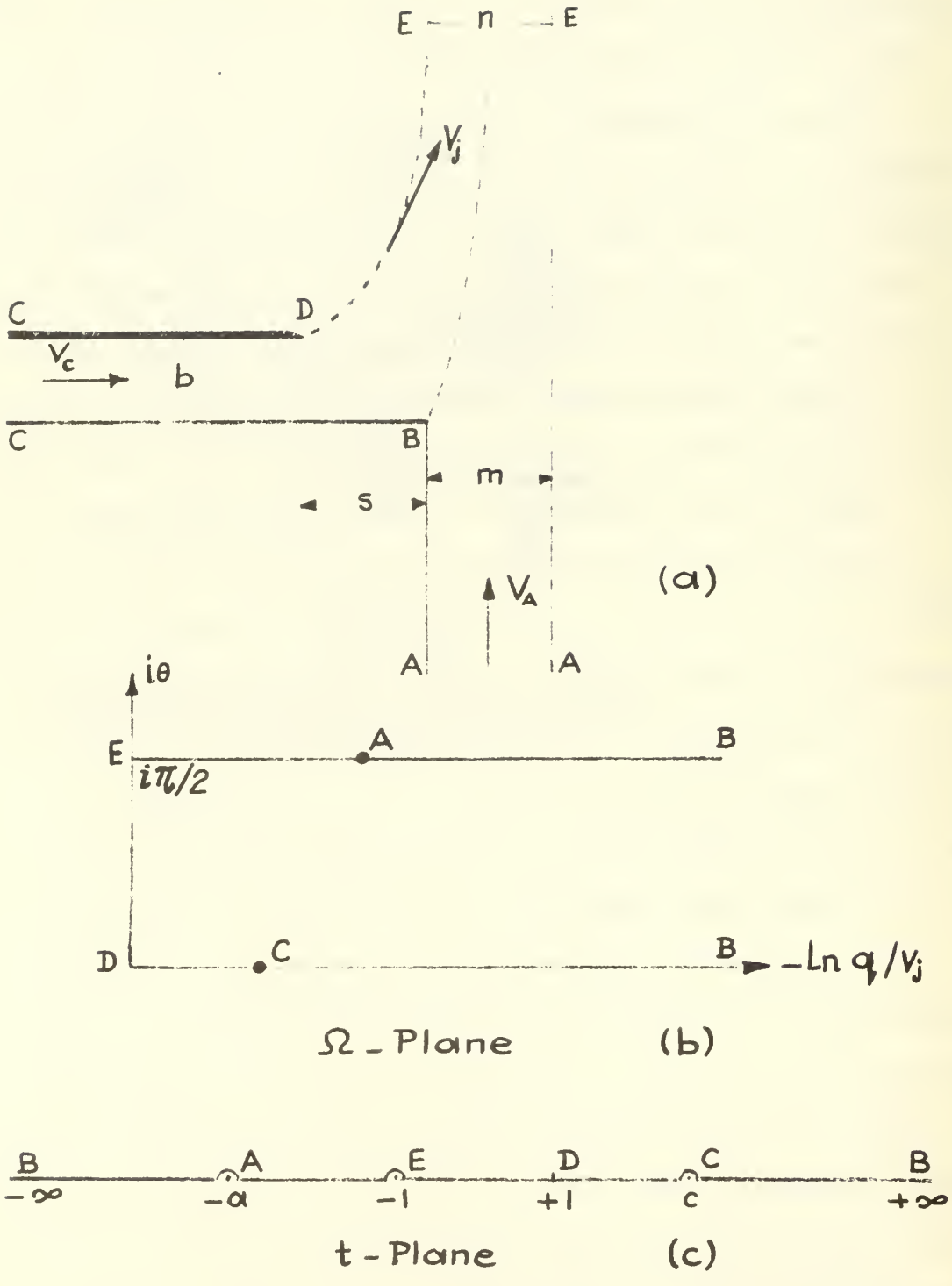

FIG. 2 Transformation planes

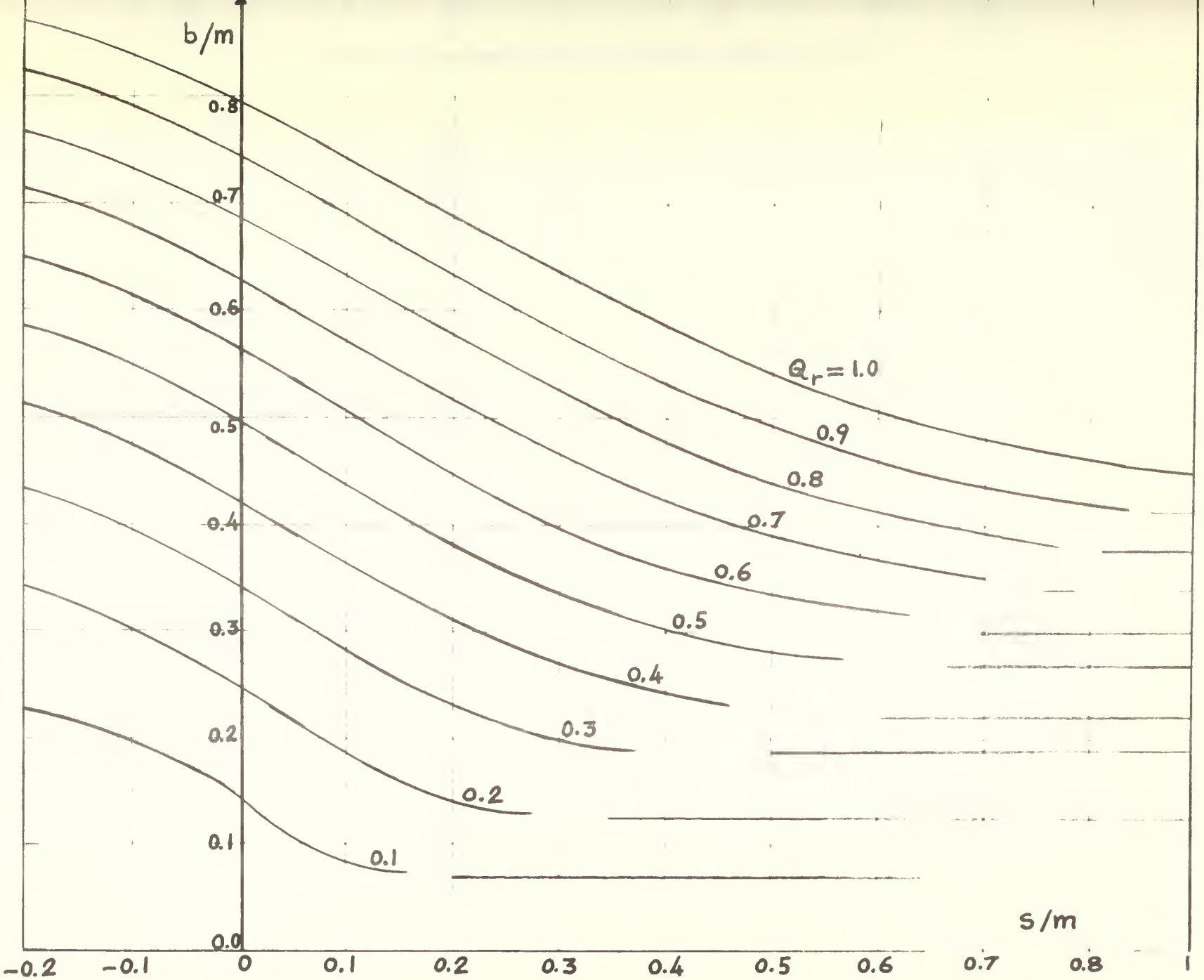

FIG. 3 b/m versus s/m for constant values of Q_r

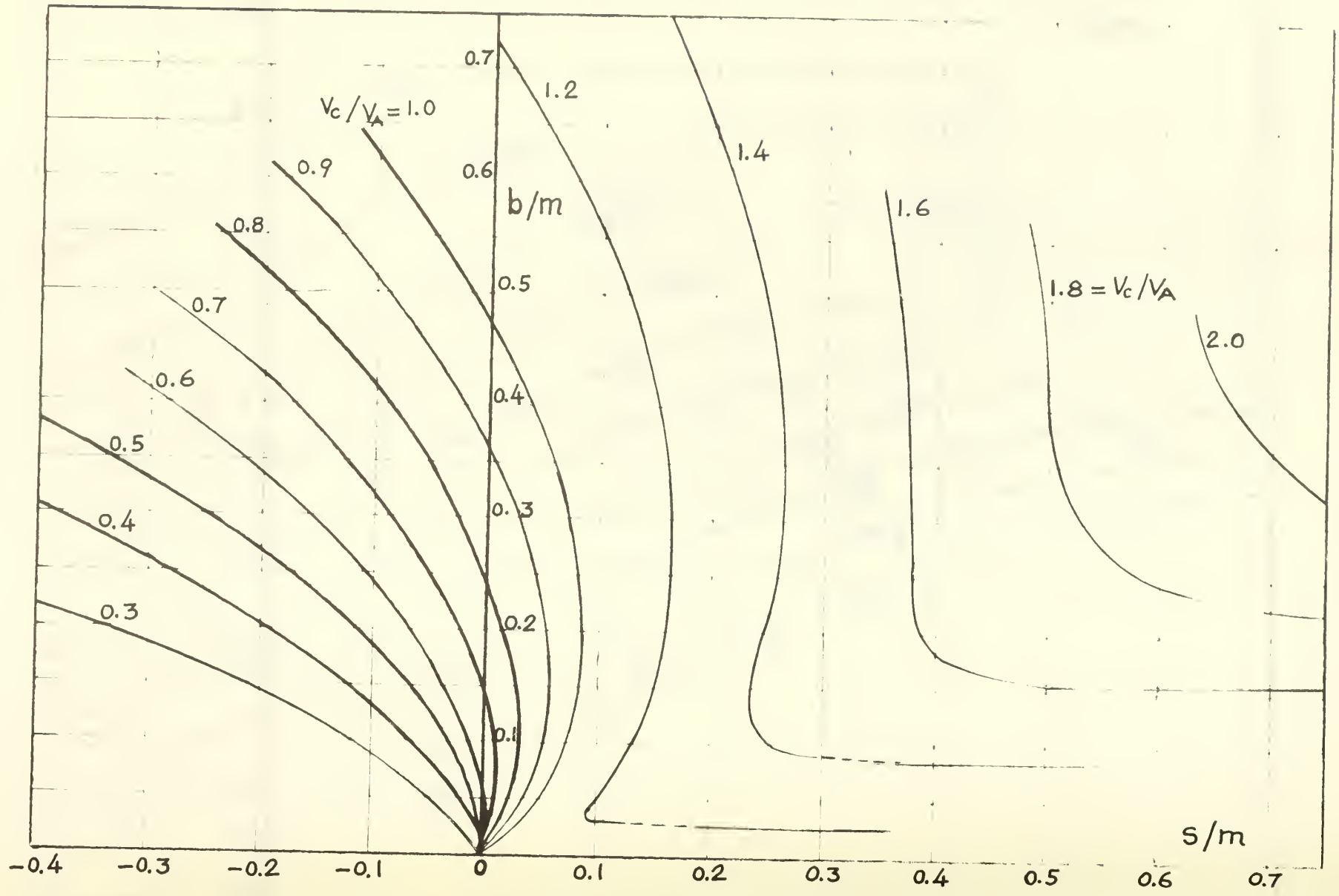

FIG. 4 b/m versus s/m for constant values of V_C/V_A

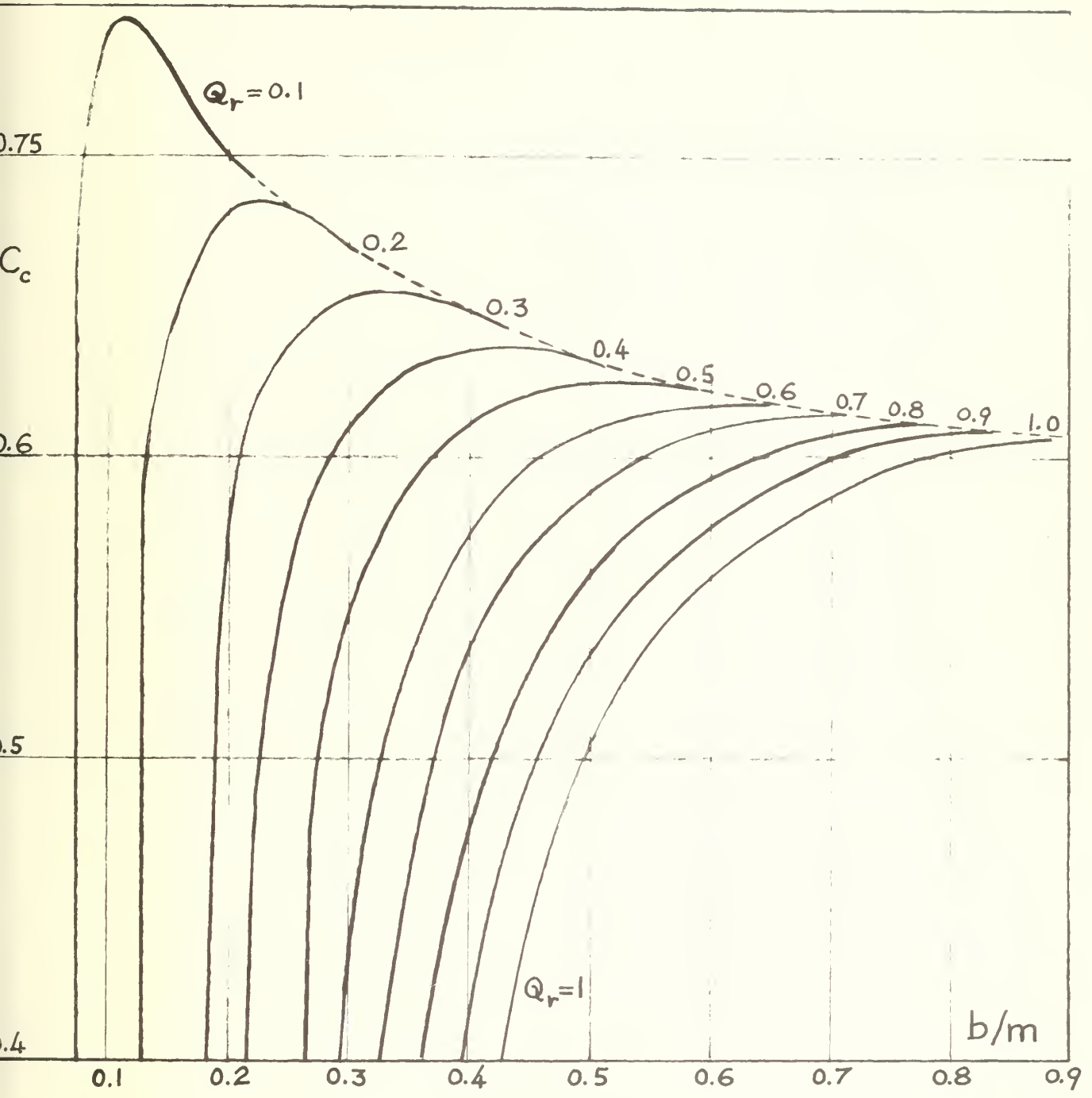

FIG. 5 C_c versus b/m for constant values of Q_r

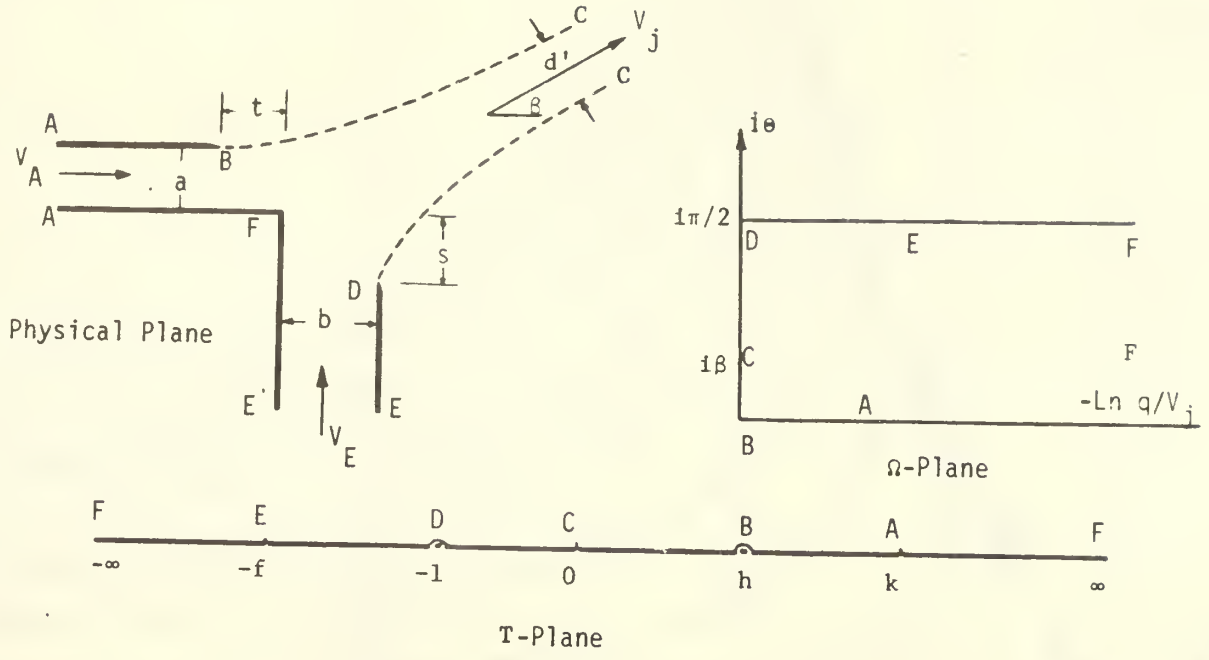

FIG. 6 Physical and transformation planes

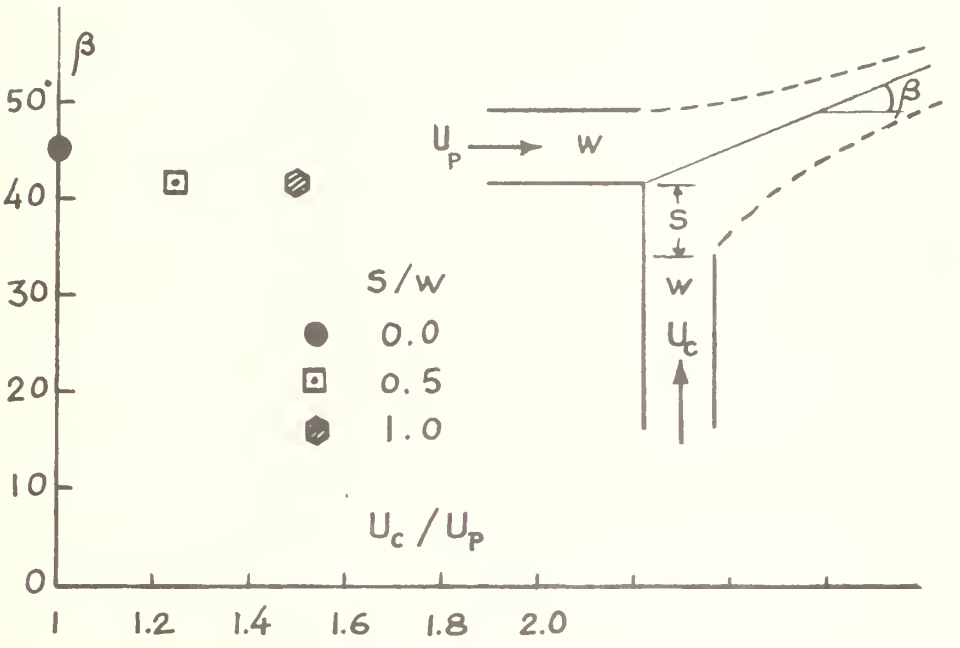

FIG. 7 Deflection angle versus U_c/U_p

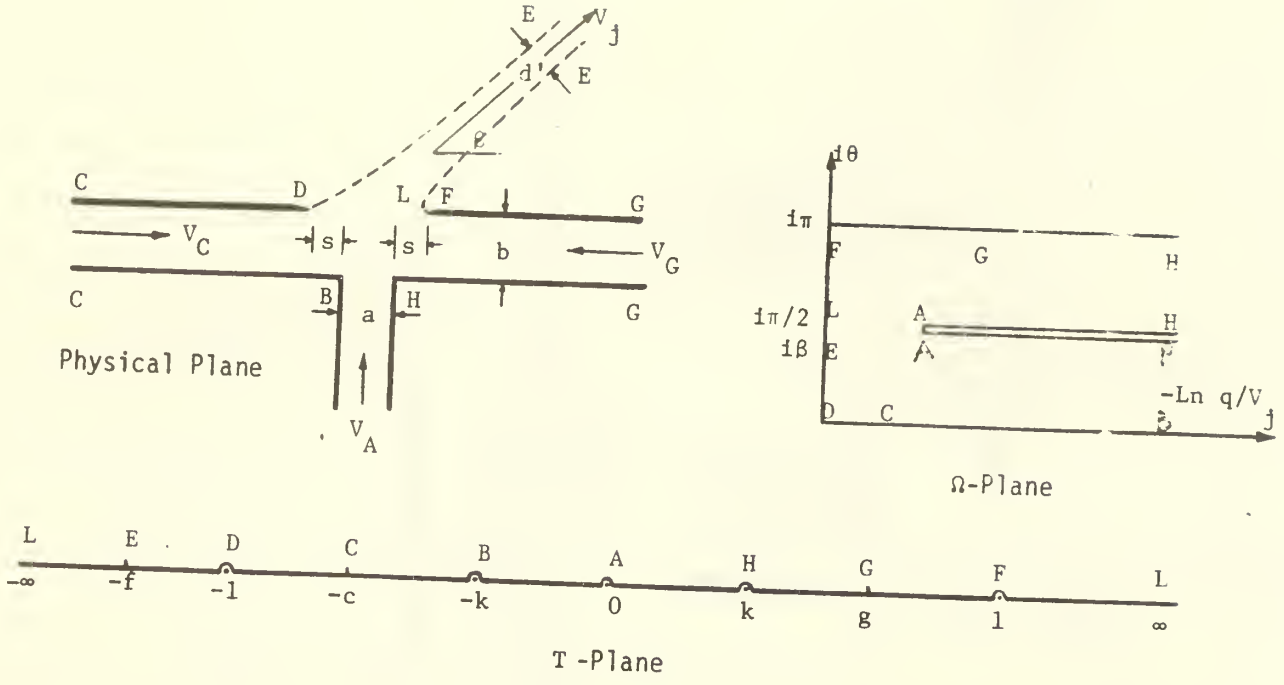

FIG. 8 Physical and transformation planes

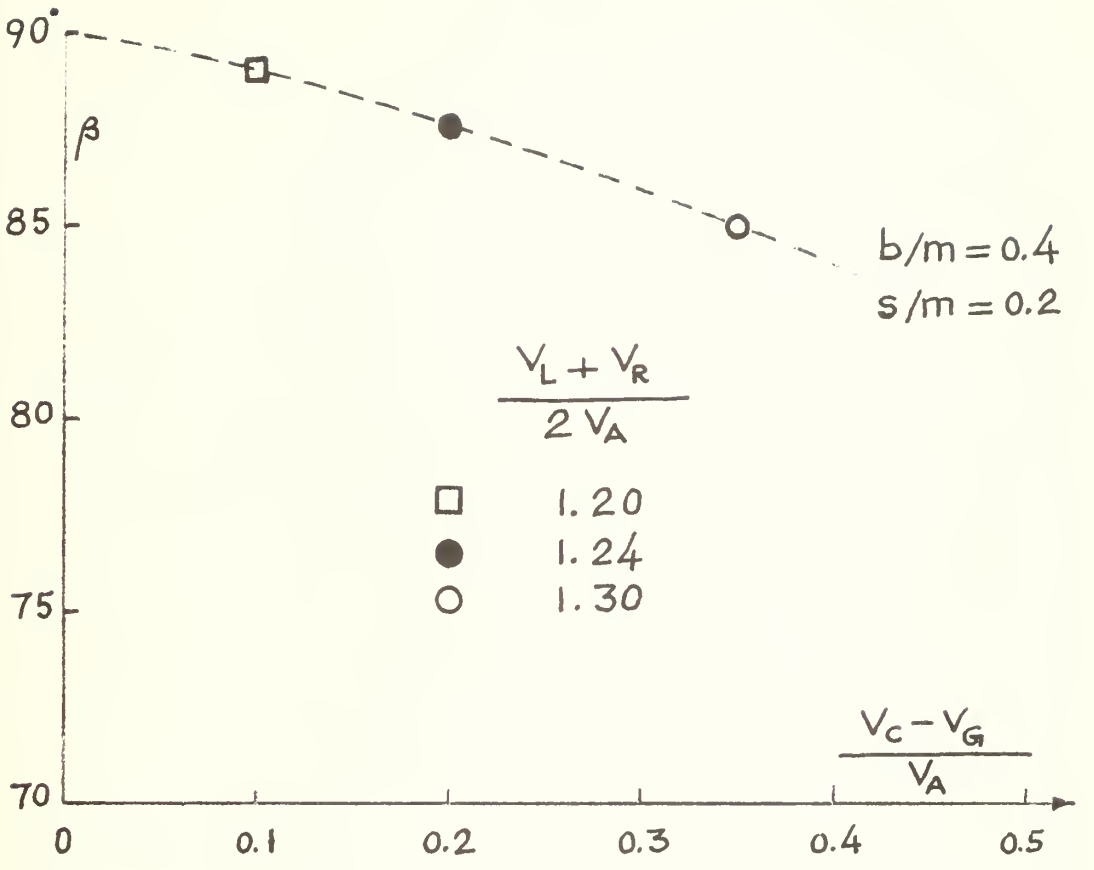

FIG. 9 Representative values of the deflection angle in terms of the normalized differential control-port velocities.

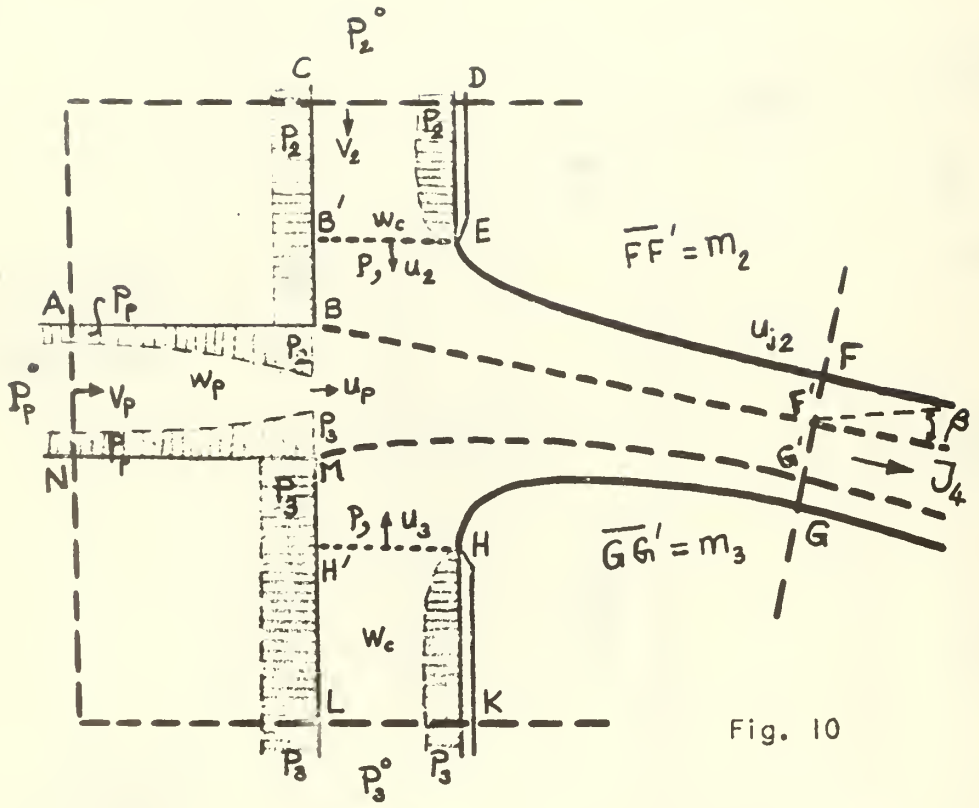

Fig. 10

$$J_P + P_P w_P + P_2 \overline{BC} + P_3 \overline{ML} - \int_D^E p\,dy - \int_K^H p\,dy = J_4 \cos\beta$$

$$J_2 - J_3 + P_2 w_c - P_3 w_c + \int_A^B p\,dx - \int_N^M p\,dx = J_4 \sin\beta$$

from which one has

$$\tan\beta = \frac{J_2 - J_3 + (P_2 - P_3) w_c + \int_A^B p\,dx - \int_N^M p\,dx}{J_P + P_P w_P + P_2 \overline{BC} + P_3 \overline{ML} - \int_D^E p\,dy - \int_K^H p\,dy}$$

Fig. 10 Control Volume and the Equations of Momentum

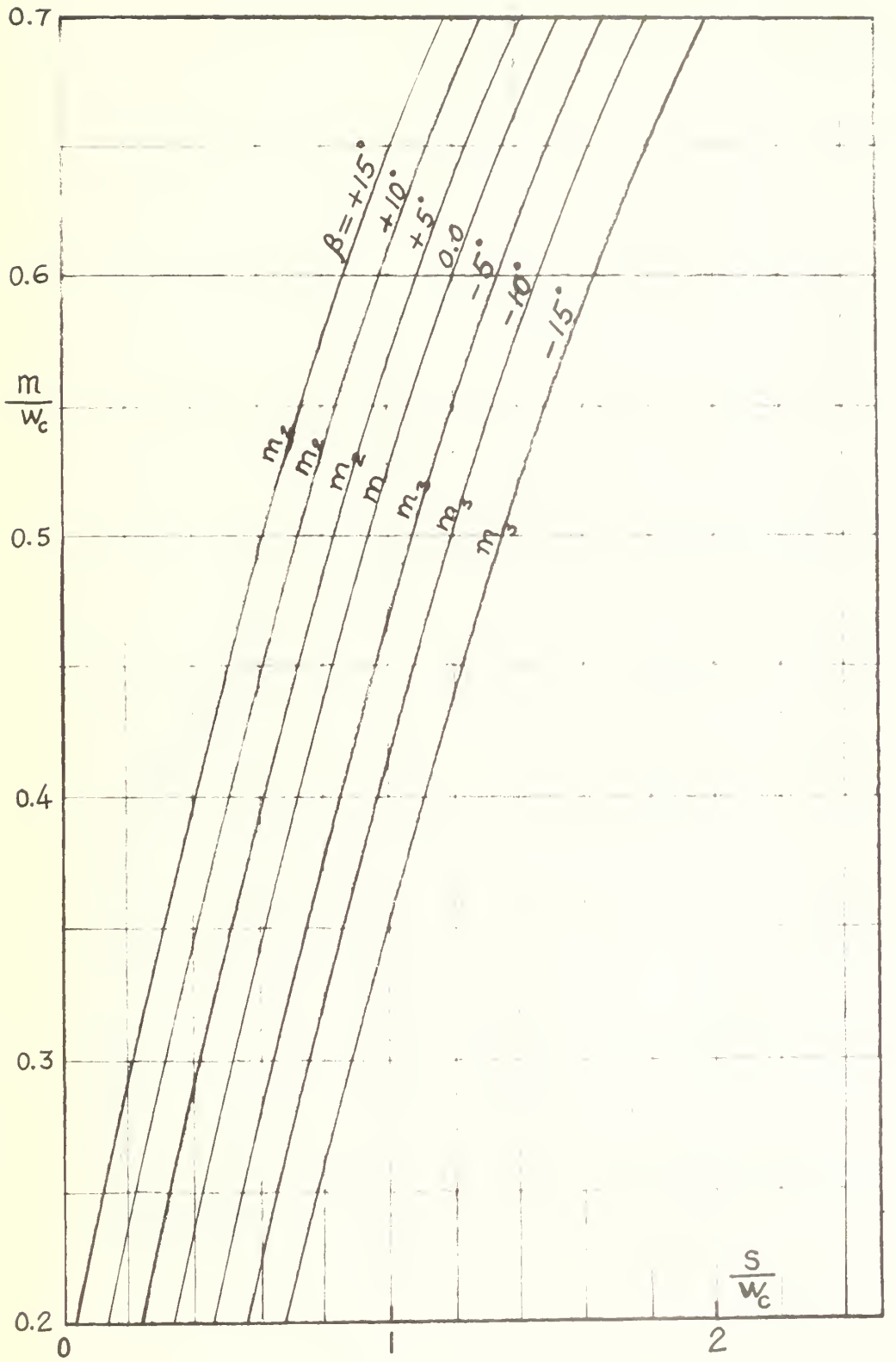

FIG. 11 m/w_c versus s/w_c for various values of β

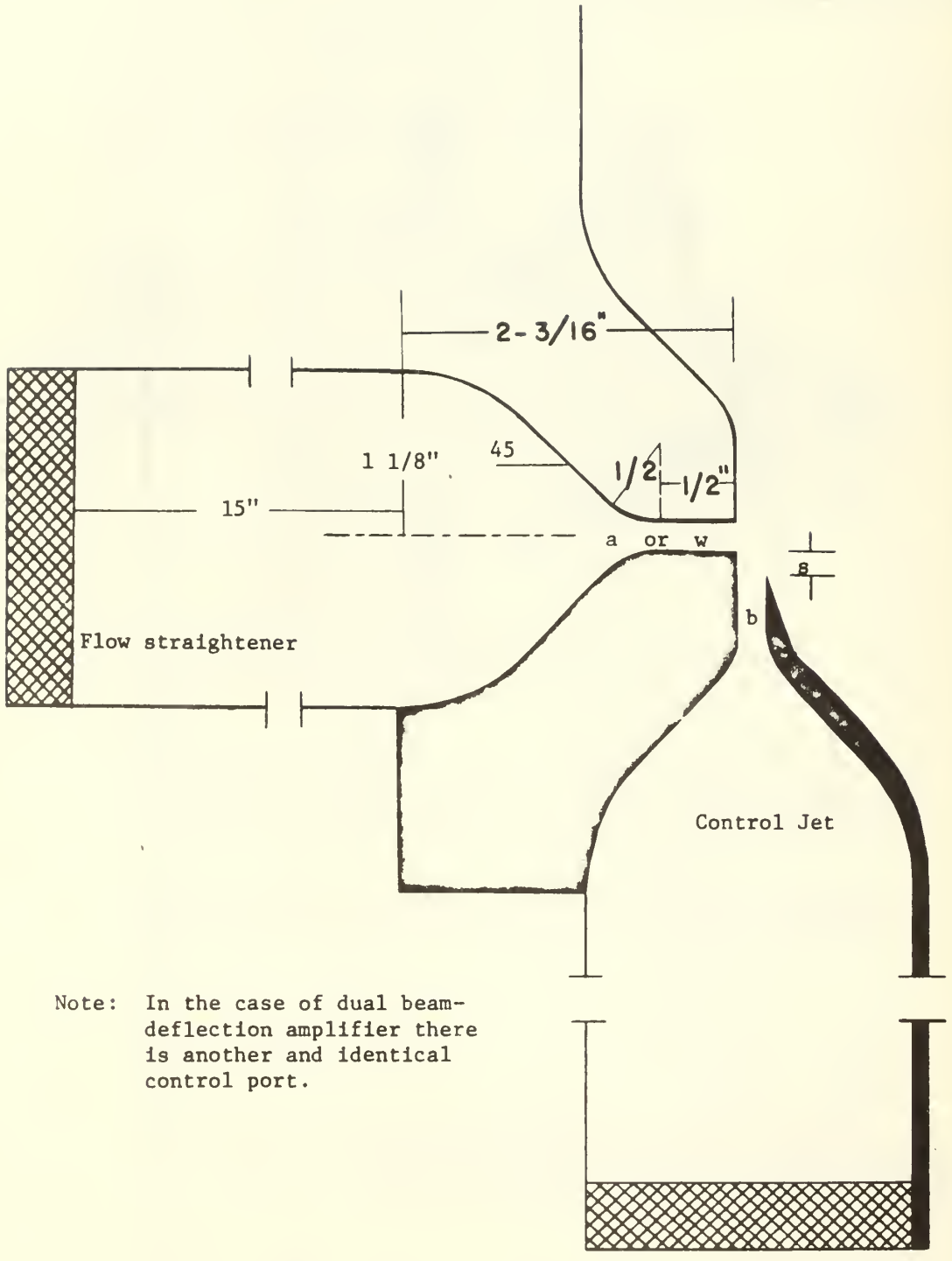

FIG. 12 Nozzle geometry used in single and double control-jet amplifiers

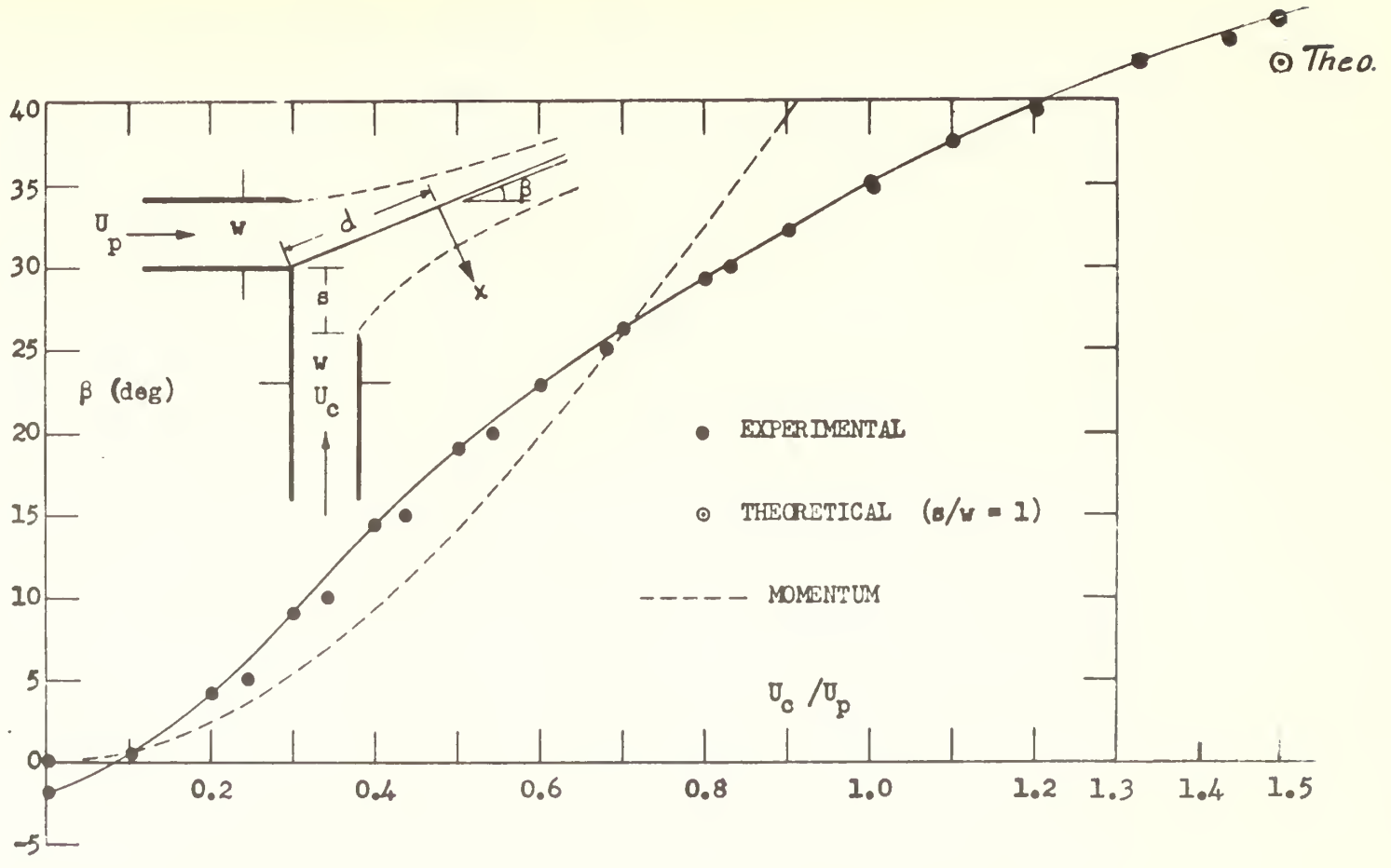

FIG. 13 Jet-deflection angle as a function of the velocity ratio for two perpendicularly impinging jets (Analysis and experiments)

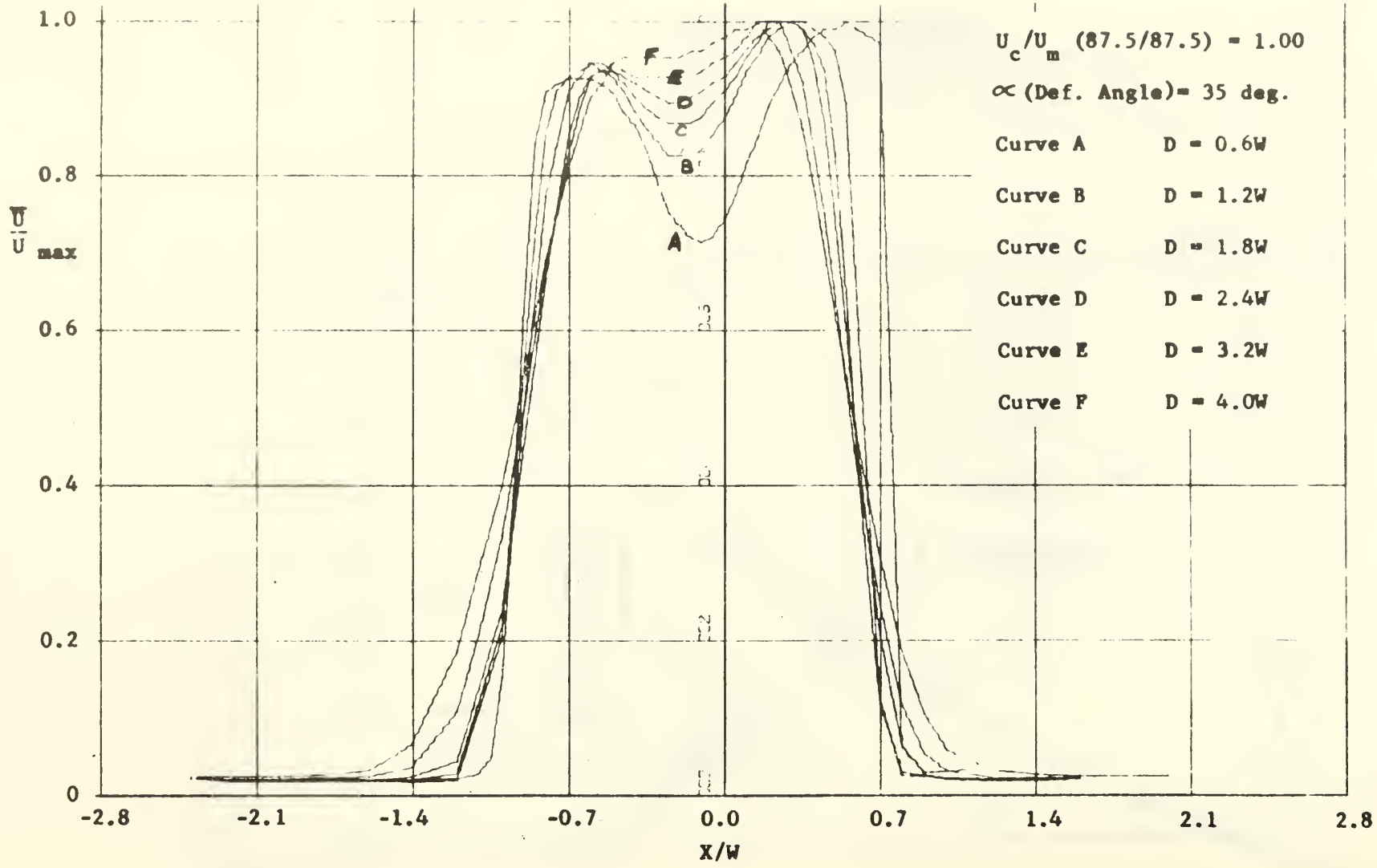

FIG. 14 Composite, normalized velocity profiles along the axis of the jet

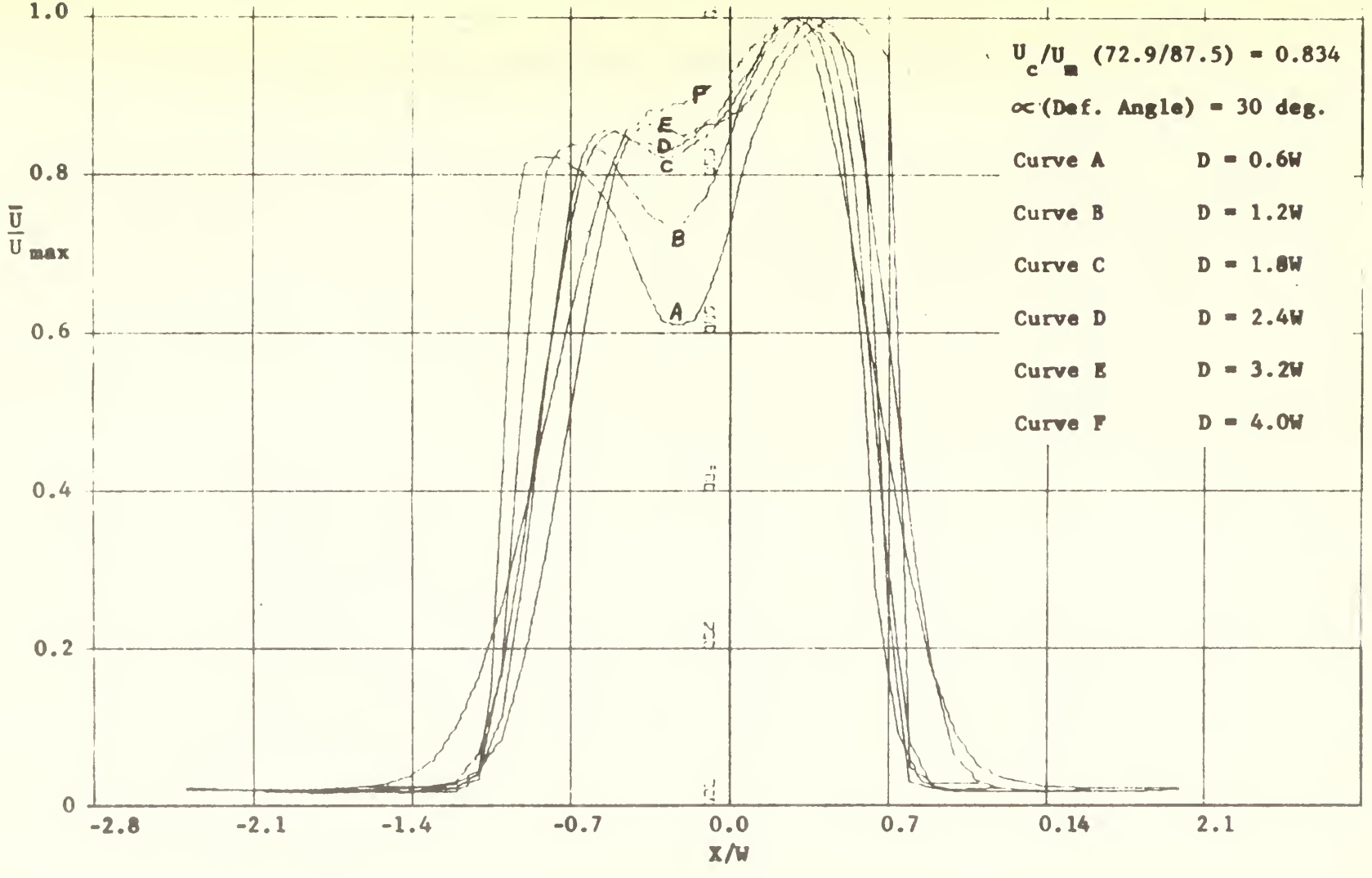

FIG. 15 Composite, normalized velocity profiles along the axis of the combined jet

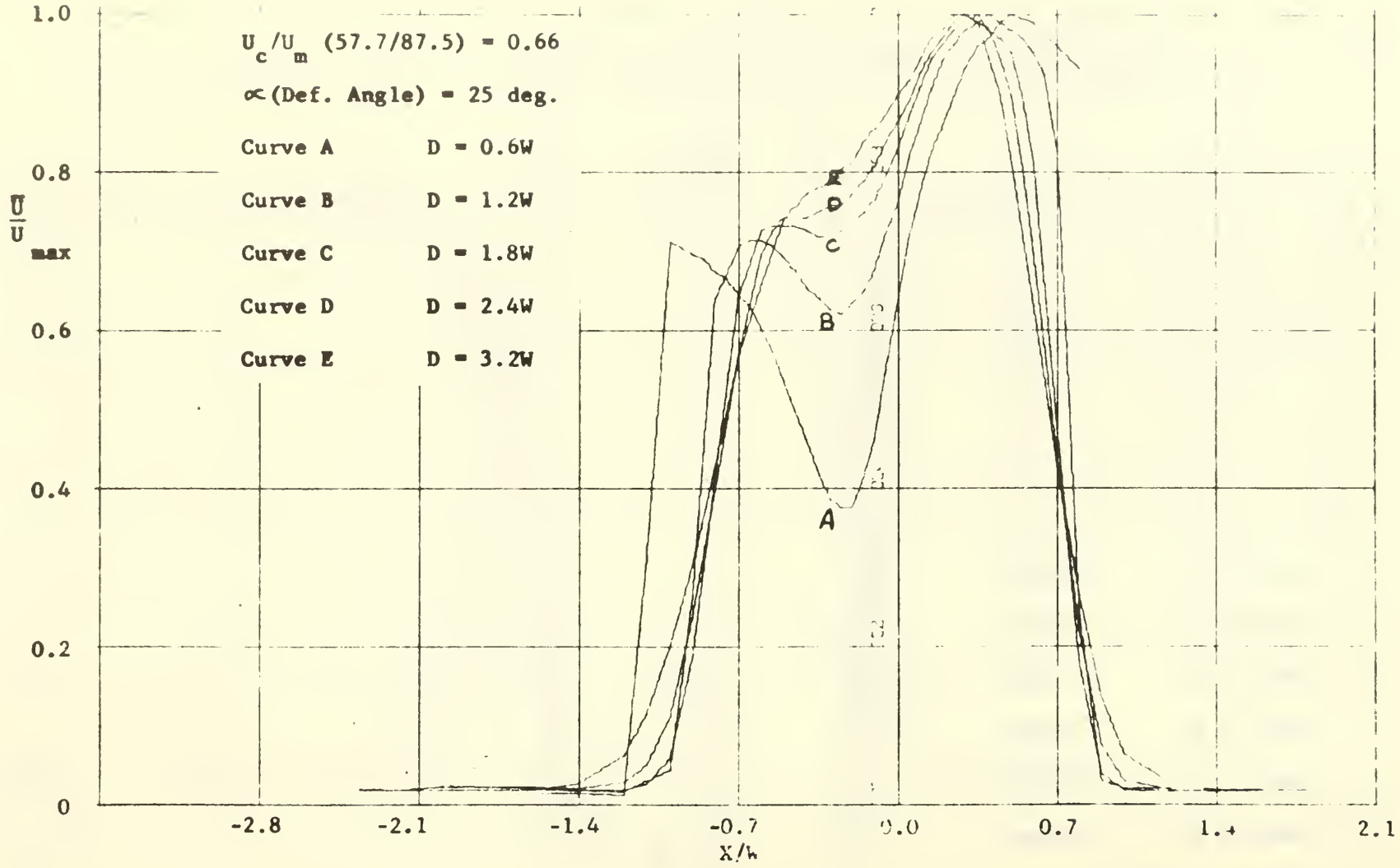

FIG. 16 Composite, normalized velocity profiles along the axis of the combined jet

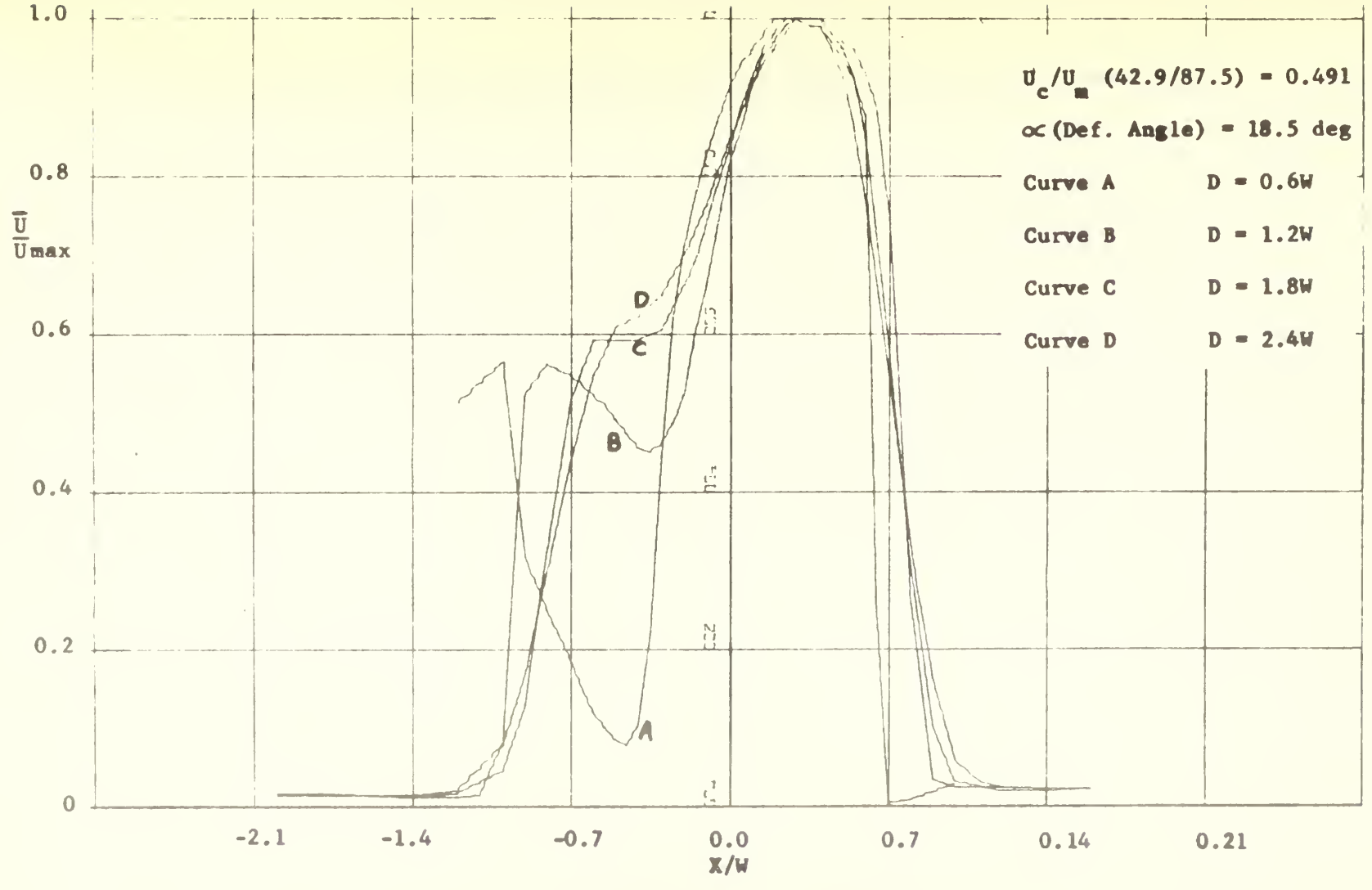

FIG. 17 Composite, normalized velocity profiles along the axis of the combined jet

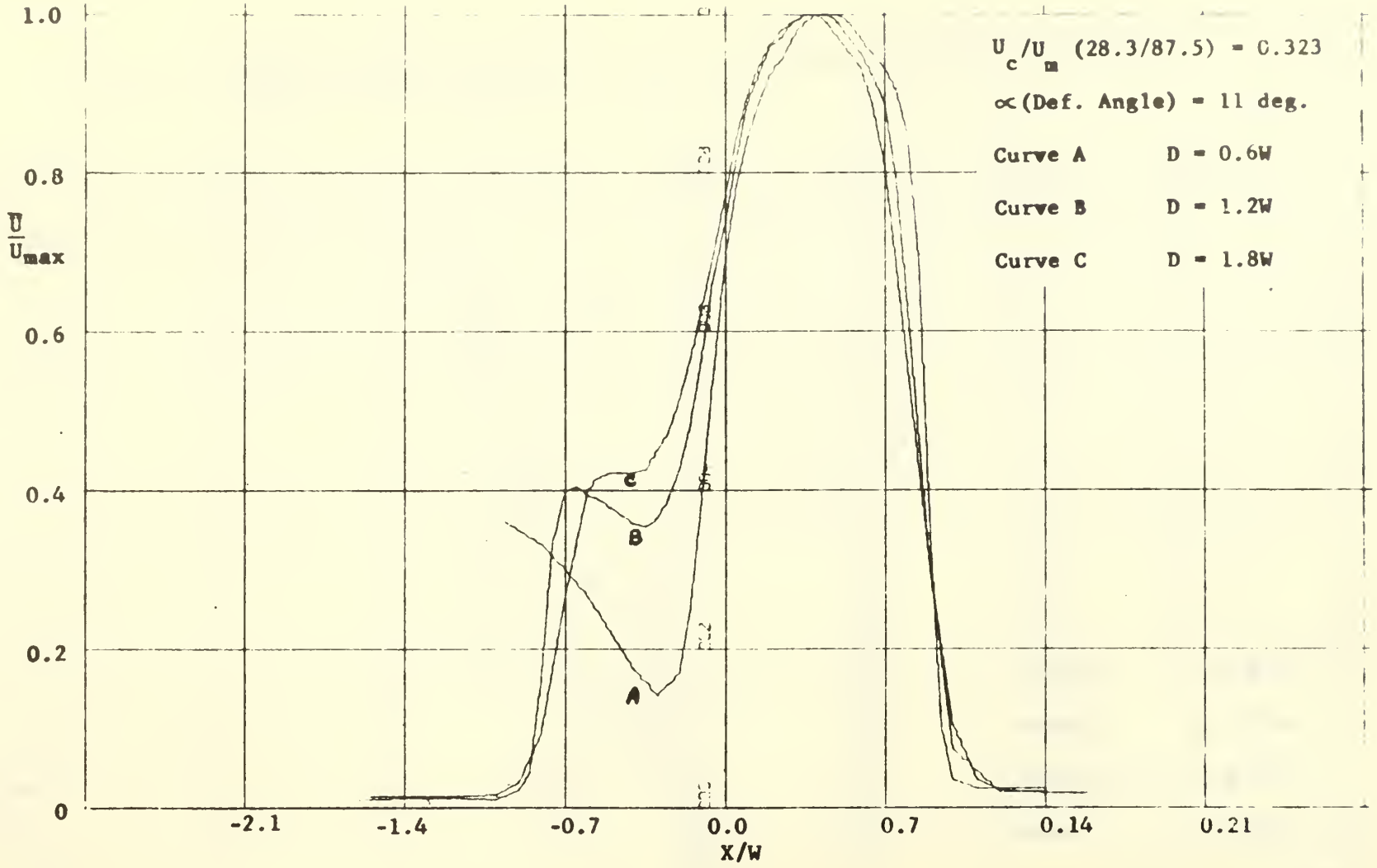

FIG. 18 Composite, normalized velocity profiles along the axis of the combined jet

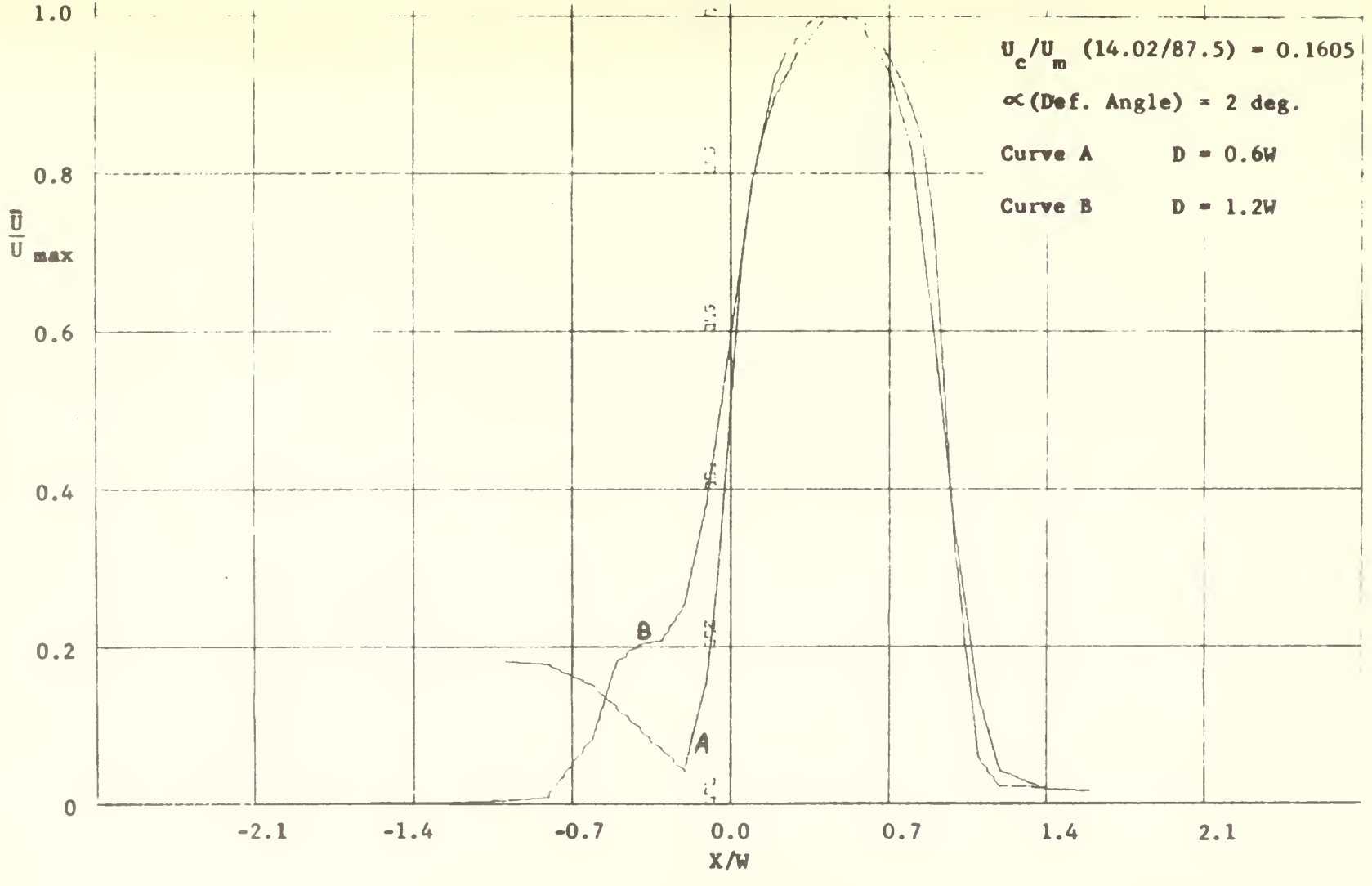

FIG. 19 Composite, normalized velocity profiles along the axis of the combined jet

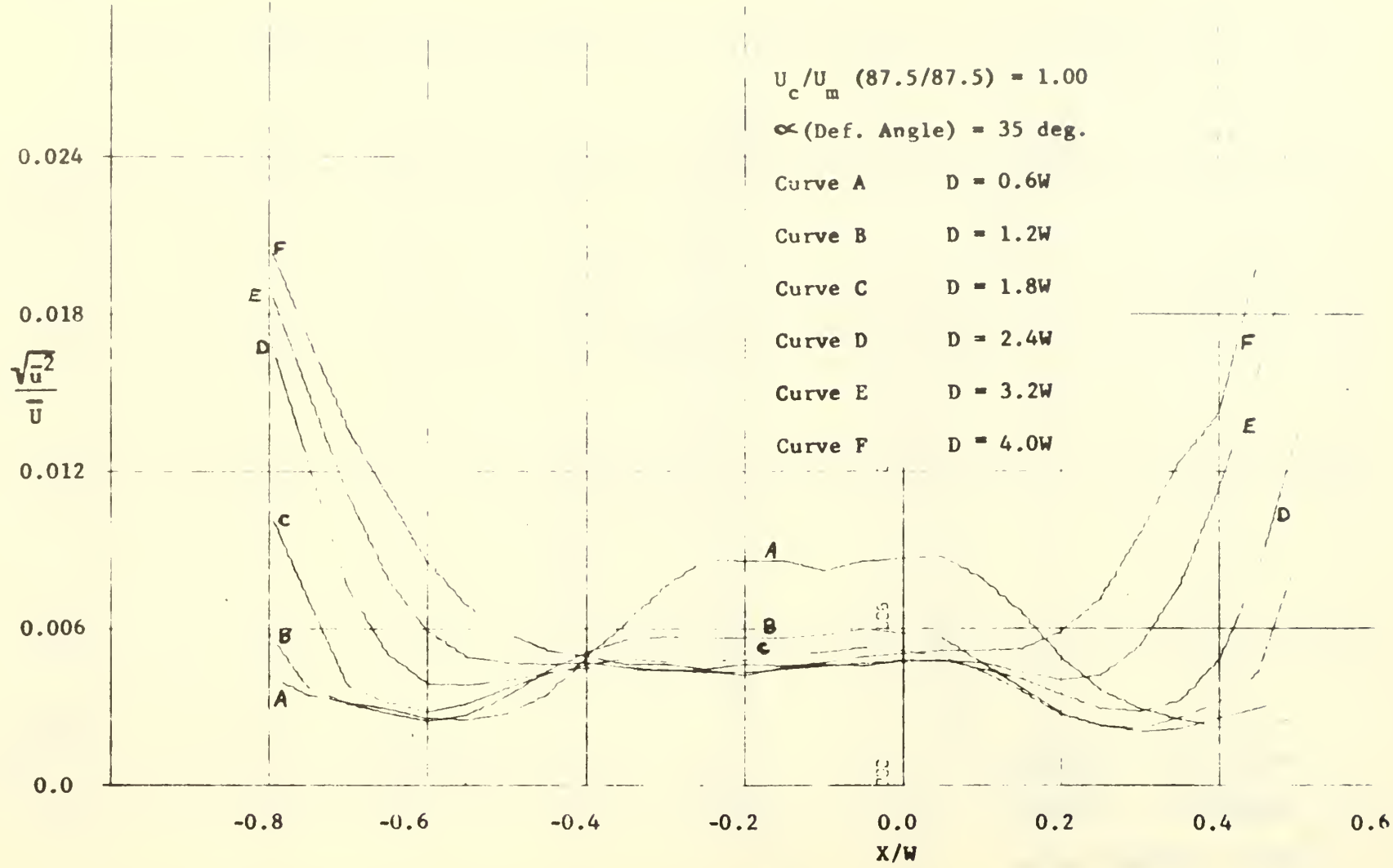

FIG. 20 Turbulence-intensity profiles along the axis of the combined jet

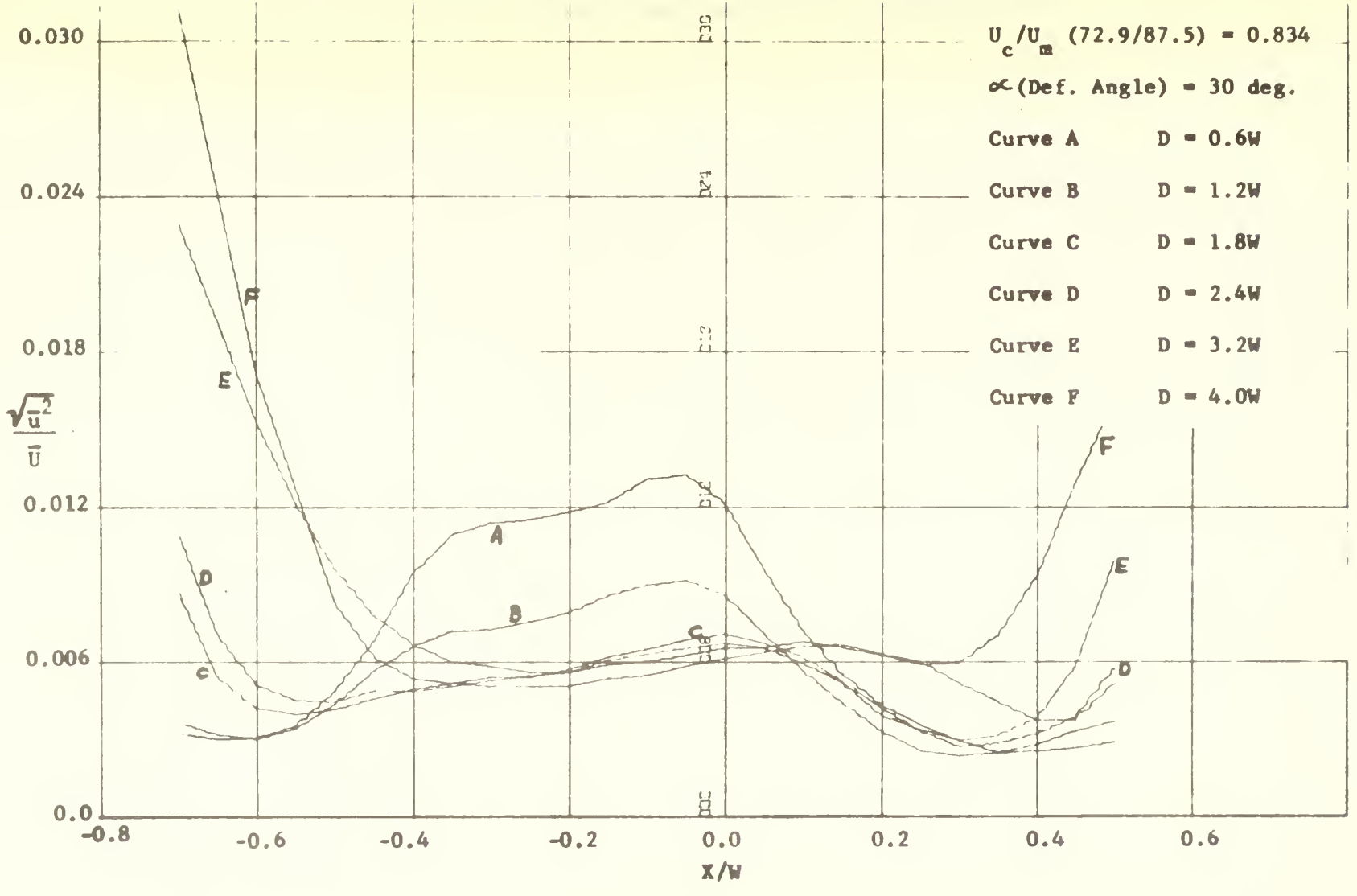

FIG. 21 Turbulence-intensity profiles along the axis of the combined jet

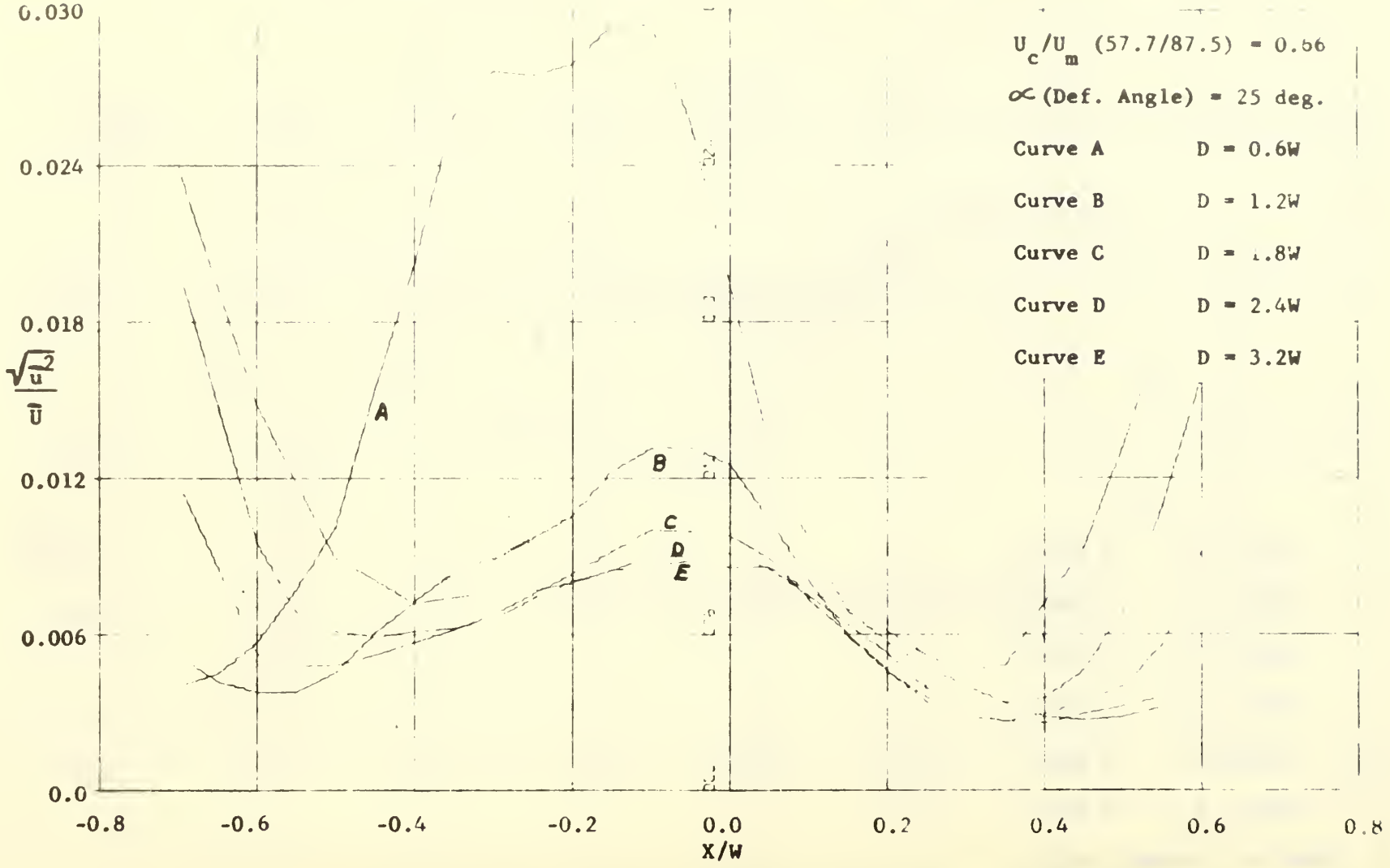

FIG. 22 Turbulence-intensity profiles along the axis of the combined jet

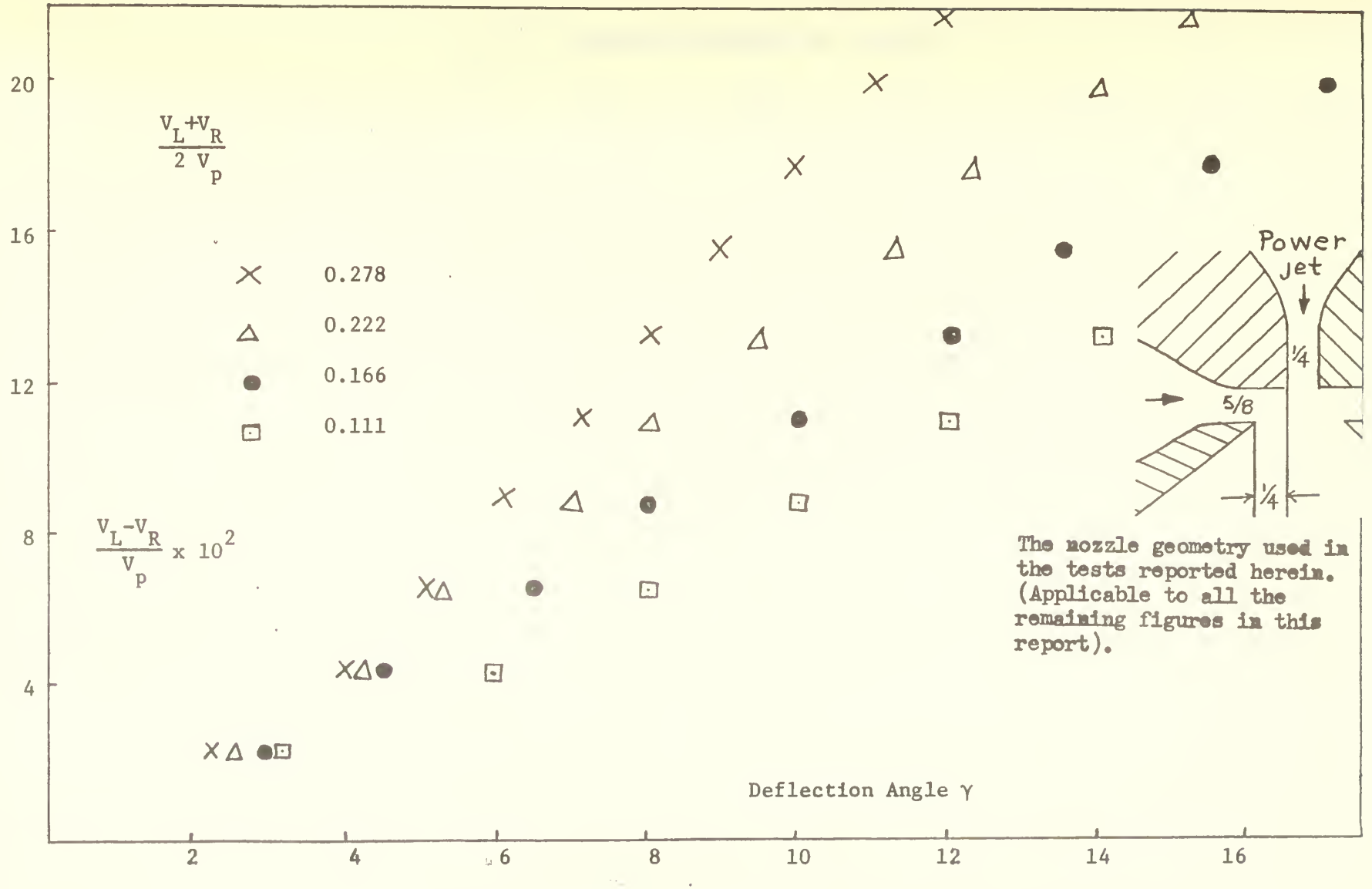

The nozzle geometry used in the tests reported herein. (Applicable to all the remaining figures in this report).

FIG. 23 Deflection Angles, Re = 31550 .

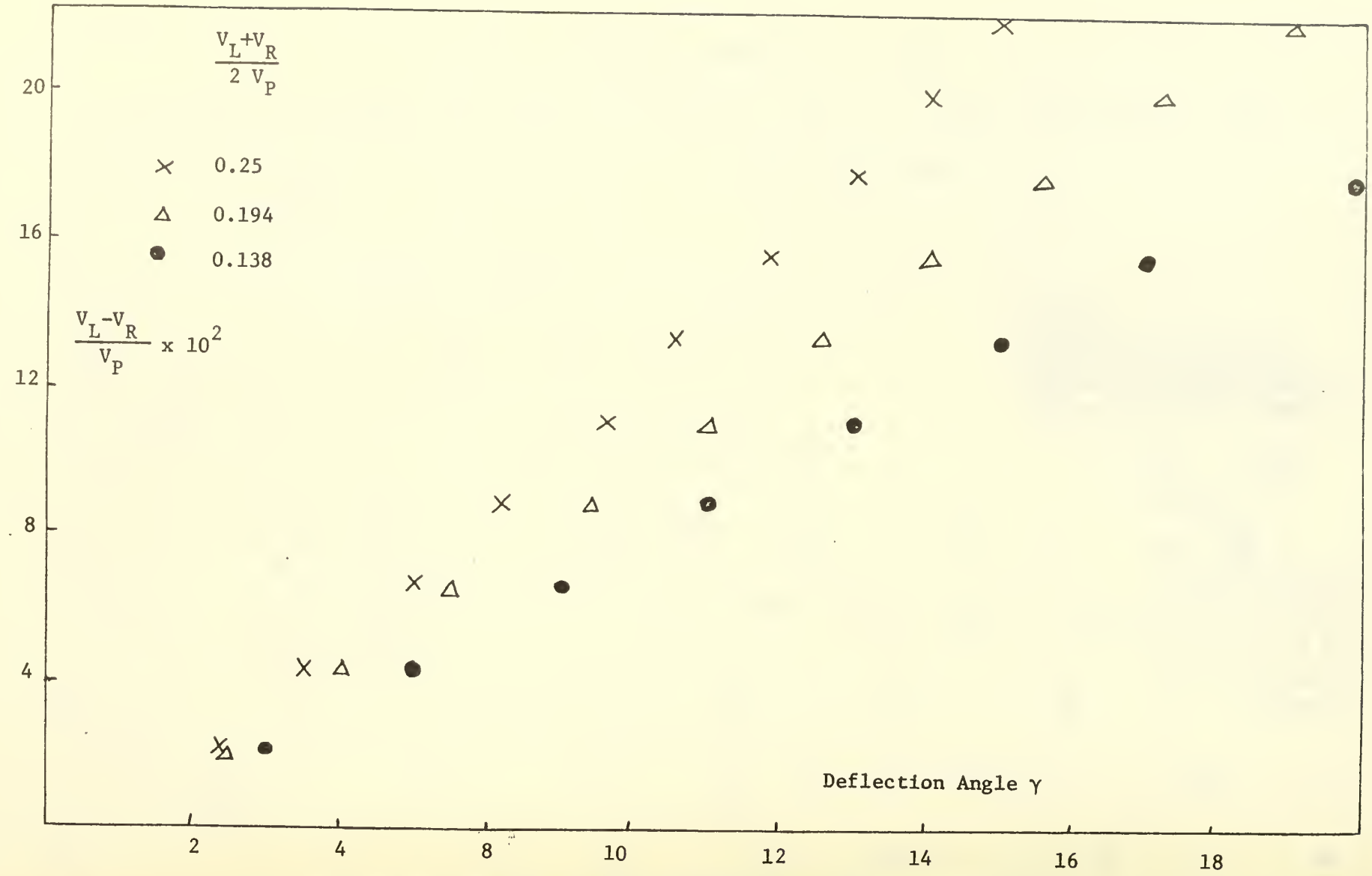

FIG. 24 Deflection Angles, Re = 31550

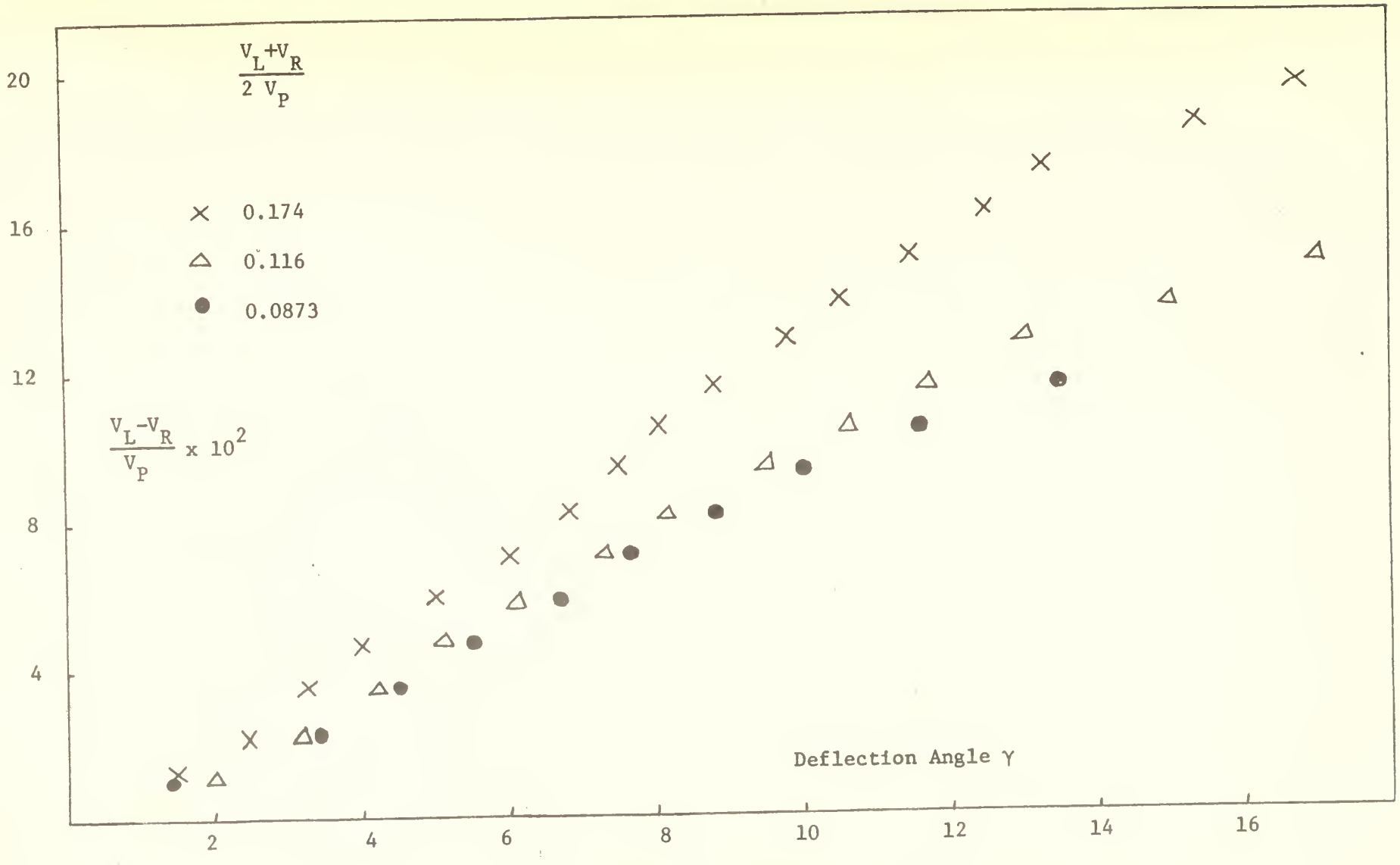

FIG. 25 Deflection Angles, Re = 15775

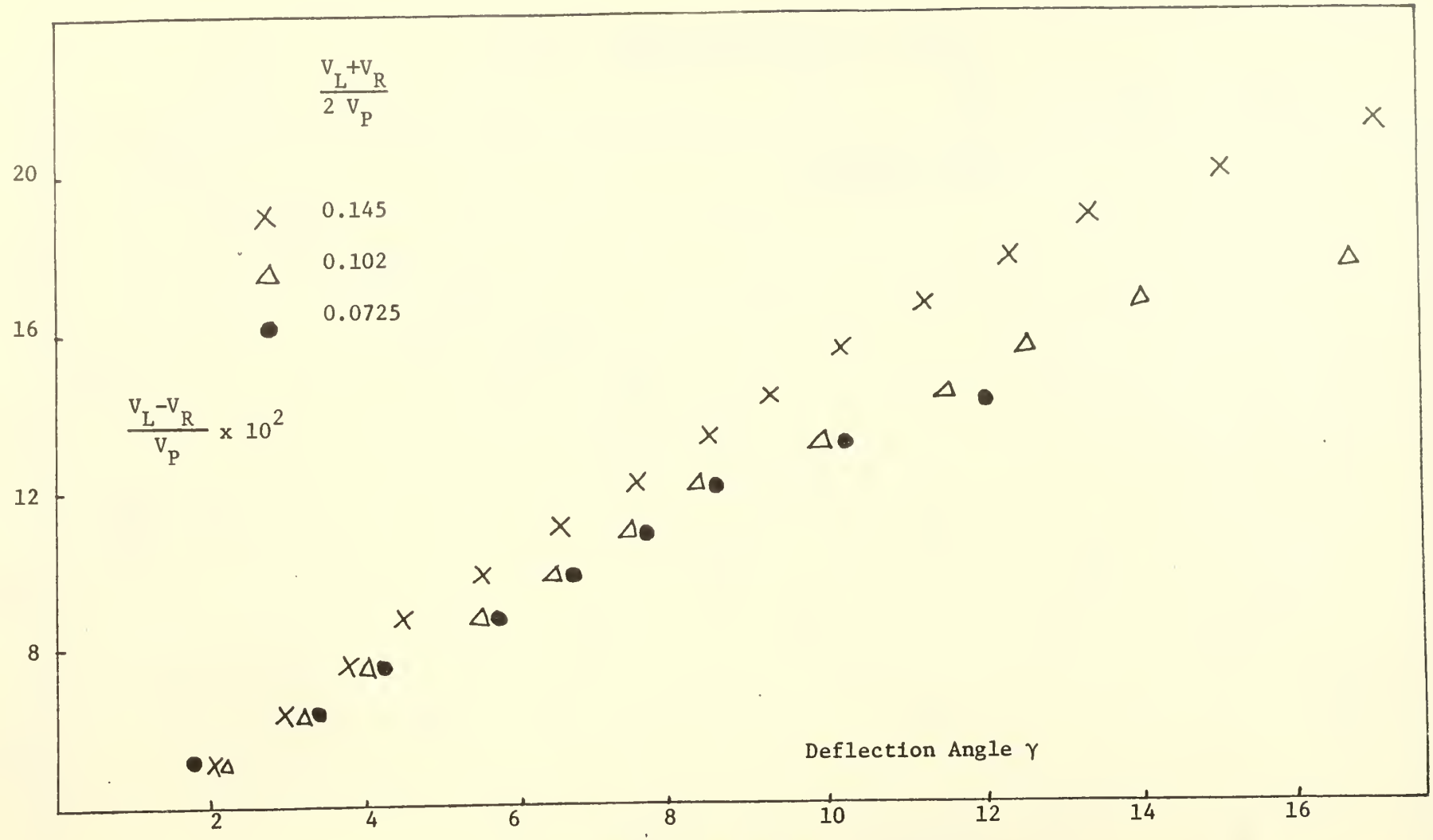

FIG. 26 Deflection Angles, Re = 15775

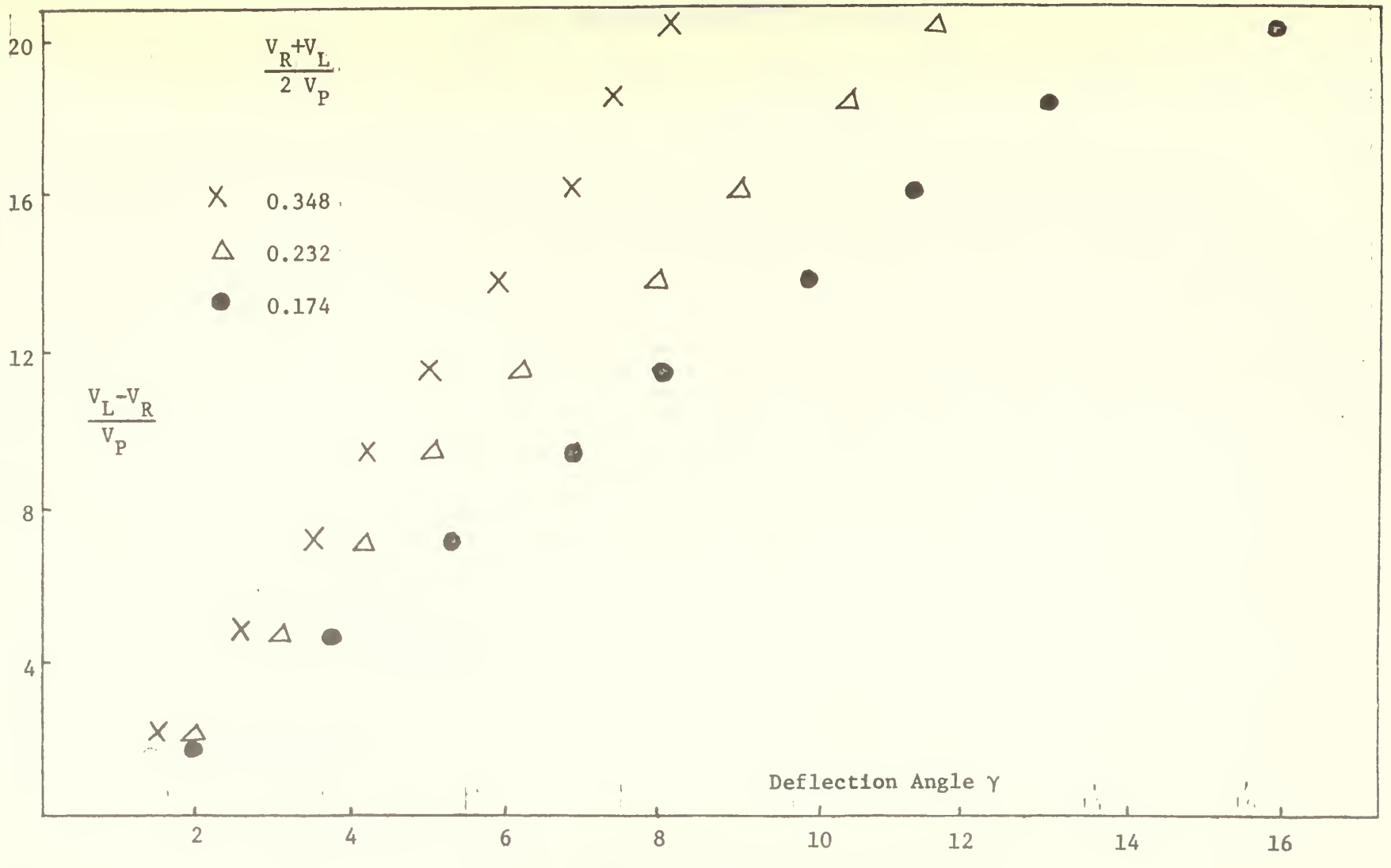

FIG. 27 Deflection Angles, Re = 7887

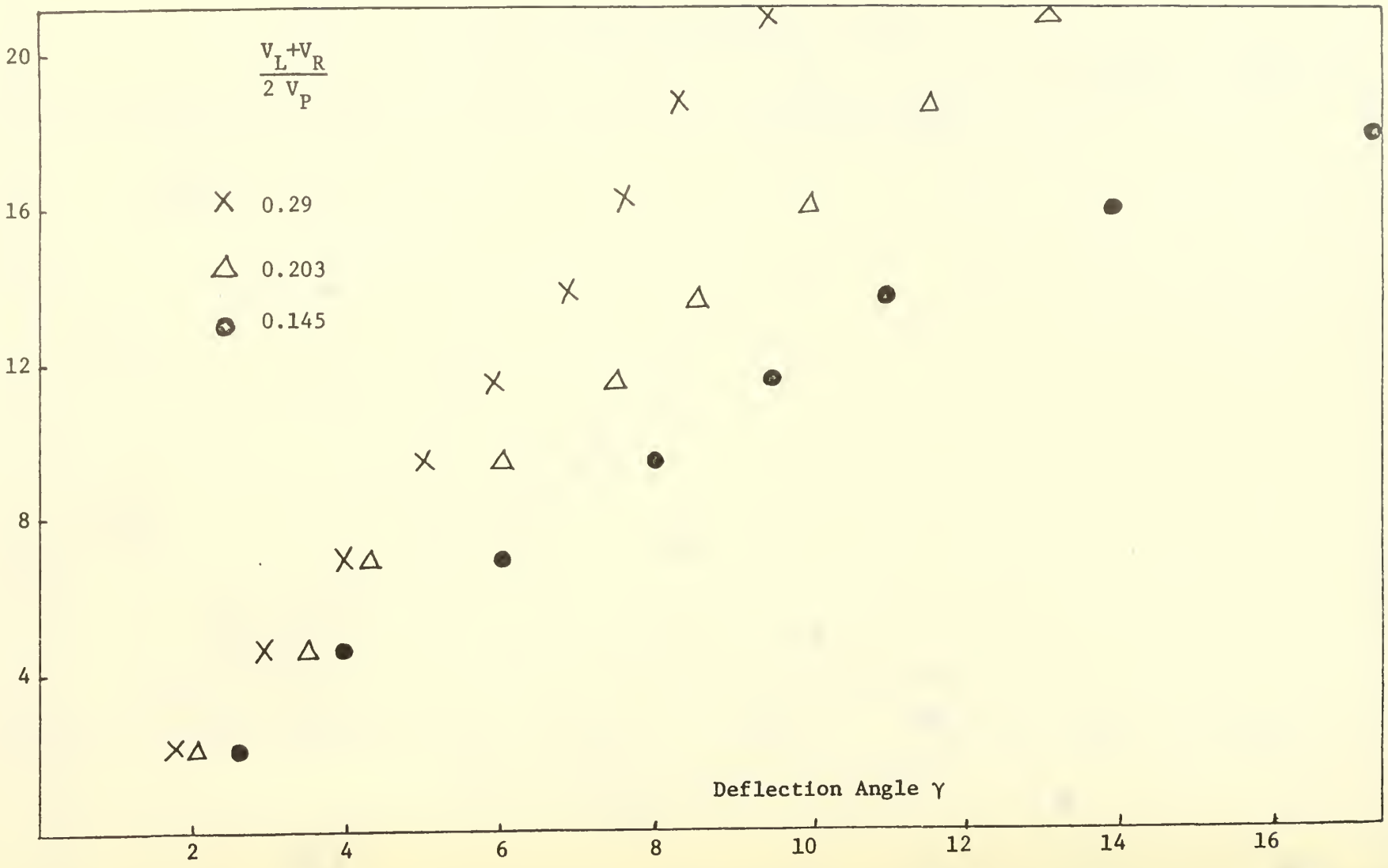

FIG. 28 Deflection Angles, Re = 7887

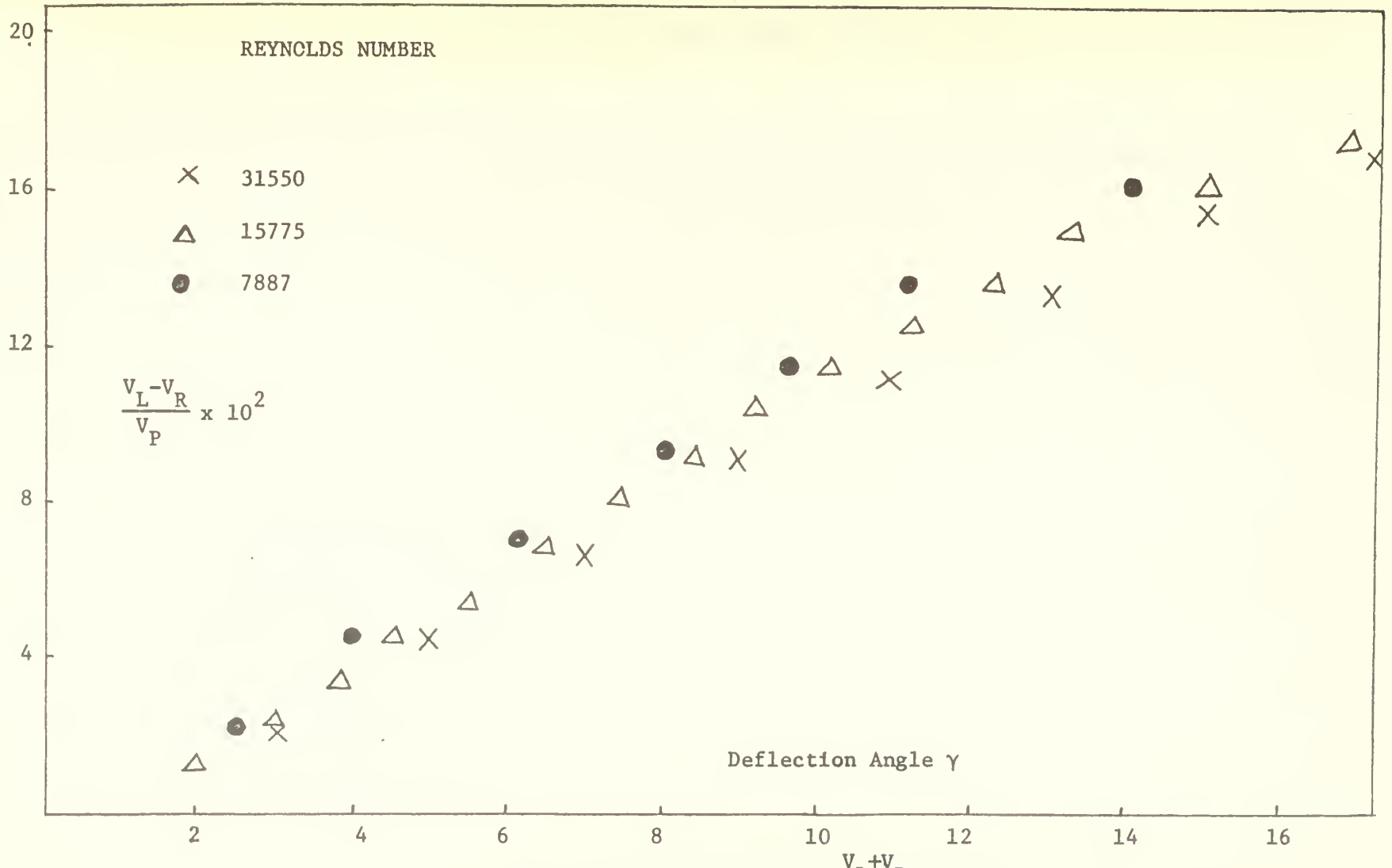

FIG. 29 Deflection Angles, $\frac{V_L + V_R}{2\ V_P} = 0.145$

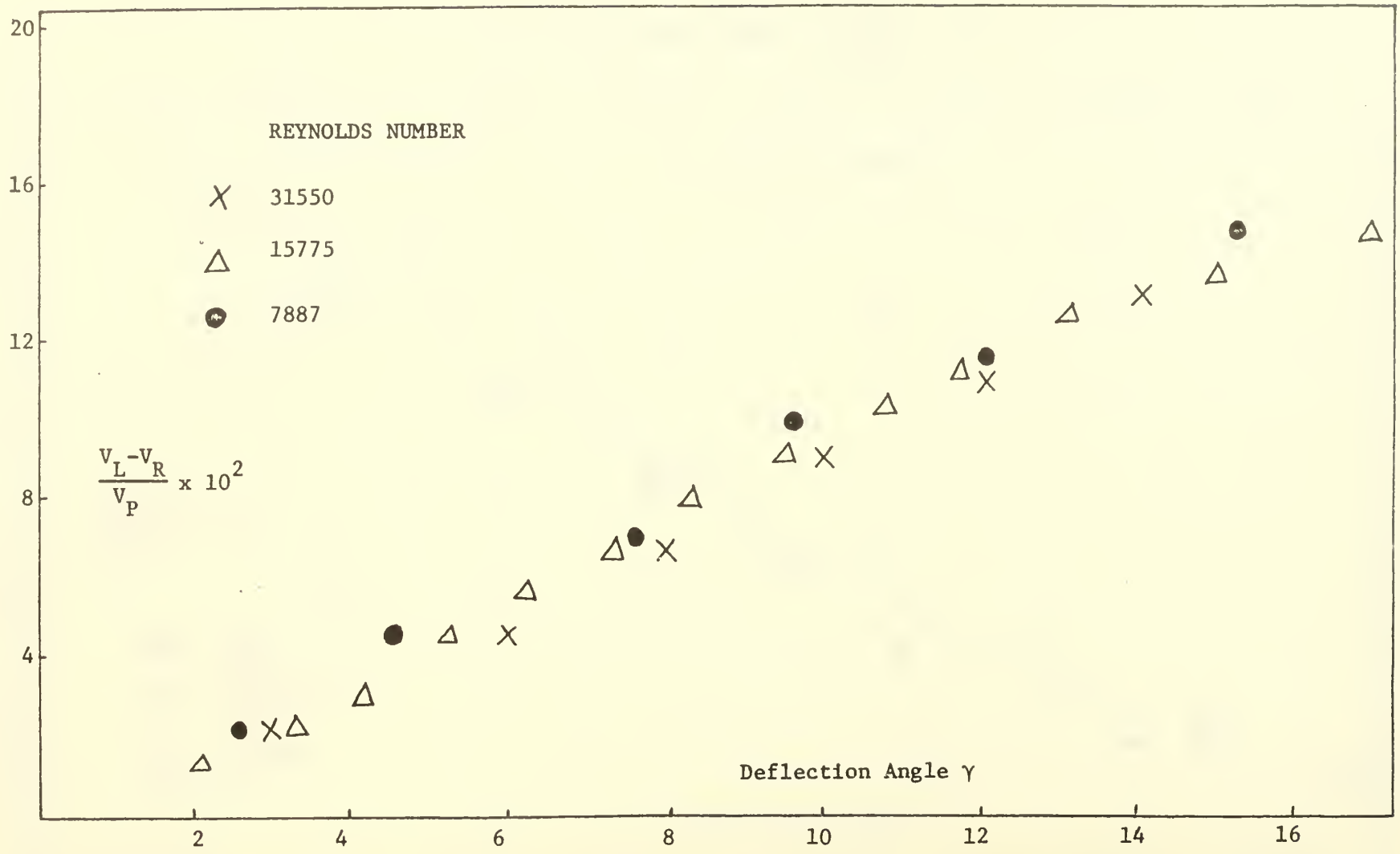

FIG. 30 Deflection Angles, $\frac{V_L + V_R}{2\ V_P} = 0.116$

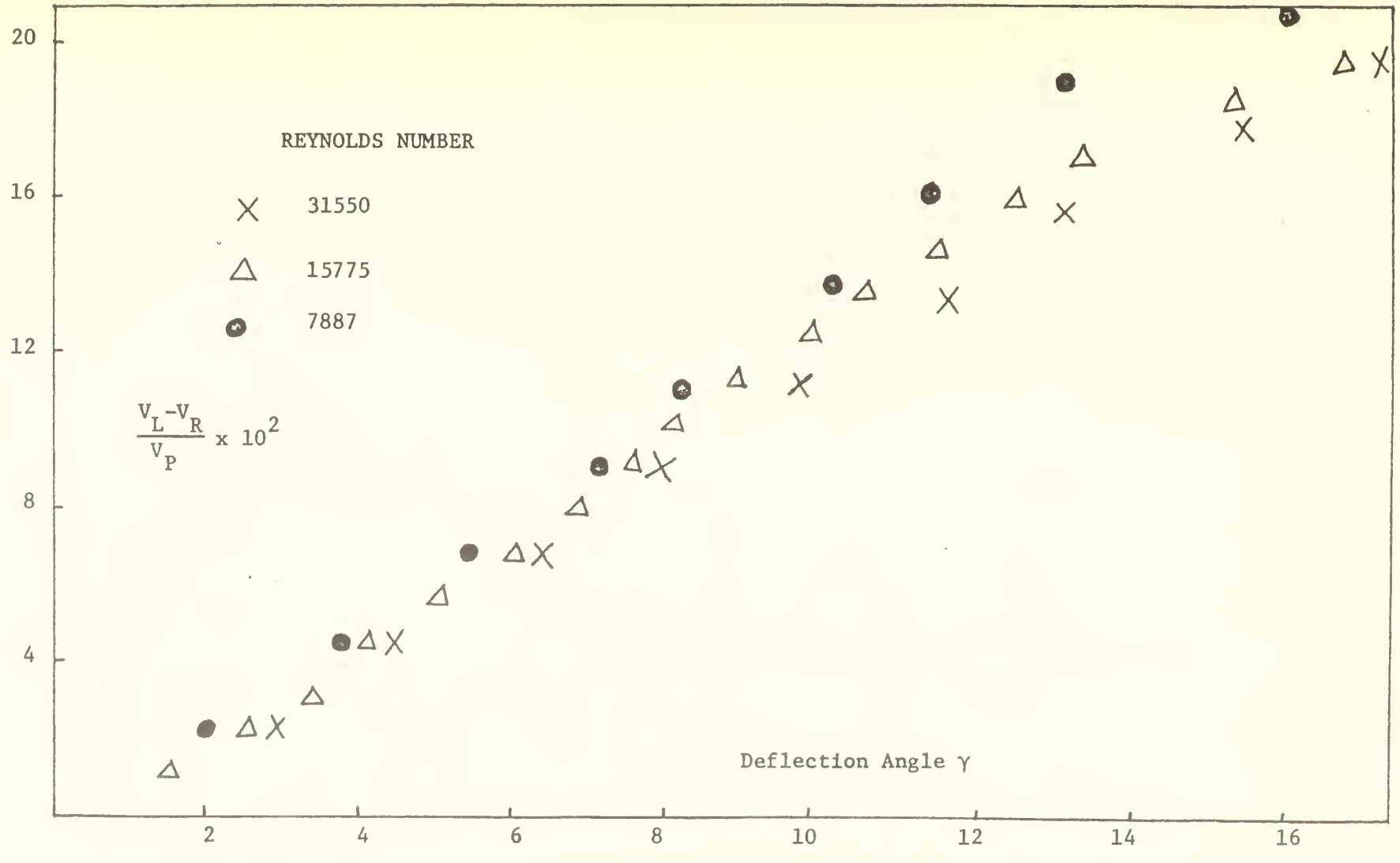

FIG. 31 Deflection Angles, $\frac{V_L + V_R}{2\ V_P} = 0.174$

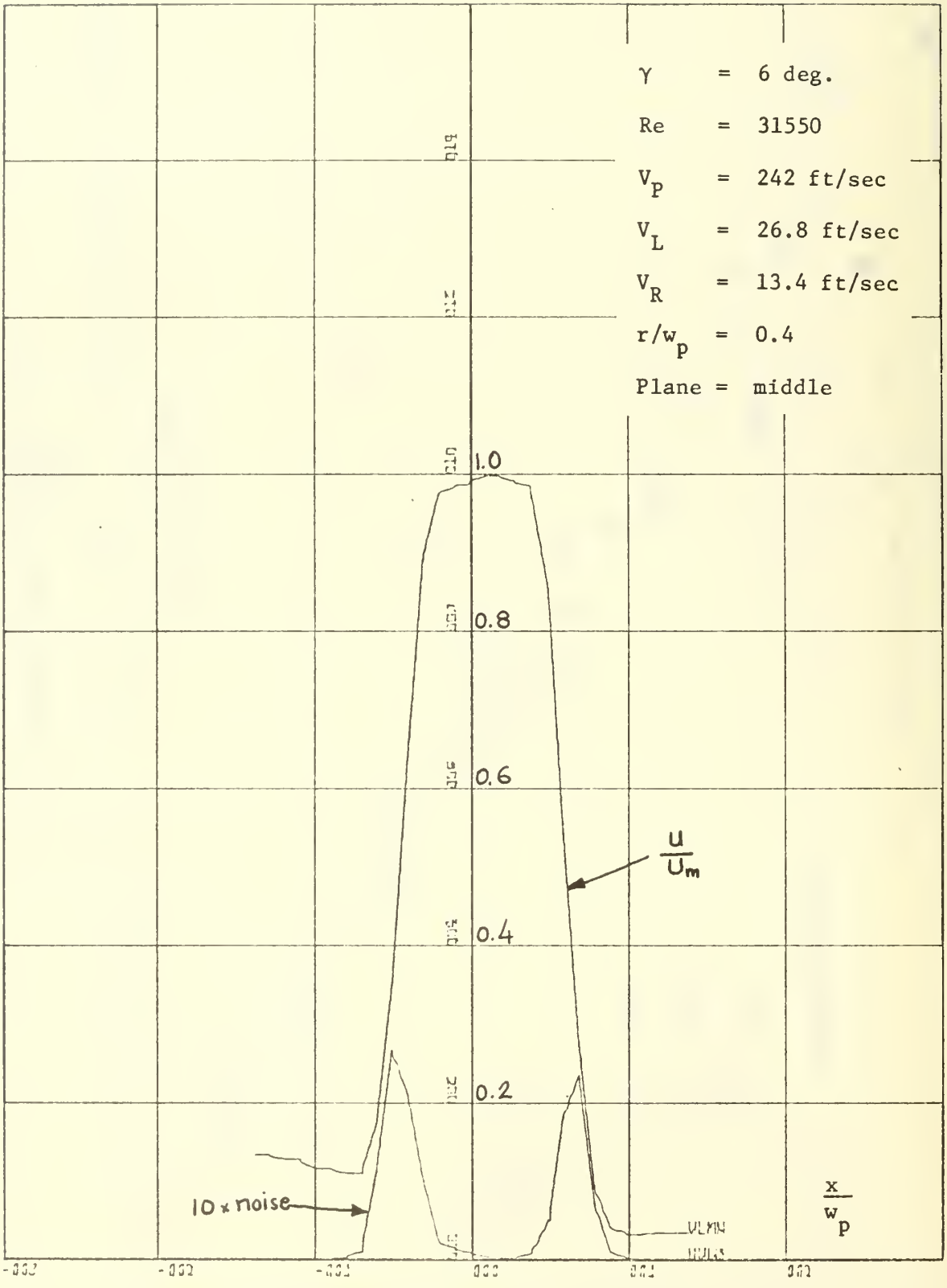

Figure 32 Mean Velocity and Noise

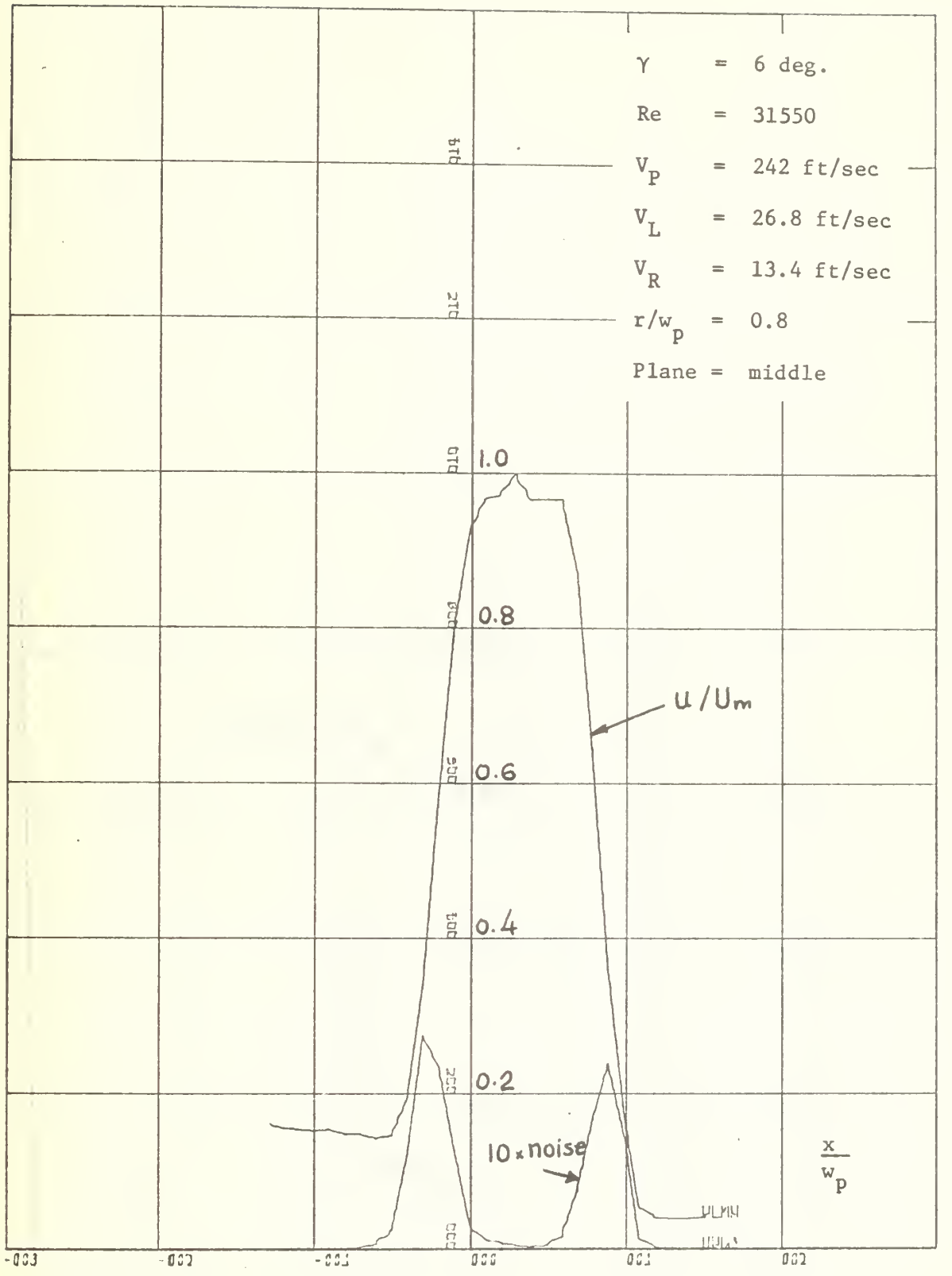

Figure 33 Mean Velocity and Noise

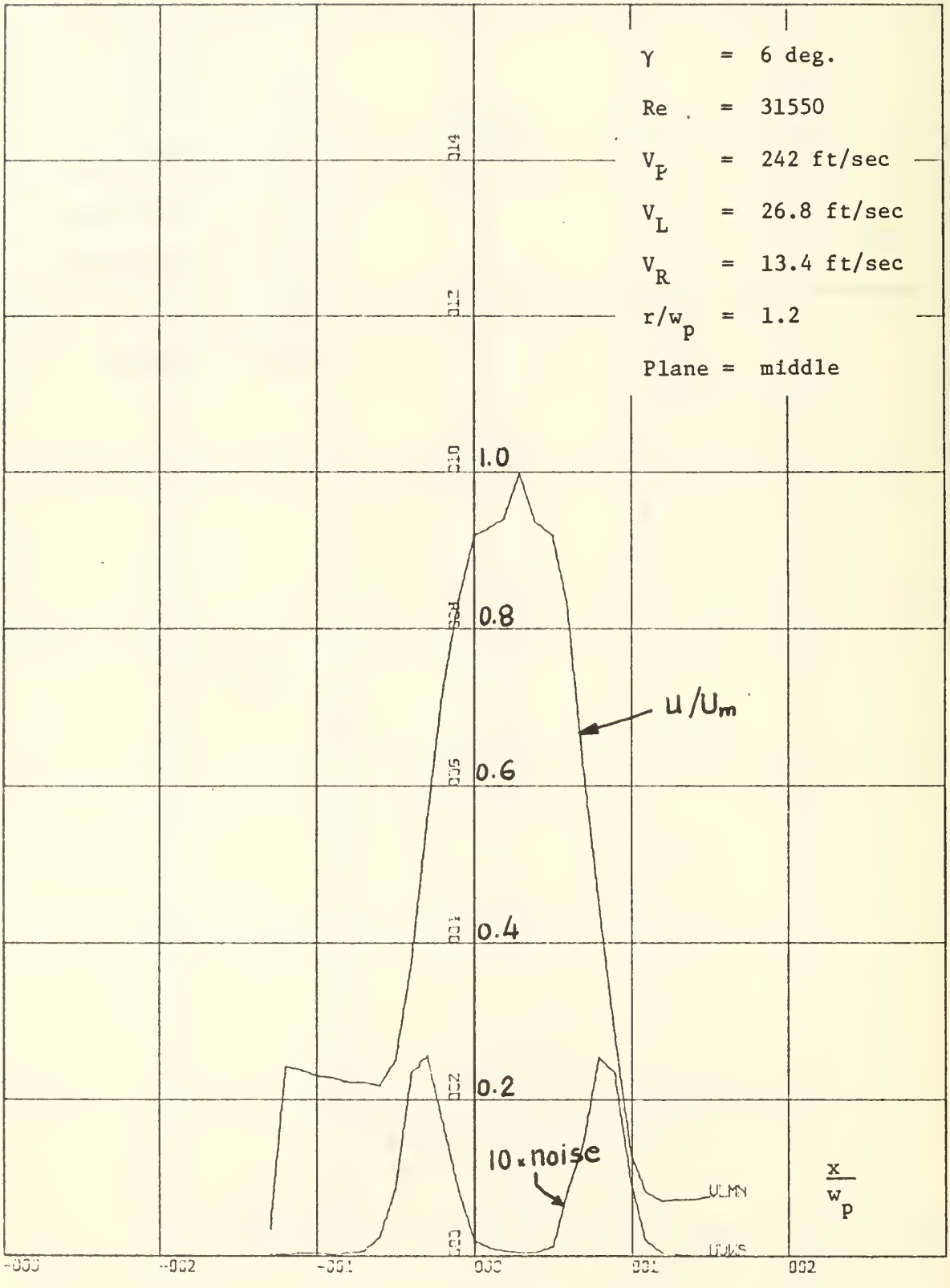

Figure 34 Mean Velocity and Noise

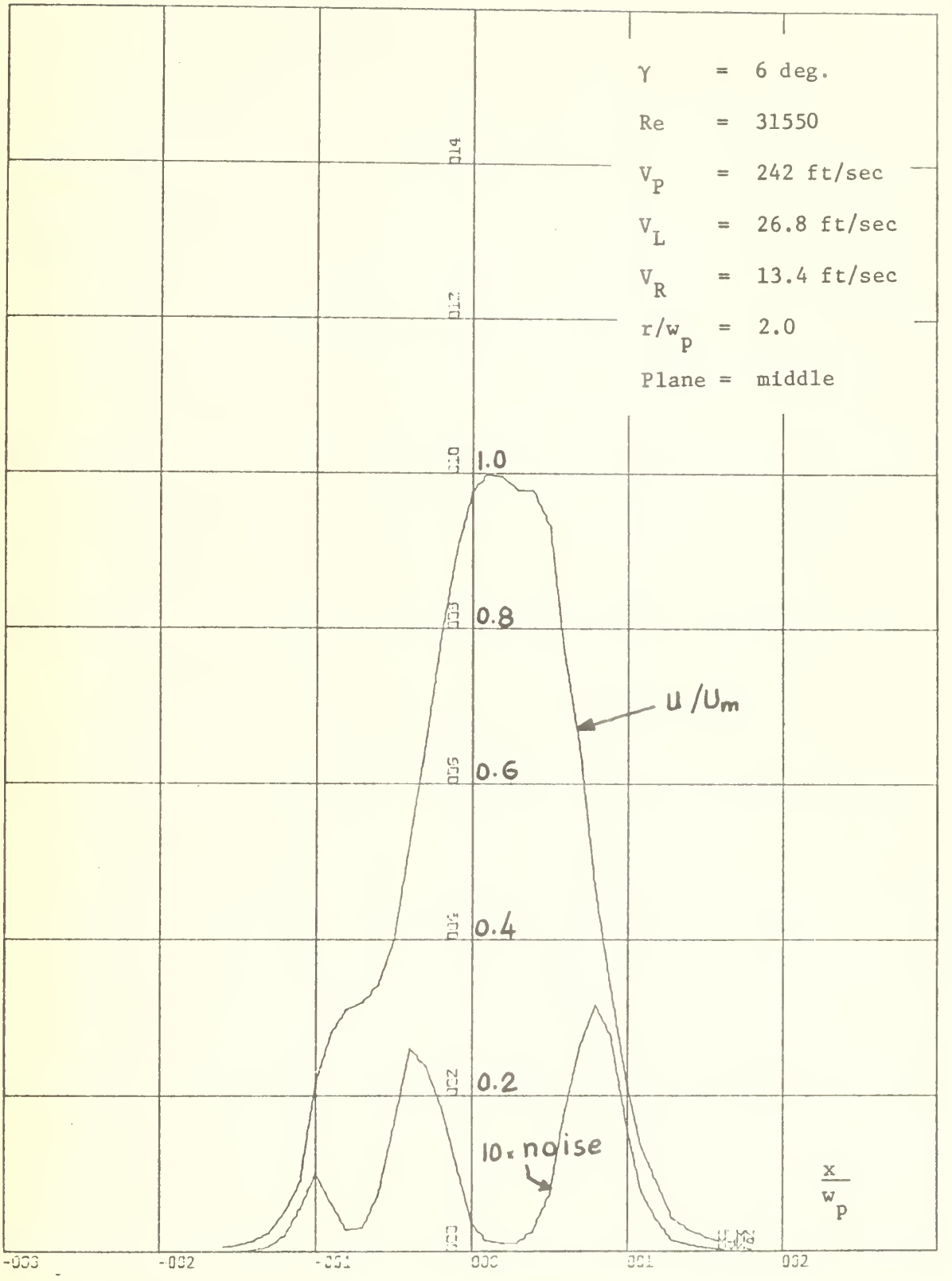

Figure 35 Mean Velocity and Noise

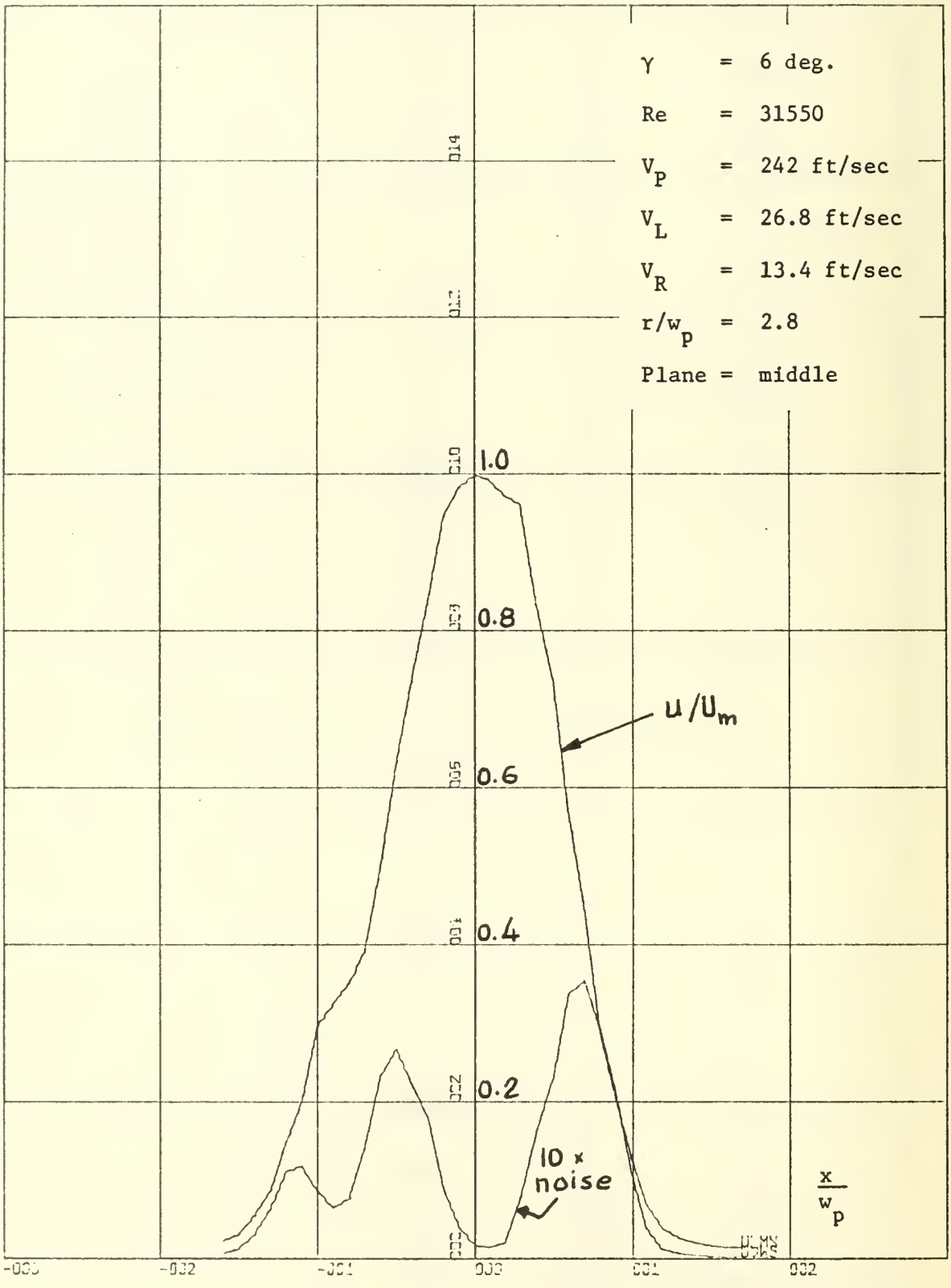

Figure 36 Mean Velocity and Noise

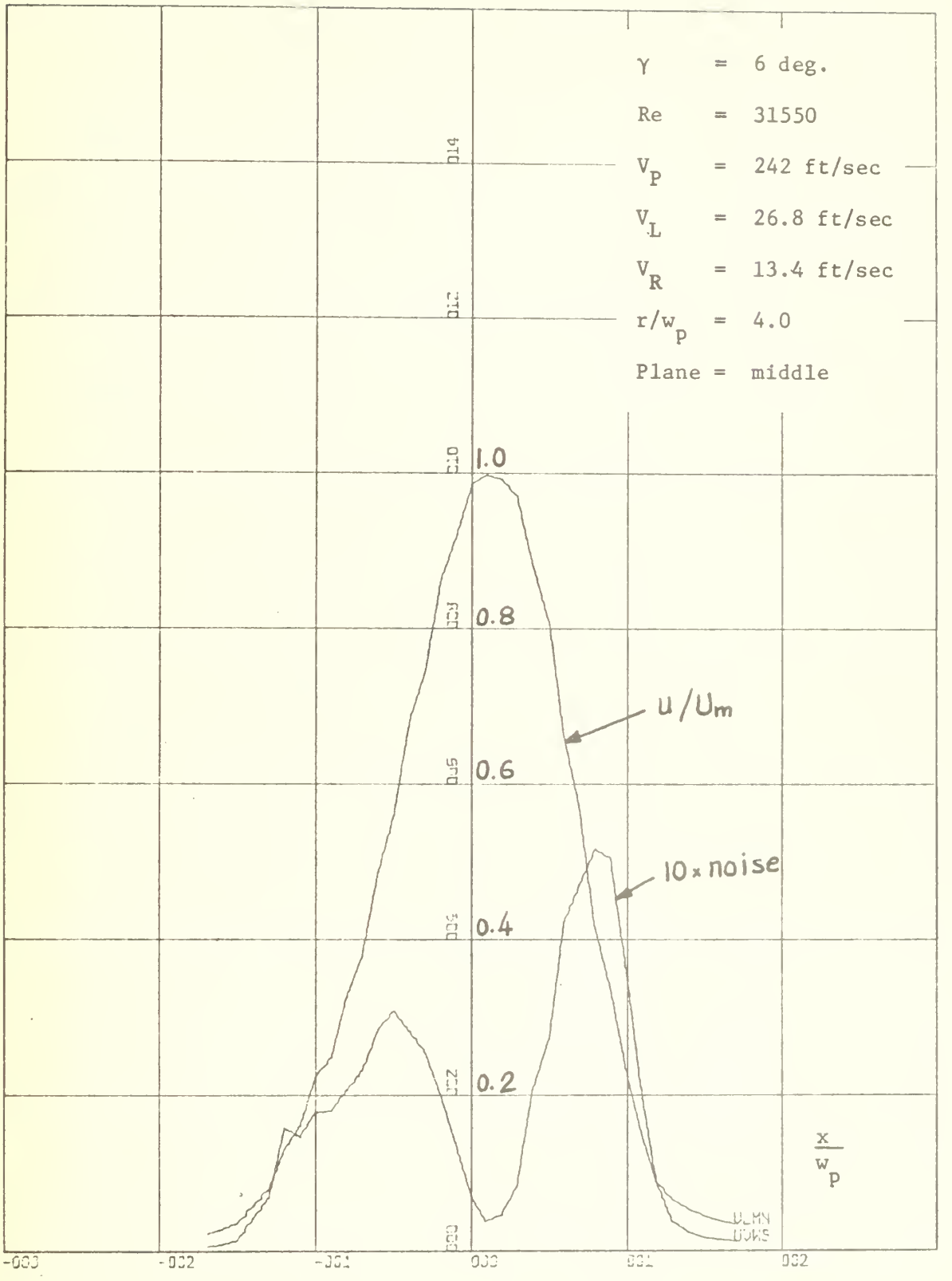

Figure 37 Mean Velocity and Noise

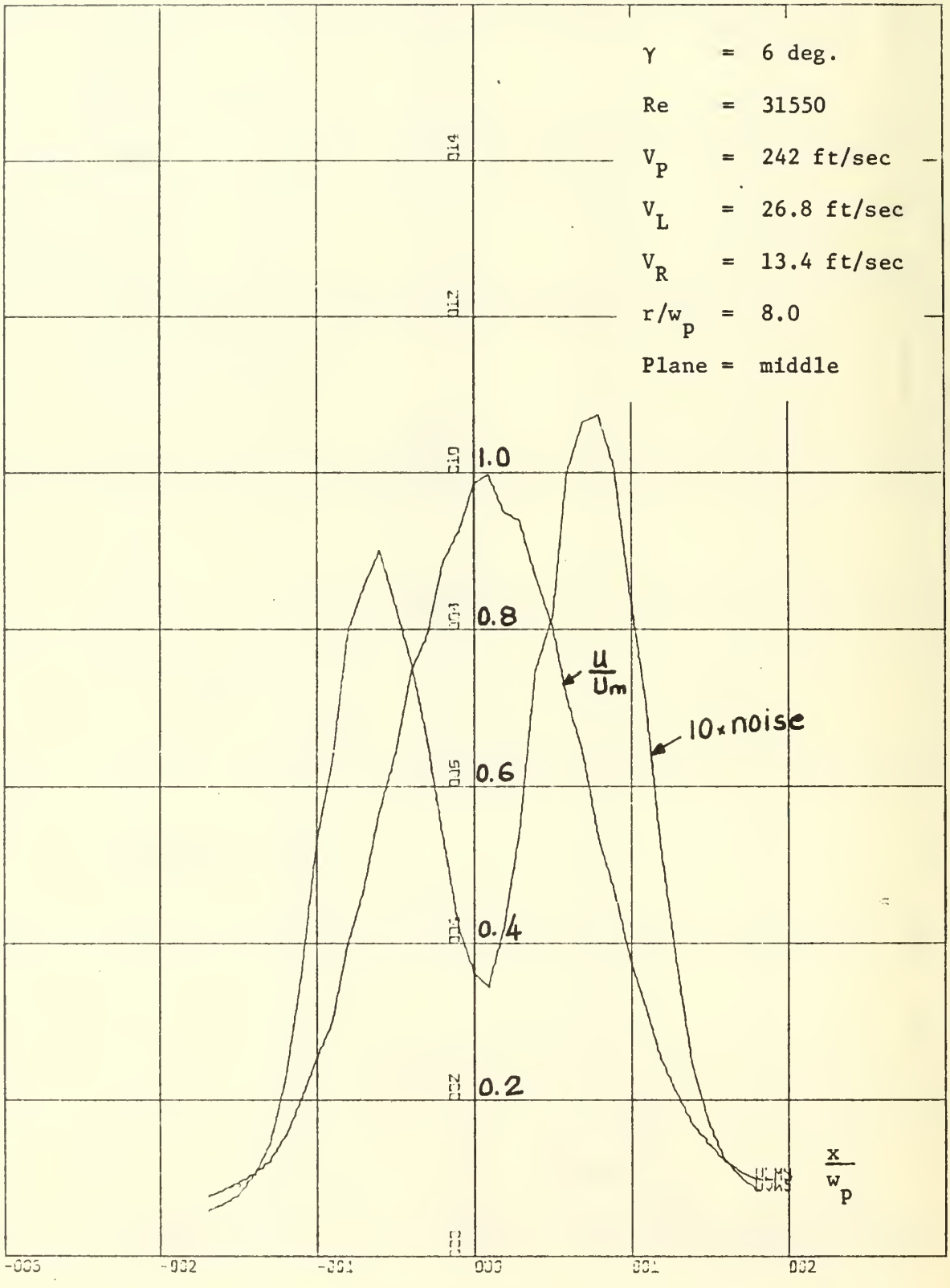

Figure 38 Mean Velocity and Noise

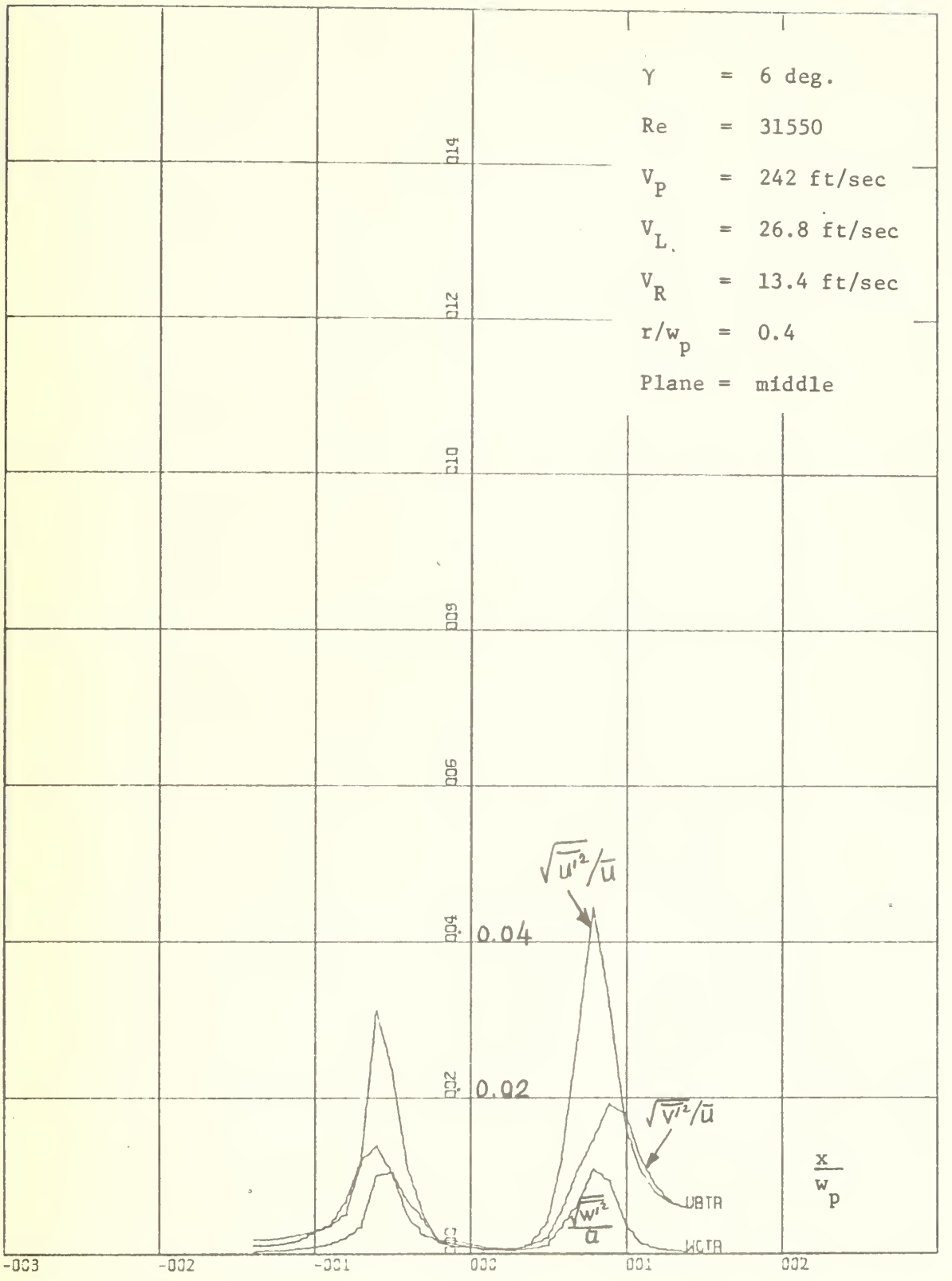

Figure 39 Turbulence Components

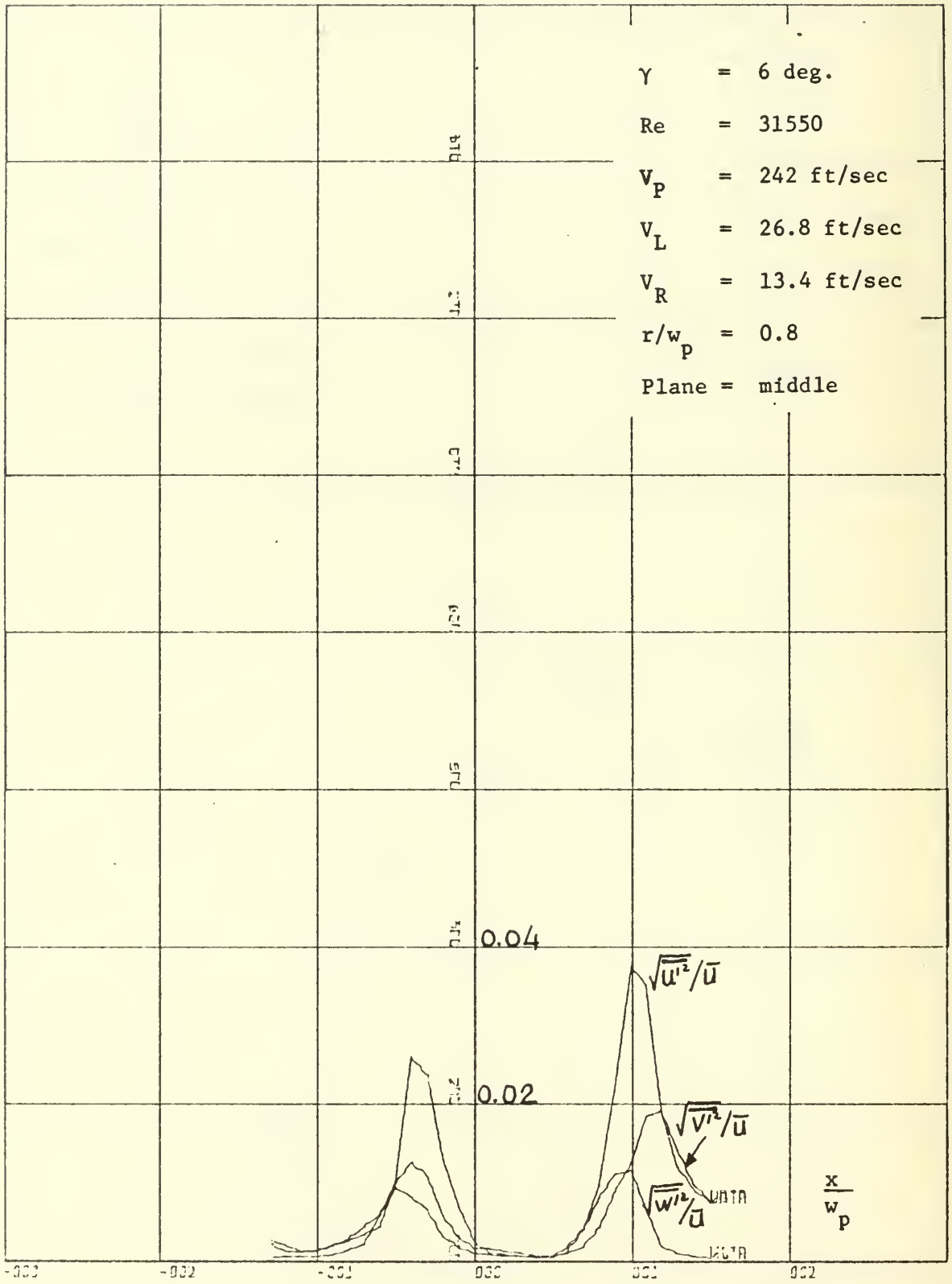

Figure 40 Turbulence Components

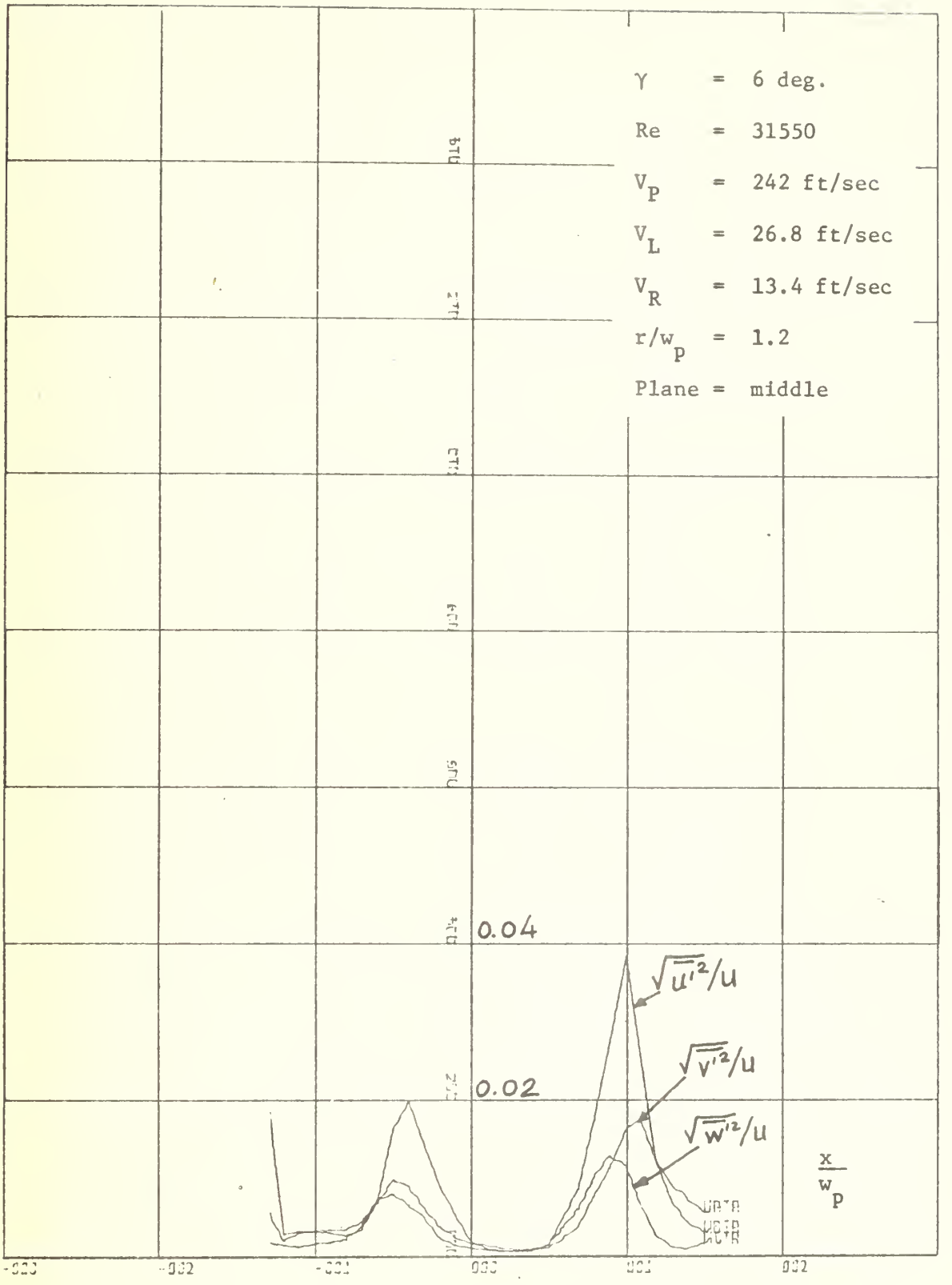

Figure 41 Turbulence Components

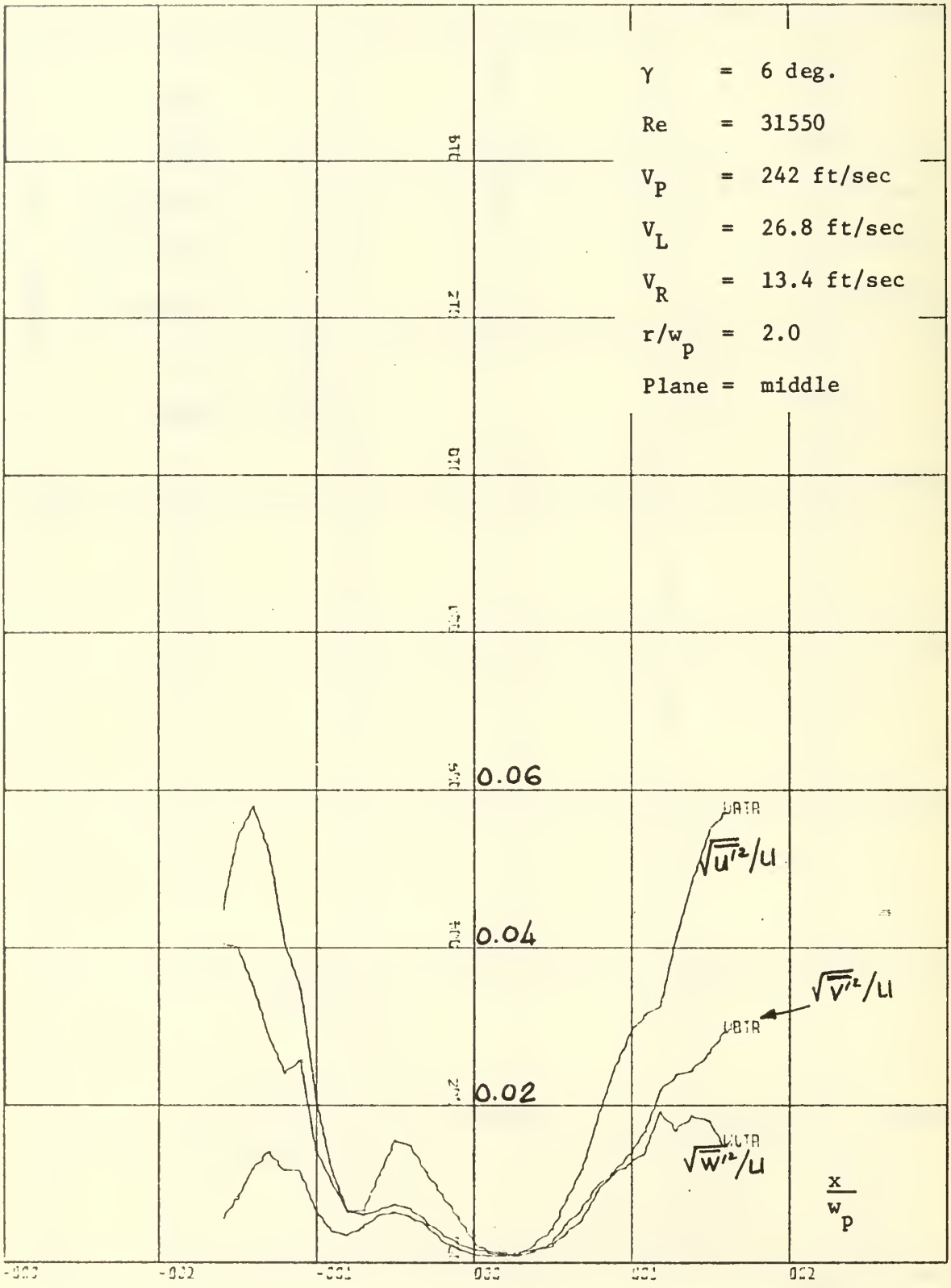

Figure 42 Turbulence Components

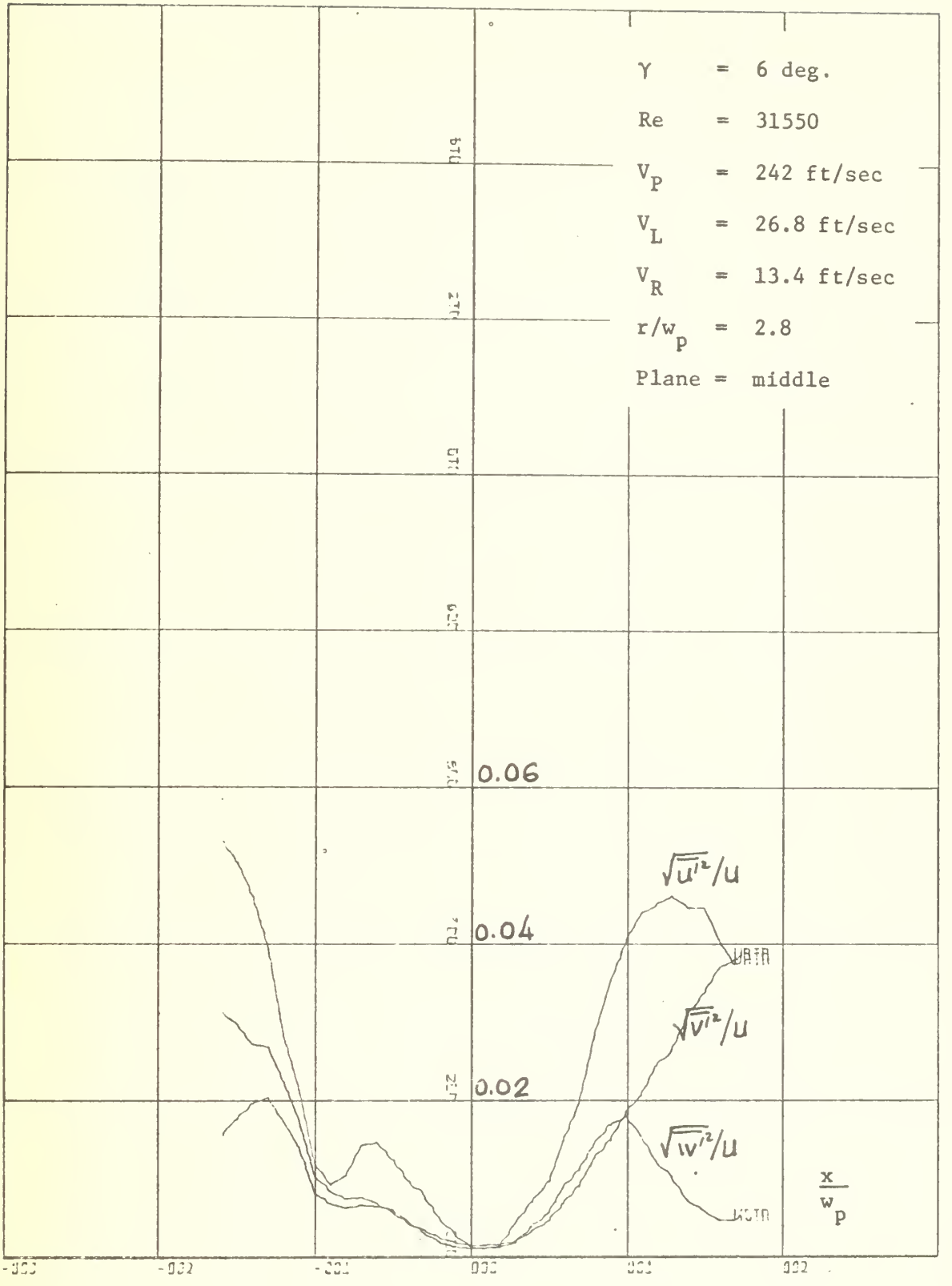

Figure 43 Turbulence Components

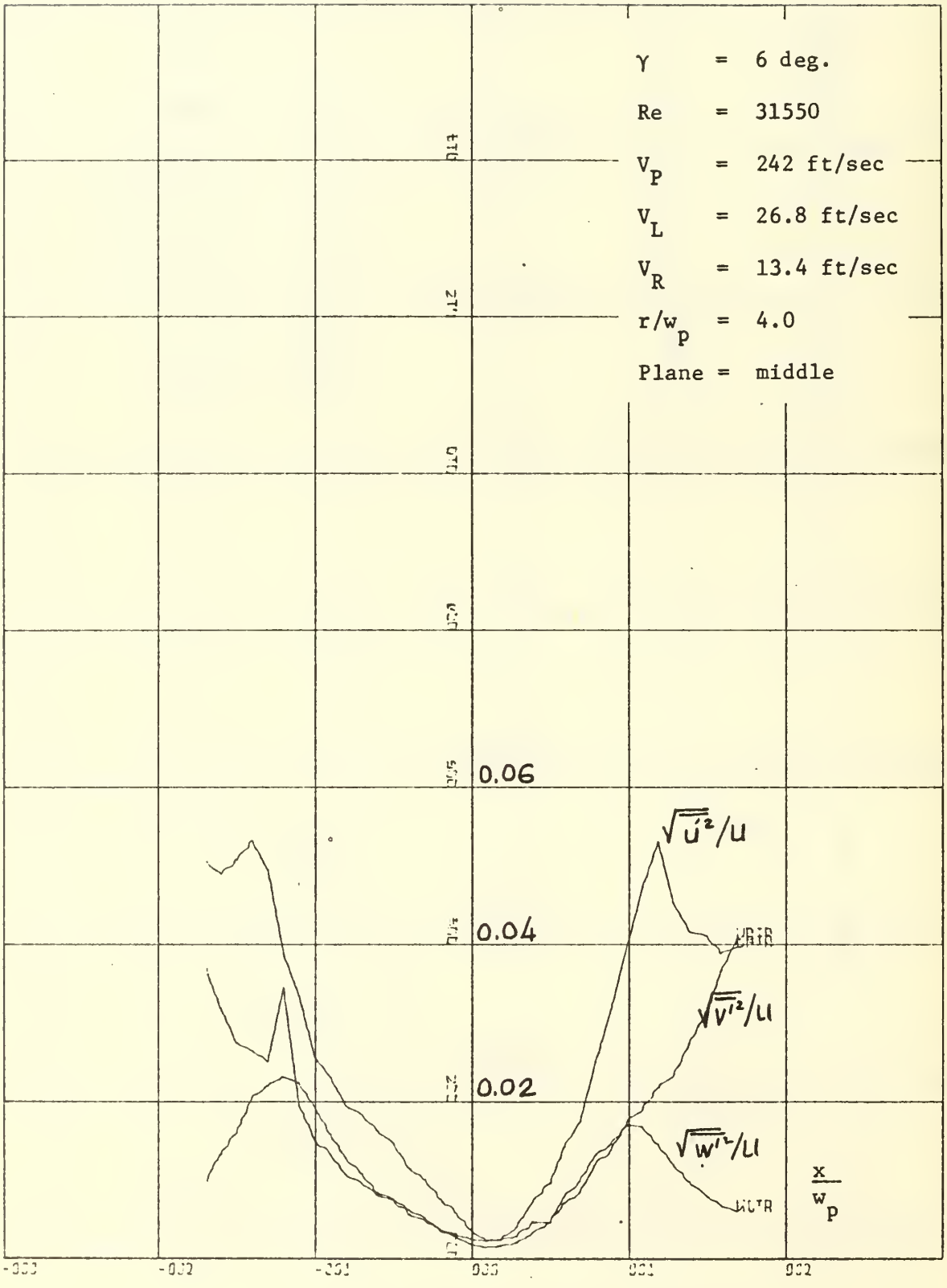

Figure 44 Turbulence Components

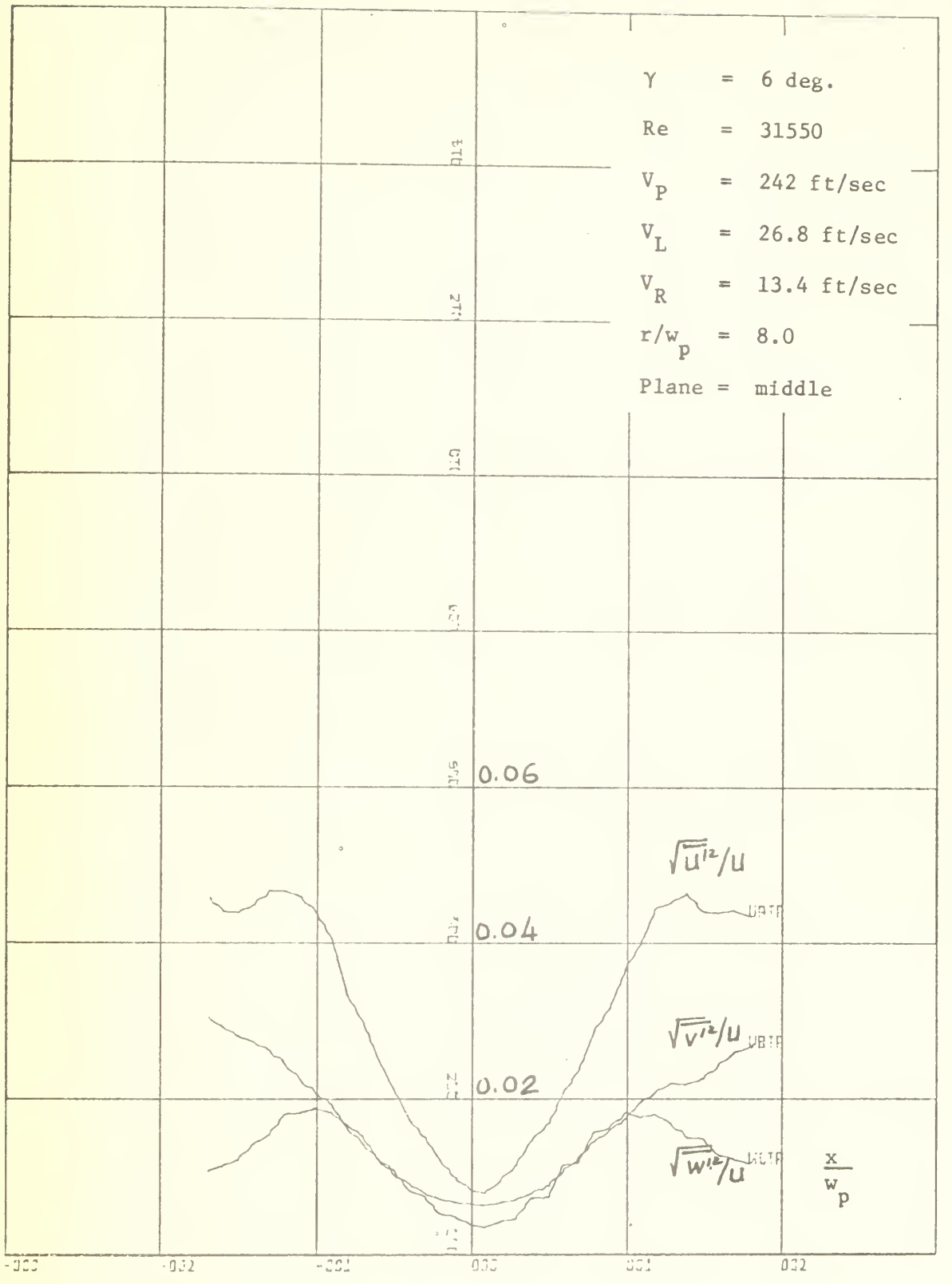

Figure 45 Turbulence Components

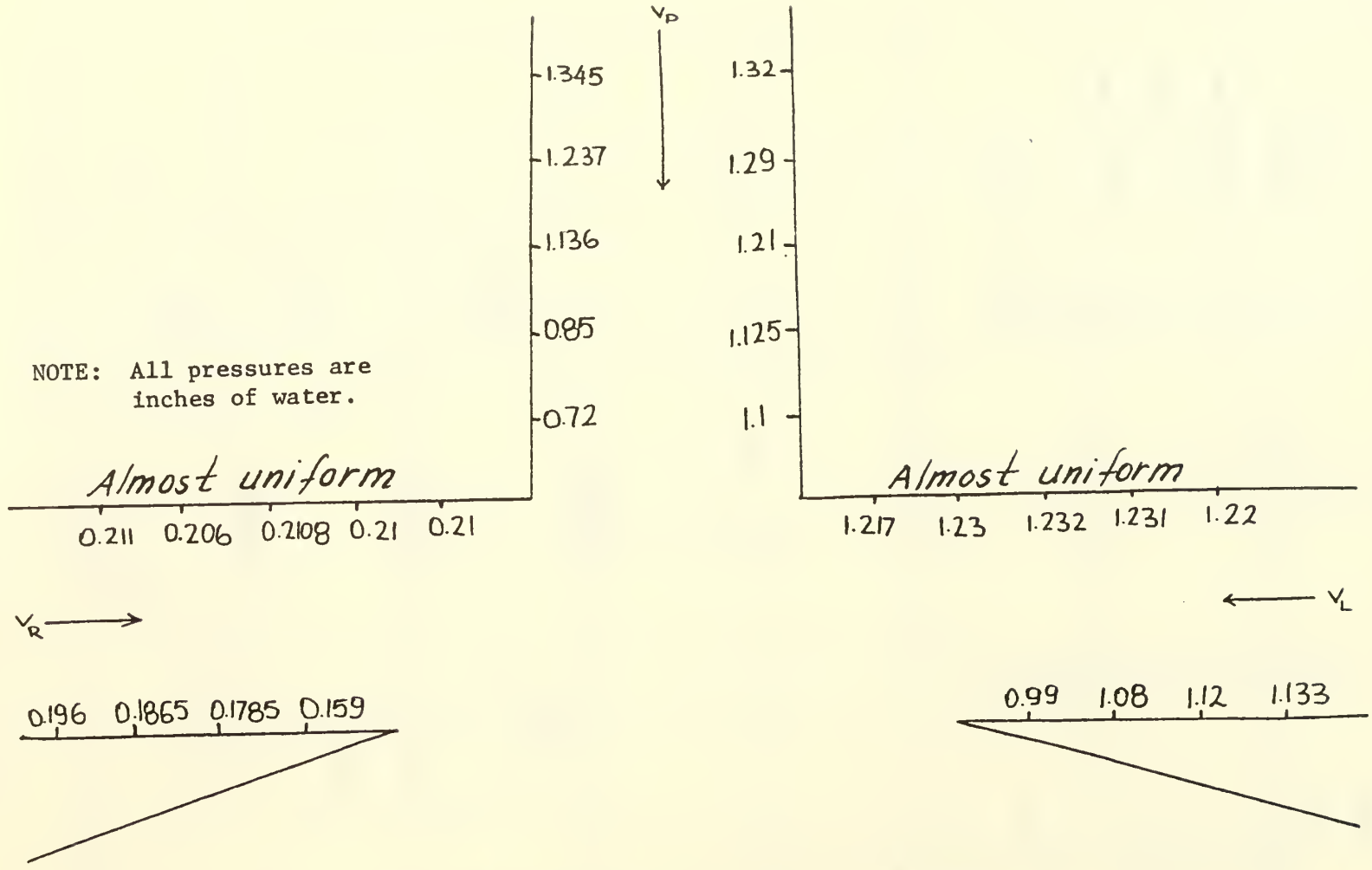

Figure 46 Static Wall Pressures, Re = 31550

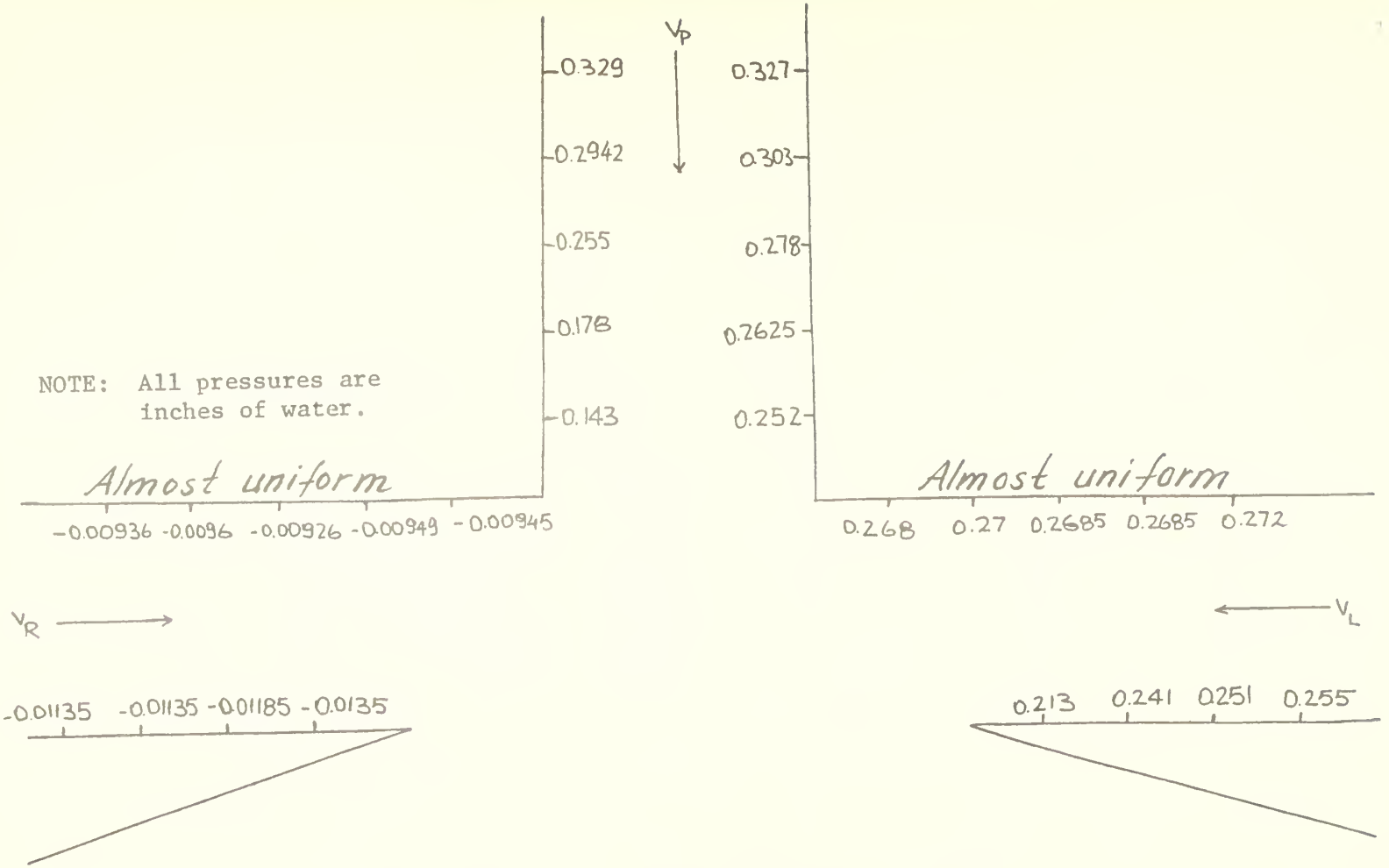

Figure 47 Static Wall Pressures, Re = 15775

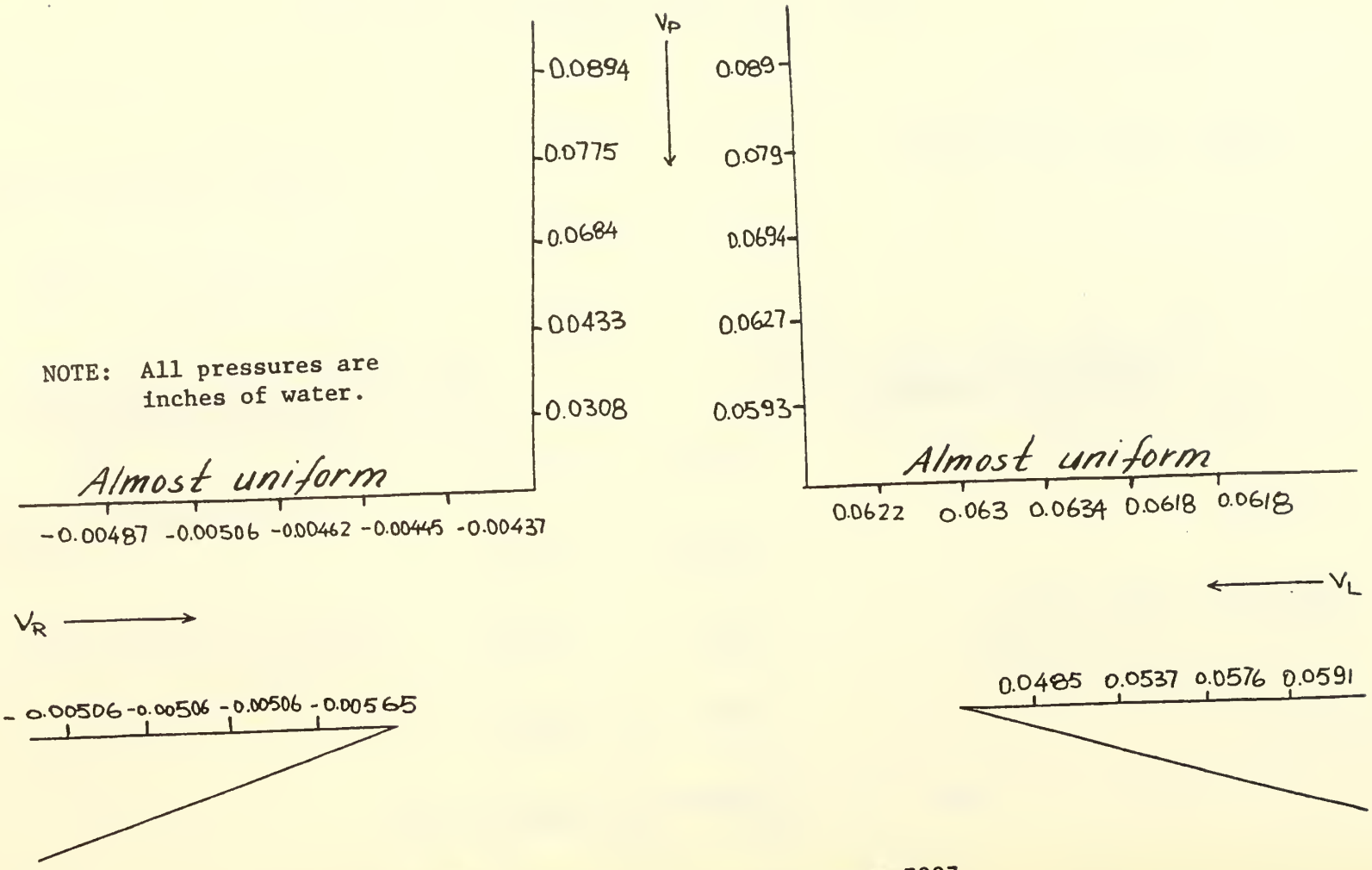

Figure 48 Static Wall Pressures, Re = 7887

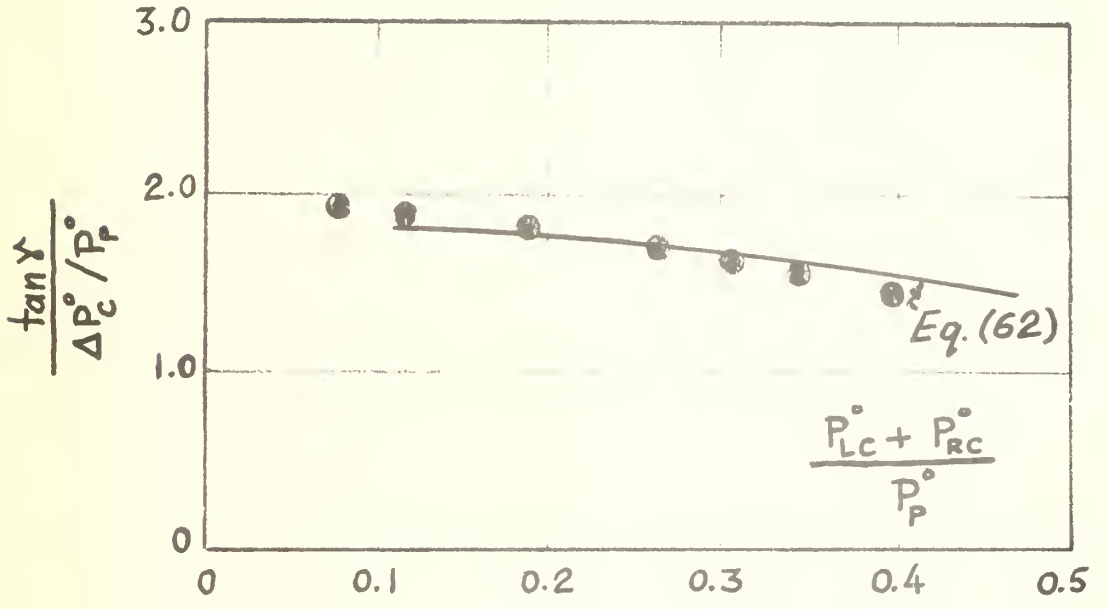

FIG. 49 Deflection Angles in terms of the control-and power-jet supply pressures and their comparison with those obtained via the momentum method. (Circles: experimental; solid line: analysis)

6. REFERENCES

1. Simson, A. K., Ph. D. Thesis, Dept. of Mech. Engineering, MIT, 1965.
2. Schlichting, H., Boundary Layer Theory, McGraw-Hill, 6th Ed. 1970.
3. Krzywoblocki, M. Z., Jet Propulsion, 26, 760-779, 1956.
4. Gurevich, M. I., The Theory of Jets in an Ideal Fluid, Acad. or Pergamon Press, 1965.
5. Davis, M. R., J. Fluid Mechs. 46, 631-656, 1971.
6. Ricou, F. P. and Spalding, D. B., J. Fluid Mechs. 11, 21, 1961.
7. Voorheis, T. S. and Howe, E. D., Proc. Pac. Coast Gas Ass. 30, 198, 1939.
8. Albertson, M. L., Dai, Y. B., Jensen, R. A., and Hunter, R., Proc. ASCE, 74, 10, 1948.
9. Grimmett, H. L., M. S. Thesis, Univ. of Illinois, 1948.
10. Polomik, E. E., M. S. Thesis, Univ. of Illinois, 1948.
11. Ricou, F. P., Ph. D. Thesis, University of London, 1959.
12. Donald, M. B. and Singer, H., Trans. Inst. Chem. Engrgs., 37, 255, 1959.
13. Hill, B. J., J. Fluid Mechs. 51, 773-779, 1972.
14. Watton, J., Proc. 4th Cranfield Fluidics Conf. Paper No. B-4, 1970.
15. Dexter, E. M., Symp. on Fluid Jet Control Devices, ASME, 1962.
16. Moynihan, F. A. and Reilly, R. J., Proc. of the Fluid Amplification Symp., HDL, Oct. 1962,
17. Douglas, J. F. and Neve, R. S., Proc. of the 2nd Cranfield Fluidics Conf., Jan. 1967.
18. Zalmanzon, L. A., Ivanov, N. N., and Limonova, M. E., Proc. IFAC Symp. on Fluidics, Paper No. A-4, 1968.
19. Sarpkaya, T., Weeks, S. B., and Hiriart, G. L., Proc. of the 4th Cranfield Fluidics Conf. Paper No. B-3, March 1970.

20. Gottron, R. N. and Weinger, S. D., Fluid Amplification Symp., HDL April 15, 1965.

21. Kelly, L. R. and Shin, J. N., Proc. 3rd Cranfield Fluidics Conf. Paper No. G-1, May 1968.

22. Gungor, N., M. S. Thesis, Dept. of Mechanical Engineering, NPS, June 1969.

23. Weeks, S. B., M. S. Thesis, Dept. of Mechanical Engineering, NPS, October 1969.

24. Pai, S., Fluid Dynamics of Jets, Van Nostrand Co., 1954, (pp: 96-136).

25. Sarpkaya, T., Proc. 2nd IFAC Symposium on Fluidics, Prague 1971.

26. Turken, E., M. S. and Engineer's Degree Thesis, Dept. of Mechanical Engineering, Naval Postgraduate School, Sept. 1971.

27. Sarpkaya, T., "Of Fluid Mechanics and Fluidics and of Analysis and Physical Insight", Proc. of the 5th Cranfield Fluidics Conf., Uppsala Sweden, June 1972.

ARMY RESEARCH OFFICE-DURHAM DISTRIBUTION LIST

Unless otherwise noted each agency will receive one copy of each Technical and Final Report emanating from this project. PSL and SC recipients are recorded and filed in IPO. Upon completion of the project they will be added to the official file. Technical and Final Reports: 85 Progress Reports: 20

AGENCY

Commanding Officer
U.S. Army Research Office-Durham
ATTN: CRDARD-IP
Box CM, Duke Station
Durham, North Carolina 27706

Commanding General
ATTN: Technical Library, Bldg. 313
Aberdeen Proving Ground, Maryland 21005

3. Commanding Officer
U.S. Army Aberdeen R&D Center
Ballistic Research Laboratories
Aberdeen Proving Ground, Maryland 21005

4. Commanding Officer
Ballistic Research Laboratories
ATTN: Technical Library
Aberdeen Proving Ground, Maryland 21005

5. Commanding Officer
Rock Island Arsenal
Rock Island, Illinois 61202

6. Commanding General
U.S. Army Tank-Automotive Command
ATTN: Technical Info Section
AMSTA-BSL
Warren, Michigan 48090

7. Commanding Officer
Frankford Arsenal
ATTN: C2500-Library, Bldg. 51-2
Philadelphia, Pennsylvania 19137

8. Commanding Officer
Picatinny Arsenal
ATTN: Technical Information Service
Dover, New Jersey 07801

9. Commanding General
U.S. Army Missile Command
ATTN: Redstone Sci. Info. Center
Redstone Arsenal, Alabama 35809

10. U.S. Army Missile Command
Directorate of Research and Development
Structures & Mechanics Lab. AMSMERS
Redstone Arsenal, Alabama 35808

11. U.S. Army Cold Regions Research and
Engineering Lab.
Hanover, New Hampshire 03755

12. Commanding General
U.S. Army Weapons Command (2)
ATTN: 9340 Documents Section
Rock Island, Illinois 61201

13. Commanding Officer
Watervliet Arsenal
ATTN: ORDBF-R
Watervliet, New York 12189

14. Commanding Officer
Army Materials & Mech Research Center
ATTN: Research & Requirements Office
Watertown, Massachusetts 02172

15. U.S. Army Electronics Command
Night Vision Lab.
Fort Belvoir, Virginia 22060

16. Commanding General
ATTN: Technical Library
White Sands Missile Range, N.M. 88002

17. Harry Diamond Laboratories
ATTN: HDL Library
Washington, D. C. 20438

18. Commanding Officer
U.S. Army Aberdeen R&D Center
Nuclear Effects Lab.
ATTN: Library
Aberdeen Proving Ground, Maryland 21005

19. U.S. Army Natick Laboratories
ATTN: Technical Library
Natick, Massachusetts 01760

20. Director
U.S. Army Munitions Command
Operations Research Group
ATTN: Technical Lib., Rm. 200 Bldg 330
Edgewood Arsenal, Maryland 21010

21. Commanding General
U.S. Army Electronics Laboratories
Fort Monmouth, New Jersey 07703

22. Commanding General
U.S. Army Electronics Command
ATTN: AMSEL-RD-PB
Fort Monmouth, New Jersey 07703

23. Commanding General
U.S. Army Mobility Equipment R&D Center
ATTN: STINFO Branch (2)
Fort Belvoir, Virginia 22060

24. Commanding Officer
Edgewood Arsenal
ATTN: Technical Director
Edgewood Arsenal, Maryland 21010

25. Director
U. S. Army Engineer Waterways
Experiment Station
P. O. Box 631
Vicksburg, Mississippi 39180

26. Commanding General
U. S. Army Aviation Systems Command
P. O. Box 209
St. Louis, Missouri 63166

27. Federal Aviation Administration
ATTN: Administrative Standards
Division (MS-110)
800 Independence Avenue, S. W.
Washington, D. C. 20590

28. Director
Army Research Office
Office, Chief Research and Development
Washington, D. C. 20310

AGENCY
29. Director of Army Research Office, Chief of Research and Development ATTN: Dr. I. R. Hershner, Jr., Chief Physical & Engineering Sciences Division Washington, D. C. 20310
30. Defense Documentation Center Cameron Station Alexandria, Virginia 22314 (12)
31. Mathematics Research Center University of Wisconsin Madison, Wisconsin 53706
32. Director National Bureau of Standards Washington, D. C. 20234
33. Deputy Director Environmental Data Service ATTN: BG B. G. Holzman, USAF (Ret.) Silver Spring, Maryland 20910
34. Director Advanced Research Projects Agency Washington, D. C. 20301
35. Defense Atomic Support Agency Washington, D. C. 20305
36. GE-TEMPO ATTN: DASA Information and Analysis Center 816 State Street Santa Barbara, California 93102
37. NASA Scientific and Technical Information Facility P. O. Box 33 College Park, Maryland 20740
38. Director National Security Agency ATTN: James Tippett R-422 Fort Meade, Maryland 20755
39. Office of Naval Research Washington, D. C. 22217
40. The Director Naval Research Laboratory Washington, D. C. 20390
41. Director, Naval Research Laboratory ATTN: Library, Code 2029 (ONRL) Washington, D. C. 20390
42. Commander U. S. Naval Weapons Laboratory ATTN: Technical Library Dahlgren, Virginia 22448
43. U. S. Naval Ordnance Laboratory ATTN: Library Division (2) White Oak Silver Spring, Maryland 20910
44. Commanding Officer U. S. Naval Propellant Plant Indian Head, Maryland 20640

AGENCY
45. Commander Naval Ordnance Systems Command ATTN: Technical Library Department of the Navy Washington, D. C. 20360
46. Air University Library, 3T-7142 Maxwell Air Force Base, Alabama 36112
47. Air Force Materials Laboratory Research and Technology Division Air Force Systems Command U. S. Air Force Wright-Patterson Air Force Base, Ohio 45433
48. Hq., Air Force Spec. Weapons Center Air Force Systems Command ATTN: Chief, Physics Division Research Directorate Kirtland AFB, New Mexico 87117
49. Air Force Office of Scientific Research Asst. Exec. Dir. Rsch. Commun. (SRGC) 1400 Wilson Boulevard Arlington, Virginia 22209
50. Library Jet Propulsion Laboratory California Institute of Technology Pasadena, California 91109
51. Director, Applied Physics Laboratory Johns Hopkins University 8621 Georgia Avenue Silver Spring, Maryland 20910
52. Defense Ceramic Information Center Battelle Memorial Institute Columbus Laboratories 505 King Avenue Columbus, Ohio 43201
53. Senior Standardization Representative U. S. Army Standardization Group, Canada Canadian Forces Headquarters Ottawa, Canada
54. The Defence Research Member Canadian Joint Staff 2450 Massachusetts Avenue Washington, D. C. 20008
55. Commanding Officer U. S. Army R & D Group (Europe) Box 15 FPO, New York 09510
56. Senior Standardization Representative U. S. Army Standardization Group United Kingdom Box 65, U. S. Navy 100 Fleet Post Office New York, New York 09510
57. Commanding Officer U. S. Army Aberdeen Research and Development Center Ballistic Research Laboratories ATTN: PSL or SC Representative Aberdeen Proving Ground, Maryland 21005

AGENCY	AGENCY
59. Commanding Officer Rock Island Arsenal ATTN: PSL or SC Representative Rock Island, Illinois 61202	72. Commanding General U. S. Army Electronics Laboratories ATTN: PSL or SC Representative Fort Monmouth, New Jersey 07703
60. Commanding General U. S. Army Tank-Automotive Center ATTN: PSL or SC Representative Warren, Michigan 48090	73. Commanding General U. S. Army Electronics Command ATTN: PSL or SC Representative Fort Monmouth, New Jersey 07703
61. Commanding Officer Frankford Arsenal ATTN: PSL or SC Representative Philadelphia, Pennsylvania 19137	74. Commanding General U. S. Army Mobility Equipment R & D Center ATTN: PSL or SC Representative Fort Belvoir, Virginia 22060
62. Commanding Officer Picatinny Arsenal ATTN: PSL or SC Representative Dover, New Jersey 07801	75. Commanding Officer Edgewood Arsenal ATTN: PSL or SC Representative Edgewood Arsenal, Maryland 21010
63. Commanding Officer U. S. Army Missile Command ATTN: PSL or SC Representative Redstone Arsenal, Alabama 35809	76. Director U. S. Army Engineer Waterways Experiment Sta. ATTN: PSL or SC Representative P. O. Box 631 Vicksburg, Mississippi 39180
64. Commanding Officer U. S. Army Cold Regions R & E Lab. ATTN: PSL or SC Representative Hanover, New Hampshire 03755	77. Commanding General U. S. Army Aviation Systems Command ATTN: PSL or SC Representative P. O. Box 209 St. Louis, Missouri 63166
65. Commanding General U. S. Army Weapons Command ATTN: PSL or SC Representative Rock Island, Illinois 61201	78. Director Ames Directorate ATTN: PSL or SC Representative U. S. Army Air Mobility R & D Laboratory NASA-Ames Research Center Moffett Field, California 94305
66. Commanding Officer Watervliet Arsenal ATTN: PSL or SC Representative Watervliet, New York 12189	79. Director Eustis Directorate ATTN: PSL or SC Representative U. S. Army Air Mobility Research and Development Center Fort Eustis, Virginia 23604
67. Commanding Officer Army Materials & Mech. Rsch. Center ATTN: PSL or SC Representative Watertown, Massachusetts 02172	80. Director Lewis Directorate ATTN: PSL or SC Representative U. S. Army Air Mobility Research and Development Laboratory NASA-Lewis Research Center Cleveland, Ohio 44135
68. U. S. Army Electronics Command Night Vision Laboratory ATTN: PSL or SC Representative Fort Belvoir, Virginia 22060	81. Director Langley Directorate ATTN: PSL or SC Representative U. S. Army Air Mobility Research and Development Laboratory Hampton, Virginia 23365
69. Commanding General ATTN: PSL or SC Representative White Sands Missile Range, N. M. 88002	
70. Harry Diamond Laboratories ATTN: PSL or SC Representative Washington, D. C. 20438	
71. Commanding Officer U. S. Army Aberdeen Research and Development Center Nuclear Effects Laboratory ATTN: PSL or SC Representative Aberdeen Proving Ground, Maryland 21005	
72. Commanding Officer U. S. Army Natick Laboratories ATTN: PSL or SC Representative Natick, Massachusetts 01762	

(OVER)

AGENCY	AGENCY
Scientific Cognizance Representative Commanding General U. S. Army Tank-Automotive Center ATTN: Mr. R. R. McGregor, SMORA-RCS Warren, Michigan 48090	
Scientific Cognizance Representative Commanding Officer Picatinny Arsenal ATTN: Mr. C. Daly, SMUPA-TT2 Dover, New Jersey 07801	
Scientific Cognizance Representative Commanding Officer U. S. Army Missile Command ATTN: W. A. Griffith, AMSMI-RGC Redstone Arsenal, Alabama 35809	
Scientific Cognizance Representative Harry Diamond Laboratories ATTN: J. M. Kirshner, Branch 310 Washington, D. C. 20438	
Naval Postgraduate School Monterey, California 93940 Attn: Code 02 (1) Code 023 (2) Code 59SL (Sarpkaya, T.) (10) Code 0212 (2)	
Department of Mechanical Engineering Naval Postgraduate School Monterey, Calif. 93940 (2)	

DOCUMENT CONTROL DATA - R&D

(Security classification of title, body of abstract and indexing annotation must be entered when the overall report is classified)

1. ORIGINATING ACTIVITY *(Corporate author)*

Naval Postgraduate School
Monterey, California 93940

2a. REPORT SECURITY CLASSIFICATION

Unclassified

2b. GROUP

3. REPORT TITLE

INTERACTION OF SEMI-CONFINED TURBULENT JETS

4. DESCRIPTIVE NOTES *(Type of report and inclusive dates)*

5. AUTHOR(S) *(Last name, first name, initial)*

SARPKAYA, TURGUT : Professor of Mechanical Engineering, Naval Postgraduate School, Monterey, California 93940

6. REPORT DATE	7a. TOTAL NO. OF PAGES	7b. NO. OF REFS
8 August 1972	105	27

8a. CONTRACT OR GRANT NO. MIPR No. ARO-D 4-69

b. PROJECT NO. ARO-D 4-69
8675-E

c. U. S. Army Research Office
Durham, N. C. 27706

d.

9a. ORIGINATOR'S REPORT NUMBER(S)

NPS-59SL72081A

9b. OTHER REPORT NO(S) *(Any other numbers that may be assigned this report)*

10. AVAILABILITY/LIMITATION NOTICES

Approved for public release; distribution unlimited.

11. SUPPLEMENTARY NOTES: No parts of this report may be translated or reproduced in any form without written permission from the author.

12. SPONSORING MILITARY ACTIVITY

DEPARTMENT OF THE ARMY
U. S. Army Research Office-Durham
Box: CM, Duke Station, Durham, N. C.

13. ABSTRACT

The present investigation is concerned with the theoretical and experimental study of the interaction of semi-confined, subsonic, turbulent jets, the application of the results to fluidics being one of the primary objectives in mind. The theoretical results obtained both through the use of the free-streamline theory and a new momentum analysis for both the single and symmetric control-jet configurations are presented in the first part of the report. The second part covers the detailed experimental investigations of the jet deflection and the velocity-and turbulence-profile measurements obtained with a hot-wire anemometer for both the single-control-jet and symmetric beam-deflection type amplifiers. Finally, the results of the two parts of the study are compared and the advantages and shortcomings of the various analyses are presented.

DD FORM 1 JAN 64 1473 0101-807-6800

14. KEY WORDS	LINK A		LINK B		LINK C	
	ROLE	WT	ROLE	WT	ROLE	WT
Jet Interaction Proportional Amplifiers Noise in Proportional Amplifiers Application of the Free-Streamline Analysis to combining jets Momentum Analysis of Proportional Amplifiers Interaction of Semi-Confined Turbulent Jets						

INSTRUCTIONS

1. ORIGINATING ACTIVITY: Enter the name and address of the contractor, subcontractor, grantee, Department of Defense activity or other organization *(corporate author)* issuing the report.

2*a*. REPORT SECURITY CLASSIFICATION: Enter the overall security classification of the report. Indicate whether "Restricted Data" is included. Marking is to be in accordance with appropriate security regulations.

2*b*. GROUP: Automatic downgrading is specified in DoD Directive 5200.10 and Armed Forces Industrial Manual. Enter the group number. Also, when applicable, show that optional markings have been used for Group 3 and Group 4 as authorized.

3. REPORT TITLE: Enter the complete report title in all capital letters. Titles in all cases should be unclassified. If a meaningful title cannot be selected without classification, show title classification in all capitals in parenthesis immediately following the title.

4. DESCRIPTIVE NOTES: If appropriate, enter the type of report, e.g., interim, progress, summary, annual, or final. Give the inclusive dates when a specific reporting period is covered.

5. AUTHOR(S): Enter the name(s) of author(s) as shown on or in the report. Enter last name, first name, middle initial. If military, show rank and branch of service. The name of the principal author is an absolute minimum requirement.

6. REPORT DATE: Enter the date of the report as day, month, year; or month, year. If more than one date appears on the report, use date of publication.

7*a*. TOTAL NUMBER OF PAGES: The total page count should follow normal pagination procedures, i.e., enter the number of pages containing information.

7*b*. NUMBER OF REFERENCES: Enter the total number of references cited in the report.

8*a*. CONTRACT OR GRANT NUMBER: If appropriate, enter the applicable number of the contract or grant under which the report was written.

8*b*, 8*c*, & 8*d*. PROJECT NUMBER: Enter the appropriate military department identification, such as project number, subproject number, system numbers, task number, etc.

9*a*. ORIGINATOR'S REPORT NUMBER(S): Enter the official report number by which the document will be identified and controlled by the originating activity. This number must be unique to this report.

9*b*. OTHER REPORT NUMBER(S): If the report has been assigned any other report numbers *(either by the originator or by the sponsor)*, also enter this number(s).

10. AVAILABILITY/LIMITATION NOTICES: Enter any limitations on further dissemination of the report, other than those imposed by security classification, using standard statements such as:

(1) "Qualified requesters may obtain copies of this report from DDC."

(2) "Foreign announcement and dissemination of this report by DDC is not authorized."

(3) "U. S. Government agencies may obtain copies of this report directly from DDC. Other qualified DDC users shall request through

_____."

(4) "U. S. military agencies may obtain copies of this report directly from DDC. Other qualified users shall request through

_____."

(5) "All distribution of this report is controlled. Qualified DDC users shall request through

_____."

If the report has been furnished to the Office of Technical Services, Department of Commerce, for sale to the public, indicate this fact and enter the price, if known.

11. SUPPLEMENTARY NOTES: Use for additional explanatory notes.

12. SPONSORING MILITARY ACTIVITY: Enter the name of the departmental project office or laboratory sponsoring *(paying for)* the research and development. Include address.

13. ABSTRACT: Enter an abstract giving a brief and factual summary of the document indicative of the report, even though it may also appear elsewhere in the body of the technical report. If additional space is required, a continuation sheet shall be attached.

It is highly desirable that the abstract of classified reports be unclassified. Each paragraph of the abstract shall end with an indication of the military security classification of the information in the paragraph, represented as *(TS)*, *(S)*, *(C)*, *or (U)*.

There is no limitation on the length of the abstract. However, the suggested length is from 150 to 225 words.

14. KEY WORDS: Key words are technically meaningful terms or short phrases that characterize a report and may be used as index entries for cataloging the report. Key words must be selected so that no security classification is required. Identifiers, such as equipment model designation, trade name, military project code name, geographic location, may be used as key words but will be followed by an indication of technical context. The assignment of links, roles, and weights is optional.